Investigating the Effect of Smectic A Temperature Range Variation on De Vries Properties

By

Qingxiang Song

A thesis submitted to the Department of Chemistry

in conformity with the requirements

for the degree of Master of Science

Queen's University

Kingston, Ontario, Canada

November, 2009

Abstract

Ferroelectric liquid crystals (FLCs) have been investigated as the basis for a new type of liquid crystal display because of their fast switching times. Commercial FLC materials are mixtures consisting of a small amount of chiral dopant in an achiral liquid crystal host with an isotropic-nematic-smectic A-smectic C (INAC) phase sequence, which is required to achieve proper alignment between glass slides with rubbed polyimide alignment layers. However, the layer contraction occurring at the SmA-SmC phase transition on cooling from isotropic liquid is a severe problem that leads to a buckling of the smectic layers and results in zigzag defects that drastically degrade the optical quality of FLC films. To solve this problem, we are focusing on a new class of liquid crystal molecules with minimal or no smectic layer shrinkage at the SmA-SmC transition which is referred to as ‘de Vries-like.’

Previous work in the Lemieux group has shown that combining structural elements promoting SmA and SmC phases in a single molecule increases de Vries-like behavior. Giesselmann *et. al.* suggest that a correlation exists between the temperature range of the SmA phase and de Vries-like behavior. In the study described herein, two homologous series of molecules with 2-phenylpyrimidine cores with siloxane-terminated side-chain (SmC promoting element) and a chloro-terminated side-chain (SmA promoting element) are synthesized and characterized by polarized optical microscopy, differential scanning

calorimetry and small-angle X-ray diffraction (SAXS). The reduction factor *R* for series **1.13** from 0.36 to 0.46 and for series **1.14** from 0.47 to 0.54. Results show that, although there is some correlation between % layer contraction and SmA temperature range, it can be explained primarily by differences in tilt angle θ. When θ is taken into account in the *R* values, there is no correlation.

Another aspect of the study described herein, two siloxane-terminated 2-phenylpyrimidine chiral dopants are synthesized and characterized by polarized optical microscopy, differential scanning calorimetry and small-angle X-ray diffraction (SAXS).

To my dear wife, Yueqiao and our parents

Acknowledgements

First and foremost I would like to express my sincere thanks and gratitude to my supervisor, Dr. Robert P. Lemieux for his support and guidance. Without Bob's guidance and encouragement this thesis would not be possible.

I would like to thank the members of my supervisory committee: Dr. Donal Macartney and Dr. Hugh Horton for offering valuable suggestions and help. I would also like to thank the past and present members of the Lemieux lab group: especially Dr. Jeff Roberts, Dr. Khurshid Ayub, Camilla Anderson, Qian Cui, Eric Ekengard, Linli Fang, Wei Gan, Christa Huntley and Li Li. I am very lucky to have been able to work alongside such an intelligent group of people. I appreciate all you have shared with me.

This thesis would not have been possible without all the people who work behind the scenes, especially Dr. Françoise Sauriol and Dr. Ruiyao Wang in the NMR facility, Dr. Yimin She and Jie Sui in the mass spectrometry lab, Ed Maracle and Robin Roberts in the electronics shop, Robert Dumont in the science store.

Finally, I would love to thank my parents, who always encourage me throughout all my life. I would like thank my dear wife Yueqiao Fu for her love, patience and faith in me. Your love and support have kept me grounded

TABLE OF CONTENTS

LIST OF FIGURES

LIST OF TABLES

Abbreviations

ΔH	Enthalpy of transition
Å	Angstrom
AC	Alternating current
Ac	Acetyl
aq	Aqueous
C_2	C_2-symmetric conformer
calcd	Calculated
χ_d	Mole fraction of the dopant
C_{dv}	'de Vries' coefficient
cm	Centimeter
Cr	Crystalline
$d(T_{AC})$	Layer spacing at transition from sma phase to smc phase
d_A	Layer spacing in sma phase
d_C	Layer spacing in smc phase
DET	Diethyl tartrate
DIAD	Diisopropyl azodicarboxylate
DIBAL	Diisobutylaluminium hydride
DMF	N,N-dimethylformamide
DSC	Differential scanning calorimetry

EI	Electron impact ionization
ESI	Electrospray ionization
Et	Ethyl
Et_2O	Diethylether
EtOAc	Ethyl acetate
EtOH	Ethanol
FLC	Ferroelectric liquid crystal
h	Hours
HPLC	High performance liquid chromatography
HRMS	High resolution mass spectrometry
I	Isotropic
i.d.	Inside diameter
^{i}Pr	Isopropyl
ITO	Indium-tin oxide
J	Coupling constant
kJ	KiloJoule
LC	Liquid crystal
LCD	Liquid crystal display
M	molar
Me	Methyl

MHz	Megahertz
min	Minutes
mm	Millimeter
mol	Mole
mp	Melting point
MS	Mass spectrometry
N	Nematic
n	Director
N*	Chiral nematic
NMR	Nuclear magnetic resonance
PCC	Pyridinium chlorochromate
Ph	Phenyl
P_o	Reduced polarization
POM	Polarized optical microscopy
PPh_3	Triphenylphosphine
ppm	Part per million
P_s	Spontaneous polarization
PTFE	Polytetrafluoroethylene
q	Tilt angle
R	A figure of merit

rt.	Room temperature
sat	Saturated
SAXS	Small-angle X-ray scattering
SmA	Smectic A
SmA*	Chiral Smectic A
SmC	Smectic C
SmC*	Chiral Smectic C
SSFLC	Surface-stabilized ferroelectric liquid crystal
TBHP	*tert*-butyl hydroperoxide
TC	Curie point
THF	Tetrahydrofuran
TOF	Time of flight
V	Volt
z	Layer normal
δ	Chemical shift
δ(T)	Chevron layer tilt angle
δP	Polarization power
μm	Micrometre

Chapter 1. Introduction

Liquid crystals are substances that exhibit a phase of matter that has properties between those of a conventional liquid, and those of a solid crystal. They were first discovered by Reinitzer[1] in 1888 and it has been widely used in liquid crystal display (LCD) applications for a variety of electronic devices. Though twisted nematic LCD devices were the first to be commercialized, they have some disadvantages such as slow response and narrow viewing angles. Ferroelectric liquid crystals (FLCs) have been investigated as an alternative technology because of their fast switching time, wider viewing angle and lower power requirement. Typically, commercial FLC mixtures consist of a small amount of chiral dopant mixed in an achiral liquid crystal host with a broad temperature range in the Smectic C phase (*vide infra*) and low viscosity.

The work described in this thesis focuses on designing new materials as liquid crystal host for FLC mixtures that have improved alignment properties in liquid crystal cell. In order to put the thesis work into proper context, the following section gives an overview of liquid crystal phases and their relevance to FLC materials.

1.1 Classification of Liquid Crystals

There are two general phases of liquid crystals, lyotropic liquid crystals and thermotropic

liquid crystals. Lyotropic liquid crystals are formed by amphiphilic molecules in the presence of a solvent and will not be discussed further in this thesis. Thermotropic liquid crystals are formed as a function of temperature in the absence of solvent. There are four general types of molecules forming Thermotropic liquid crystal phases (mesogens) as shown as Figure 1-1, which are classified according to their shapes. Calamitic mesogens are rod-shaped with a rigid core and flexible alkyl side-chains (**1.1**). Discotic mesogens are disc-shaped, typically formed by a flat polyaromatic core and multiple alkyl side-chains (**1.2**). Polycatenar mesogens are normally formed by a narrow rigid core and multiple alkyl side-chains (**1.3**). Bent-core (banana-shaped) mesogens have recently received a great deal of attention due to their unique chiral layer structure (**1.4**).[2]

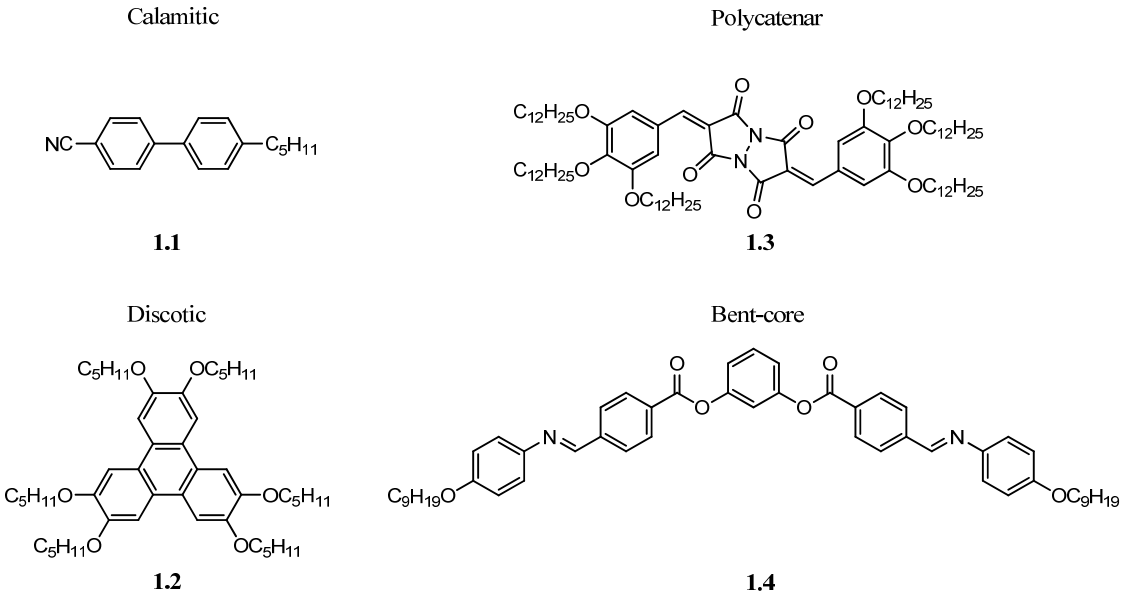

Figure 1-1: Examples of calamitic, discotic, polycatenar and bent-core liquid crystals.

1.2 Calamitic Liquid Crystals phase

Calamitic mesogens form two major types of liquid crystal phases, the Nematic phase (N) and Smectic phases. In the nematic phase, the molecules only exhibit orientational order; in smectic phases the molecules exhibit orientational order with a diffuse layer structure. There are several types of smectic phases, but we will focus only on the smectic A (SmA) and smectic C phases (SmC).

1.2.1 The Nematic Phase

Nematic liquid crystals are usually formed by rod-like molecules with a large aspect ratio (L/*d*) (Figure 1-2) and the molecules have long-range orientational order but no positional order. Therefore, their center of mass positions are randomly distributed as in a liquid and the molecules flow, but all of them are oriented in same direction along a vector **n** (director).

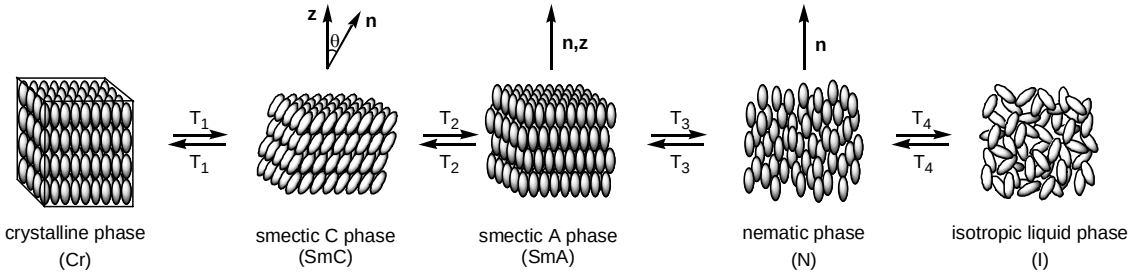

Figure 1-2: Schematic representation of isotropic (I), nematic (N), smectic A (SmA), smectic C (SmC) and crystalline (Cr) phases of calamitic liquid crystals.

1.2.2 The Smectic A Phase

The SmA phase can be described as a nematic phase which self-assembles into a layered structure, as shown in Figure 1-2. The long axes of molecules are oriented along a director **n** which is parallel to the layer normal **z**. The molecules can rotate about their long axes and the layer spacing *d* is approximately equal to the molecular length L. There is no packing order within each layer. The X-ray scattering profile of a SmA phase normally shows only a first order diffraction peak at small angle due to the diffuse layer structure. Molecules featuring have nanosegregation elements, a concept which will be described later in this chapter, such as siloxane-terminated or perfluorinated side-chains, tend to form smectic phases.

1.2.3 The Smectic C Phase

The structure of the Smectic C phase is similar to that of the Smectic A phase, the only difference being that the molecular orientation is uniformly tilted with respect to the layer normal **z** as shown in Figure 1-2. The tilt angle θ formed by **n** and **z** is dependent on the temperature, and increases with decreasing temperature.

1.2.3.1 Molecular origins of tilt

Several models have been proposed to discribe the origin of the molecular tilt in the SmC phase. The earliest one was proposed by McMillan who noted that 4,4'-di-*n*-alkoxyazoxybenzenes (**1.5**) form SmC phases, but not the analogous 4,4'-di-*n*-alkylazoxybenzenes (**1.6**).[3] Based on this observation, he postulated that a mesogen must have polar groups such as ether or ester linking the core to each side chain.[4] According to this model, upon cooling, the rotational order about **n** increases and results in a coupling of these 'outboard dipoles', as shown as in Figure 1-3. The resulting induced torque results in the tilt. However, this model is far from being universal because there are many known examples of molecules with outboard dipoles that do not form a SmC phase in the phase sequence.[5]

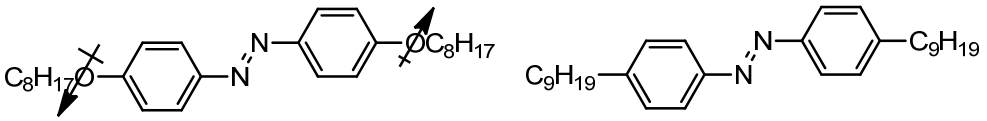

1.5 **1.6**

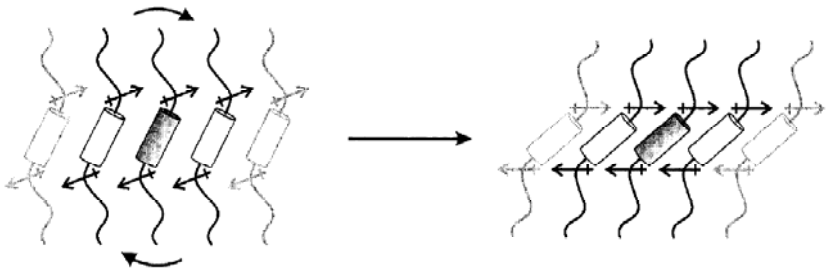

Figure 1-3: Schematic representation of McMillan model for origin of tilt in SmC phase

Another model by Wulf suggests that steric interaction and packing force play a more significant role than the coupling of outboard dipoles.[6] He proposed that the time-average molecular shape is a cylinder in SmA phase, and that molecules can rotate freely about the long axis **n**. Upon cooling into the SmC phase, the conformational order increases and the rotational freedom is reduced. On the time average, the molecular shape corresponding to the lowest energy conformation of the calamitic mesogens is zigzag. The most efficient means of packing zigzags involves tilting of the molecular long axes, as shown as Figure 1-4. Durand and coworkers showed by X-ray diffraction that the cores of calamitic mesogens are more tilted than the side-chains in the SmC phase.[7] Recently, Clark and coworkers confirmed this finding using polarized infrared absorption spectroscopy.[8]

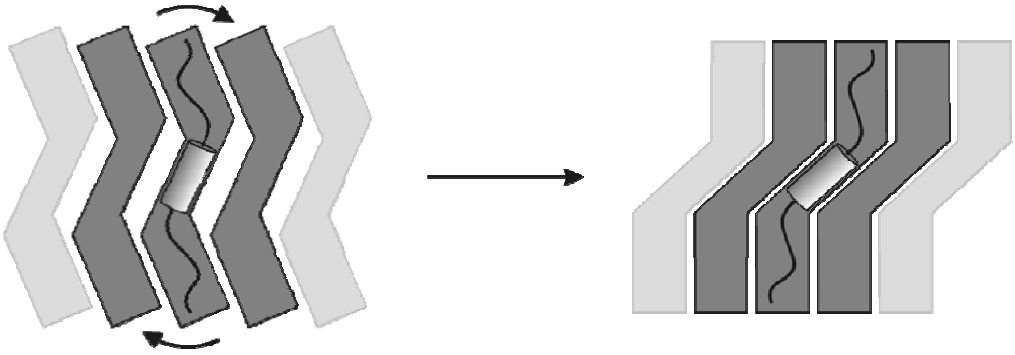

Figure 1-4: Schematic of the Wulf model where the zigzags pack closer when the core is more tilted than the side chains.

1.2.4 Structural Elements Favoring Smectic Phases

The formation of nematic or smectic phases depends on the degree of amphiphilicity of the mesogen and the anisotropy of molecular polarization. Nanosegregation, which refers to the assembly of blocks within the mesogens into distinct microdomains due to chemical incompatibility, plays a key role in the formation of mesophases[9]. In the specific case of calamitic mesogens, the formation of layers is favored by the difference in rigidity and van der waals interactions between aromatic cores and alkyl side-chains. One can further promote the formation of smectic phases by incorporating certain groups such as (semi)perfluorinated alkyl groups or an organosiloxane end-group, which are nanosegregation elements.[9] The stability of smectic phases generally increases with an increase in the alkyl chain length, *i.e.*, as the molecular amphiphilicity increases. Thus, the tendency of smectic phase formation increases with increasing the alkyl chain length.

1.3 Chirality in Calamitic Liquid Crystals Phase

1.3.1 Structure of Chiral SmC Phase

The SmC phase is biaxial and is described by two vectors, the director **n** and the layer normal **z**, which form the tilt plane. The vector **n** and **z** are related by the tilt angle θ. There are three symmetry elements: a symmetry plane σ which is congruent with the tilt

plane, a C_2 axis which is perpendicular to the tilt plane and an inversion centre. In 1976, Meyer and coworkers predicted that when the SmC phase is chiral (SmC*), the symmetry plane vanishes, thus reducing the symmetry of the phase from C_{2h} to C_2, as shown in Figure 1-5. The resulting polar order along the C_2 axis result in a spontaneous polarization, P_s, and the chiral SmC* material should be ferroelectric.[10]

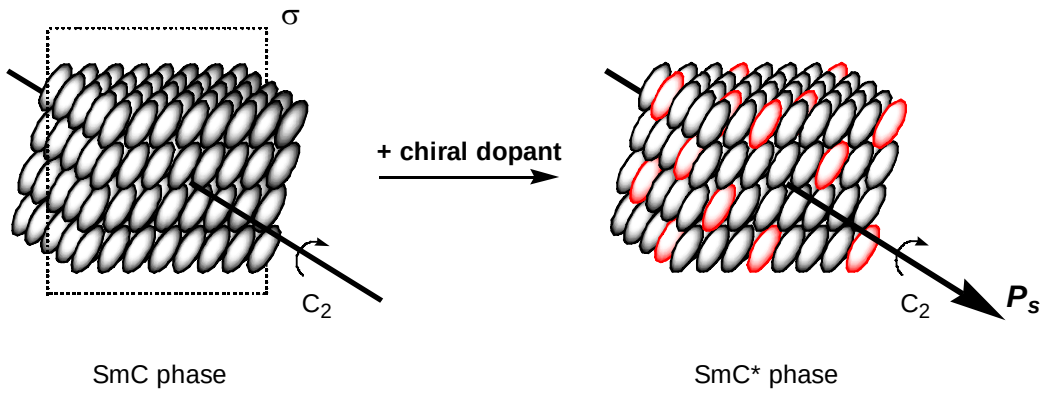

Figure 1-5: Symmetry elements of the SmC and SmC* phases.

1.3.2 Ferroelectric liquid crystals

Without any external constraints, the SmC* phase forms a helical structure, and the direction of P_s rotates from one layer to the next. Thus, the spontaneous polarization of the bulk material averages to zero (Figure 1-6(a)). However, Clark and Lagerwall showed that when a SmC* material is aligned between two polyimide-coated glass slides, the SmC* helix spontaneously unwinds if the gap between the slides is equal to, or smaller than the helical pitch (Figure 1-6(b)). Such materials are referred to as surface-stabilized

ferroelectric liquid crystals (SSFLCs).[11]

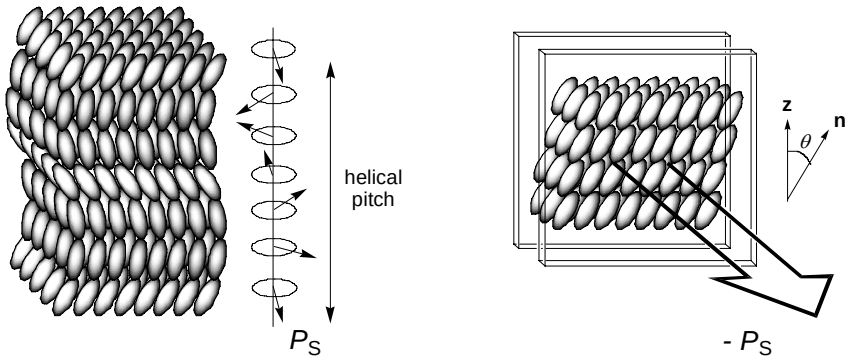

Figure 1-6: (a) Unwinding of the helical structure of the SmC* phase due to boundary conditions. (b)The sign of the spontaneous polarization is defined by the vector product of (**z** × **n**), and is shown here as negative.

By coupling the polarization to an external electric field applied across the SSFLC film, the tilt orientation can be switched from $+\theta$ to $-\theta$, by precession of the molecules about **z** as shown in Figure 1-7. This behavior is known as Goldstone mode switching. Because liquid crystalline materials are birefringent due to refractive index anisotropy, we can make a light shutter by placing an SSFLC film between two crossed polarizers. Application of a field of one sign produces an "ON" state, whereas application of the opposite field produces the "OFF" state.

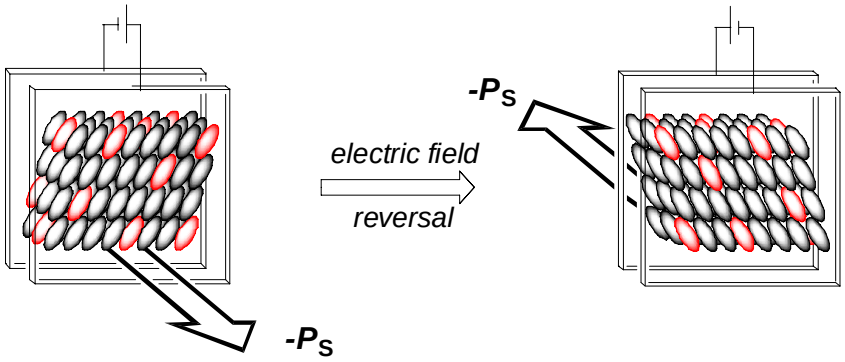

Figure 1-7: Switching of a SSFLC induced by changing direction of external electric field

Although SSFLC displays have many advantages such as bistability and low energy requirement, device applications based on neat SmC* materials tend to have switching times that are much longer than desired due to the high viscosity of the material. Fortunately, Kuczyński and Stegemeyer showed that when a small amount of chiral dopant is added to an achiral SmC liquid crystal host, a SmC* phase is induced[12]. In order to be useful, the chiral dopant must induce a high P_s. The ability of a dopant to induce a spontaneous polarization in an achiral SmC host is expressed as the polarization power (eq. 1-1), where χ_d is the mole fraction of the dopant, P_o is the reduced polarization (eq. 1-2), which is a normalized form of P_s that accounts for variation in tilt angle from one host to the next.[12,13]

$$\delta_P = dP_0(\chi_d)/d\chi_d \qquad \text{(eq. 1-1)}$$

$$P_0 = P_S/\sin\theta \qquad \text{(eq. 1-2)}$$

1.3.3 Molecular origins of P_s: The Boulder Model

In order to design dopants with large δ_p values, we need to understand the relationship between molecular structure and spontaneous polarization. In 1986, a model for predicting the sign of polarization of SmC* mesogens was proposed by Walba and co-workers[14,15]. It assumes that the alkyl side-chains extend in all-*anti* conformations and the overall shape is that of a zigzag, which has been confirmed by both deuterium NMR studies[16,17] and X-ray diffraction studies.[18]

In 1978, Durand and co-workers compared SmC tilt angles measured by polarized optical microscopy (θ_{opt}) with those derived from X-ray diffraction measurements ($\theta_{x\text{-}ray}$).[7] The optical tilt depends on the polarizability anisotropy of the molecule and corresponds approximately to the angle between the layer normal and the long axis of the aromatic core. The X-ray tilt is simply calculated as the inverse cosine of the smectic layer spacing *d* over the molecular length L. Normally, θ_{opt} is bigger than $\theta_{X\text{-}ray}$, which suggests that the core is more tilted than the side-chains, as shown in Figure 1-8. In a mixture of an achiral SmC host and a chiral dopant, the ordering of the dopant molecules in the SmC phase is modeled by a mean-field potential analogous to a binding site with a bent cylinder shape, as shown in Figure 1-9. Once in the binding

site, the sign of *Ps* can be predicted by conformational analysis of any structural unit combining a polar functional and stereogenic centre.

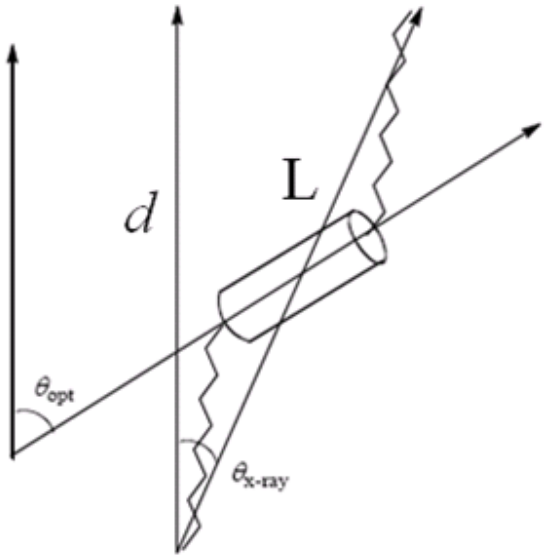

Figure 1-8: Schematic of the observed optical (θ_{opt}) and X-ray ($\theta_{x\text{-}ray}$) tilt angles. The core of SmC mesogens is more tilted than the side-chains.

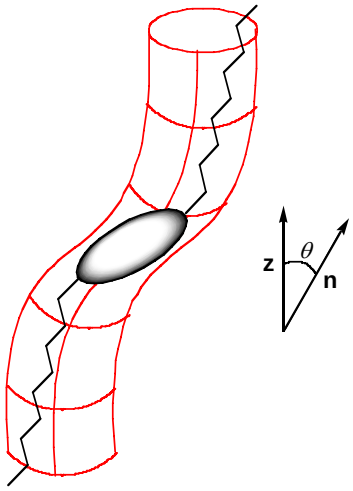

Figure 1- 9: Schematic of the binding site of SmC mesogens as described by the Boulder model.

For example, the analysis of the phenyl benzoate chiral dopant **1.7** based on Boulder Model is shown in Figure 1-10. According to the model, the molecule is constrained by the bent cylinder geometry and the alkyl chains are in all-*anti* conformations. Because there are several polar functional groups in this molecule, one must determine which one will contribute to the *Ps*. In the case of **1.7**, the decyloxy and ester groups cannot contribute to *Ps* because they are decoupled from the stereogenic center, and one should only consider the "stereopolar unit" formed by the stereogenic centre at C-2 and the ether group next to it. There are three possible conformations about the C_2-C_3 bond in the (*S*)-2-octyloxy side-chain, and they are shown in Figure 1-10 as Newman projections. Conformer I can be ignored because the alkoxy dipole lies in the tilt plane and does not contribute to *Ps*. The remaining conformers, II and III, show *Ps* of opposite signs. However, conformer II is the lowest energy conformer because the methyl group is *anti* relative to the alkyl chain. According to the physics convention, *Ps* should point to right and the sign is negative, which is consistent with experiments.[19]

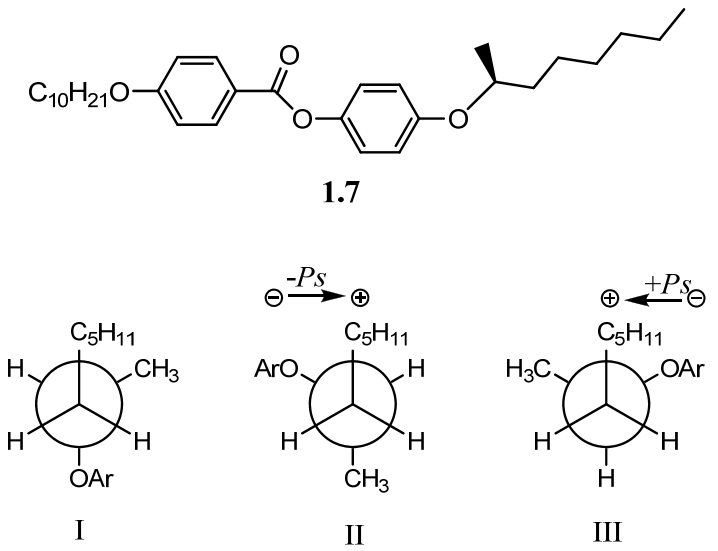

Figure 1-10: Conformational analysis of the (*S*)-2-octyloxy side-chain of the chiral phenyl benzoate dopant **1.7** confined to the SmC binding site according to the Boulder model. Newman projections are along the C_2-C_3 bond. The sign of P_s according to the physics convention points from negative to positive

1.3.4 Problems with SSFLC Technology

There are many advantages to SSFLCs such as fast switching time, bistability and high viewing contrast. However it is difficult to achieve uniform alignment that produces high contrast because the smectic layers usually shrink at the transition from the orthogonal SmA* phase to the tilted SmC* phase. In order to achieve good alignment between rubbed polyimide-coated glass slides, liquid crystal mixtures with a I-N-SmA*-SmC* sequence are slowly cooled from isotropic liquid down to the SmC* phase. Figure 1-11(a) shows the so-called bookshelf geometry of the SmA* phase aligned along the rubbering direction between two glass substrates in a display device. At the transition to the tilted

SmC* phase, the layers contract while the molecules are pinned at the surfaces. The resulting layer contraction in this confined geometry as the molecules tilt results in the layers buckling into the chevron geometry shown in Figure 1-11(b). In 1987, Rieker and coworkers confirmed the existence of these chevrons by experiments.[20] When the chevrons separate from each other in opposite directions, zigzag defects are produced as shown in Figure 1-12. The formation of chevrons and zigzags severely degrades the optical quality of SSFLC devices.

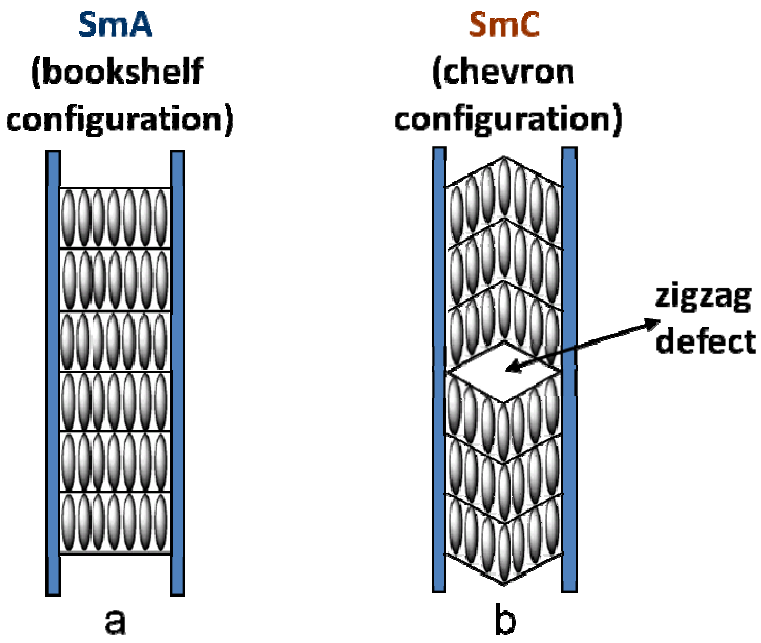

Figure 1-11: SmA* sample aligned between the glass substrates in the bookshelf configuration (a) transforms into the chevron configuration (b) when entering the SmC* phase.[21]

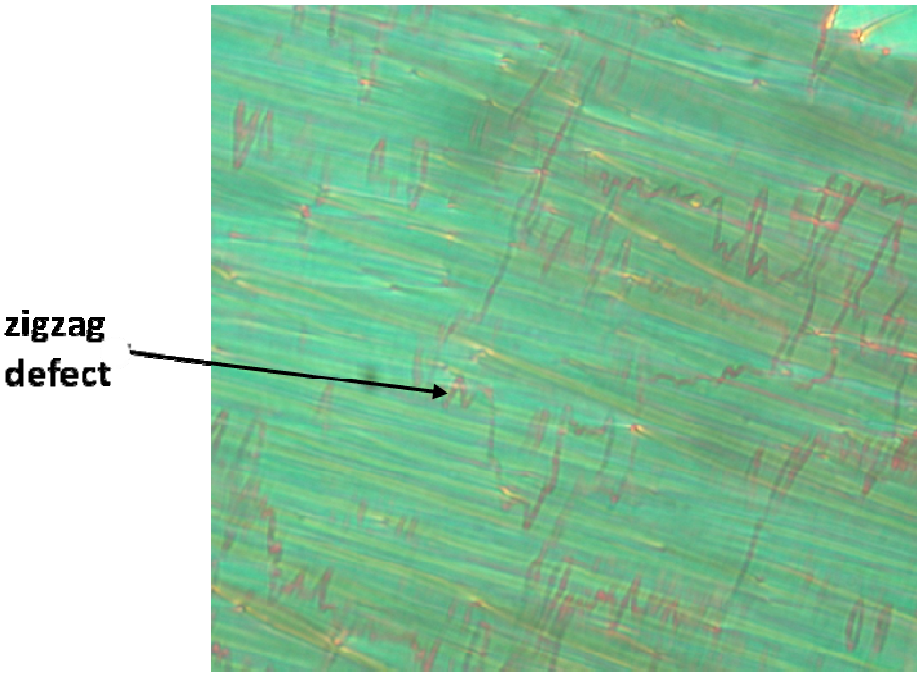

Figure 1-12: Example of zigzag defects in the SmC phase

1.4 de Vries-Like Materials

To solve the problem of chevron formation, research has focused on a new class of liquid crystal materials with little or no smectic layer contraction at the SmA-SmC transition, which are referred to as ‘de Vries-like’ materials. The transition from the SmA to SmC phase of these unusual materials is not well understood, but two models have been described to help understand their behavior. The description of any SmA–SmC phase transition may be found somewhere along a continuum between these two limiting cases, the classic rigid rod model and the diffuse cone model proposed by de Vries.

1.4.1 Classic Rigid Rod Model

As shown in Figure 1-13(a), molecules in the SmA phase are oriented along the director **n**. Upon transition to the SmC phase, the molecules tilt uniformly at an angle θ. The relationship between the layer spacing d_C and d_A is expressed by eq.1-3, and the layer contraction $(d_A - d_C)/d_A$ is a function of the tilt angle θ according to eq.1-4.

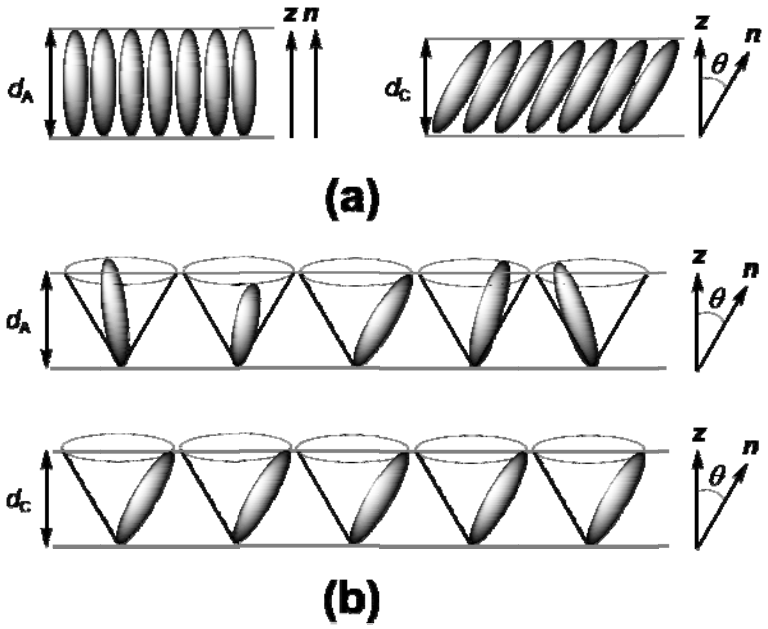

Figure 1-13: (a) Classic rigid rod model; (b) deVries Diffuse Cone Model.[22]

$$d_C = d_A \cos\theta \qquad \text{(eq. 1-3)}$$

$$(d_A - d_C)/d_A = 1 - \cos\theta \qquad \text{(eq. 1-4)}$$

1.4.2 De Vries Diffuse Cone Model

In 1979, de Vries proposed a tilted diffuse cone model to explain the minimal layer contraction of some unusual (de Vries-like) materials at the transition from SmA to SmC phase.[23] According to this model, the molecules in the SmA phase are tilted with a random azimuthal distribution, and the average orientation is along the layer normal **z**. Upon transition from the SmA to SmC phase, the molecules switch from a random to an ordered molecular tilt, as shown in Figure 1-13(b). In order to assign any decrease in layer contraction to an increase in 'de Vries' character based on the diffuse cone model, Radcliffe and coworkers defined the figure of merit *R*, which is used in the following chapters.[24] *R* is the ratio of the "chevron layer tilt angle" δ(T), which is the tilt angle required to give the layer contraction relative to the layer spacing $d(T_{AC})$ at the SmA-SmC transition temperature according to the rigid rod model, over the optical tilt angle $\theta_{opt}(T)$ measured by POM (eq. 1-6). According to this expression, the *R* value of ideal 'de Vries-like' materials should approach zero whereas that of a classic rigid rod material should approach 1. They also defined an expression for de Vries character that takes into account negative thermal expansion in the SmA phase (*i.e.* increase in layer spacing with decreasing temperature) (eq. 1-7). The "X-ray tilt angle" $\theta_{X\text{-}ray}(T)$ is the tilt angle required to give the layer contraction relative to $d_A(T)$ extrapolated into the SmC phase according to a least-squares fit of the data in the SmA phase (solid line in Figure

1-14).

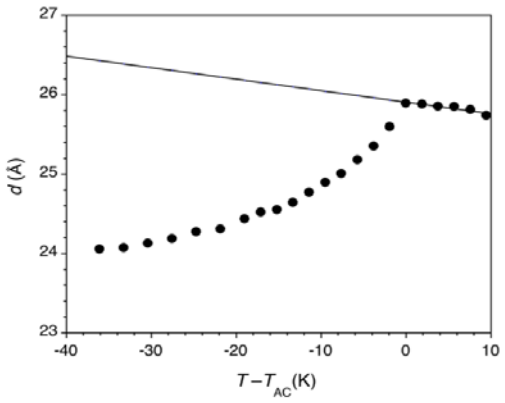

Figure 1-14: Smectic layer spacing *d* as a function of reduced temperature T-T_{AC}. The dashed line corresponds to the least-squares fit of the data points at T-$T_{AC} \geqslant 0$K.[24,25]

$$R = \delta(\mathrm{T})/\theta_{opt}(\mathrm{T}) = \cos^{-1}(d_C(\mathrm{T})/d(\mathrm{T_{AC}}))/\theta_{opt}(\mathrm{T}) \qquad \text{(eq. 1-6)}$$

$$\mathrm{f} = \theta_{Xray}(\mathrm{T})/\theta_{opt}(\mathrm{T}) = \cos^{-1}(d_C(\mathrm{T})/d_A(\mathrm{T}))/\theta_{opt}(\mathrm{T}) \qquad \text{(eq. 1-7)}$$

Recent studies demonstrated that calamitic materials with low orientational order and high lamellar order may exhibit de Vries-like behavior.[26-28] Moreover, Saunders and coworkers suggested that materials with 'de Vries-like' property will almost always follow the phase sequence *I*-SmA-SmC.[29] These are consistent with the fact that most 'de Vries-like' materials involve nanosegregating structural elements such as siloxane end-groups or partially fluorinated side-chains that strongly promote lamellar order and that the phase sequences of 'de Vries-like' materials normally exclude nematic phase (*vide infra*).[21]

1.4.3 Known "de Vries-Like" Materials

Although there is currently no rational design strategy for liquid crystals with "de Vries-like" properties, there are several known "de Vries-like" materials. In most "de Vries-like" materials, the layer spacing *d* increases with decreasing temperature in the SmA phase (negative thermal expansion).[21] This behavior, unlike that of normal thermal expansion behavior of solid, is likely due to an increase in orientational order and an increase in effective molecular length as the alkyl side-chains become more extended.

1.4.3.1 Nanosegregation

The use of oligomeric siloxane end-groups in conventional calamitic liquid crystals has been shown to promote the formation of smectic phases at the expense of nematic phases without increasing the viscosity dramatically.[9] It is because the siloxane end-groups are incompatible with both paraffinic and aromatic segments and therefore have a tendency to nanosegregate. In 1999, Coles and coworkers showed that although the alkene-terminated compound **1.8** is not liquid crystalline before attachment of the siloxane group, the organosiloxane derivative **1.9** exhibits liquid crystal properties above room temperature,[30] forming SmA and SmC phases. Siloxane end-groups are thought to form a "virtual siloxane backbone", which is shown schematically in Figure 1-16, and can be used to increase the miscibility of two incompatible molecules. In the Lemieux

group, Li's recent work demonstrated that the trisiloxane end-group does impart some 'de Vries' character based on a comparison of the parent compound **PhP1** with the siloxane-terminated analogue compound **1.10**[31] and two chiral siloxane-terminated analogue compound **E11** and **E6**.

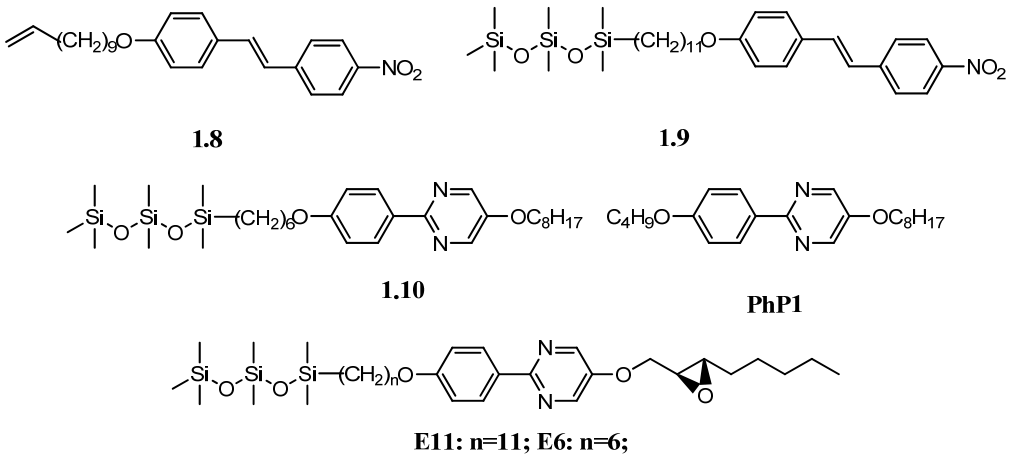

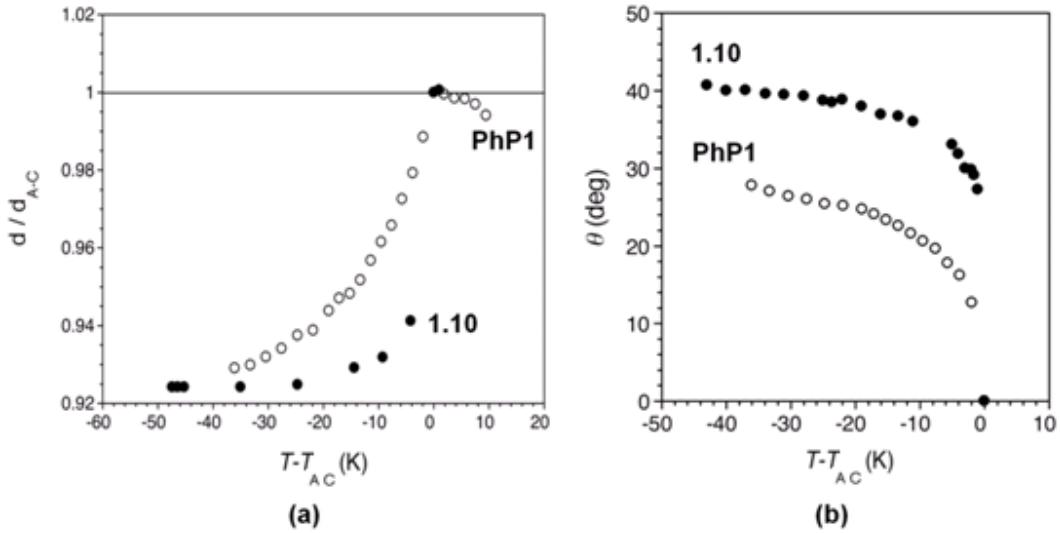

Figure 1-15: (a) Normalized smectic layer spacing d/d_{AC} versus reduced temperature $T\text{-}T_{AC}$ for compound **1.10**(●), **3.2**(○); (b) Optical tilt angle θ versus $T - T_{AC}$ of compound **1.10**(●), **3.2**(○);

As shown in Figure 1-15, the effect of siloxane end-group is not to reduce the layer

contraction but to increase tilt, therefore reducing *R*.

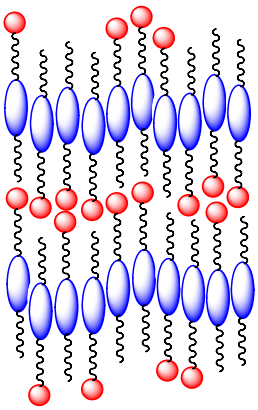

Figure 1-16: Representation of the segregation of siloxane groups (red ball) from the cores (blue ovals) and side chains (zigzag chain)

Semi-perfluorinated alkanes are the simplest class of molecules known to form a lamellar mesophase. The perfluorinated alkyl side chains can be used to promote smectic phases because of the fluorophobic effect.[9] Perfluoroalkanes are widely used as component(s) in FLC mixtures because they are very chemically stable and tend to have low viscosities.[9] In 1995, Reiker and coworker suggested that these materials organize in an anti-parallel structure, as shown in Figure 1-17, due to the large excluded volume of perfluorinated tails.[32] This offsets the lateral bulk and allows for efficient packing. Some of the best "de Vries-like" liquid crystals contain perfluorinated alkyl side chains. For instance, **3M 8422**, one of the top materials with de Vries-like properties has a maximum layer contraction of only 0.4%.[24]

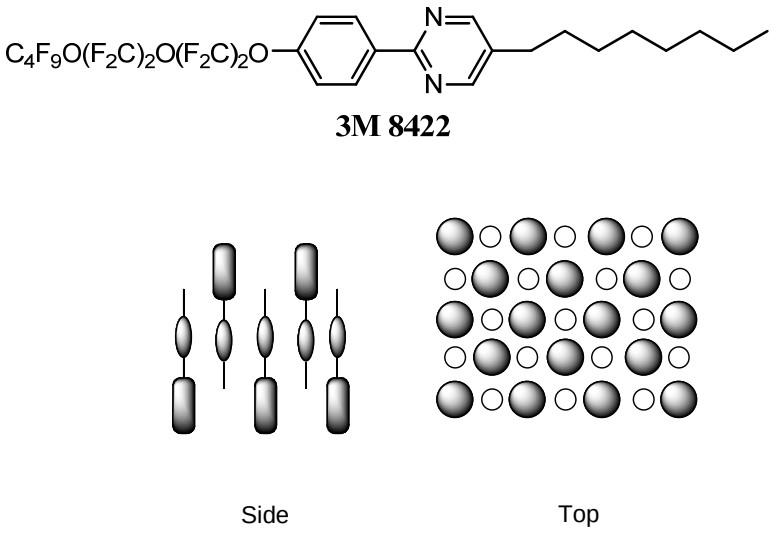

Figure 1-17: Representation of the antiparallel alignment of molecules with fluorinated alkyl side-chains. The cores (ovals) are aligned and the perfluorinated side-chains (blocks) invert orientation along smectic layer.

1.4.3.2 Alkyl Chain Length Effect

Previous work suggests that materials with de Vries-like properties tend to form SmA phases with broad temperature range. The stabilization of a SmA phase is normally observed in calamitic materials with a shortening of the alkyl side-chain. Hence, in order to search for a correlation between de Vries-like property and the alkyl chain length, Bezner and coworkers investigated the homologous series **nHL** (n=9, 10, 12) in 2007.[33] In this work, they showed that the temperature range of the SmA* phase decreases with increasing length of the nonchiral side chain by more than 50 K, as shown in Figure 1-18, and the range of smectic layer constraction decreases sharply with decreasing molecular length, as shown in Figure 1-19. This result suggests that the degree of smectic layer

contraction in the homologous series can change gradually and correlate with the temperature degree of SmA* phase. Because the smectic order parameter monotonically increases from the isotropic to SmA* transition point, the homologue with the broadest SmA* phase should have the highest smectic order at the transition point to SmC* phase, which is consistent with theoretical models.[28]

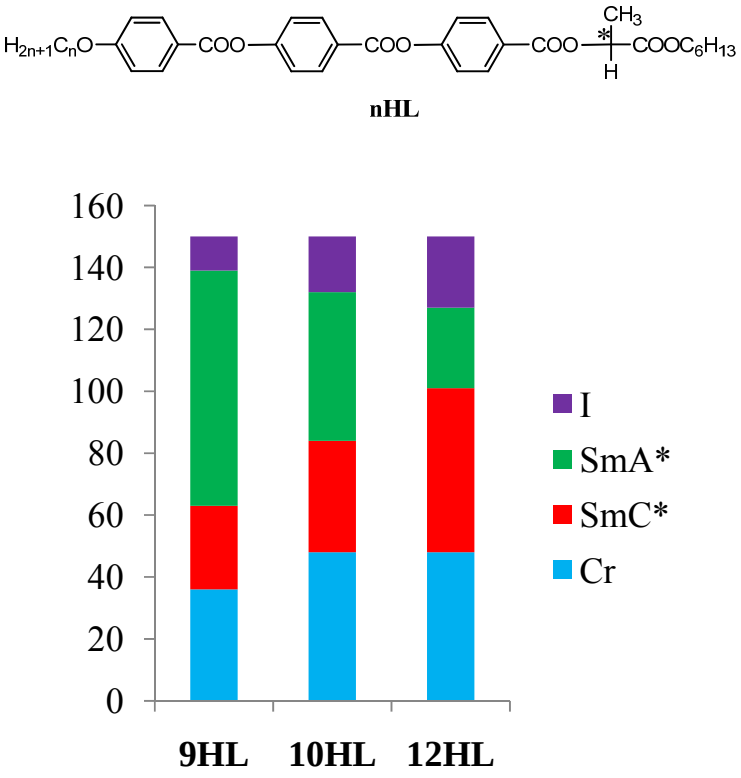

Figure 1-18: Phase sequences of ***n*HL** (*n*=9, 10, 12). With increasing molecular length the SmA* temperature range increases and the SmC* range decreases.

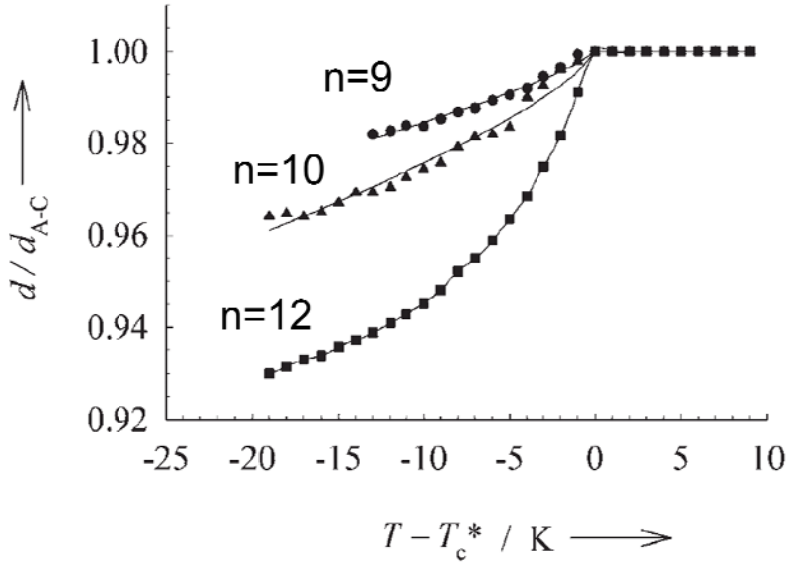

Figure 1-19: Relative layer contraction $d/d_{A\text{-}C}$ increases from **9HL** to **12HL** (taken from ref.33).

1.5 Design of "de Vries-like" Materials

1.5.1 SmA Promoting Elements

Previous work suggests that materials with de Vries-like properties tend to form SmA phases with a broad temperature range. In search of materials with small layer contraction, one should introduce a SmA phase promoting element in a liquid crystal molecule. In 2004, Hegmann and coworkers showed that a non-planar 5-phenylpyrimidine core is a SmA promoting element. A comparison of the phase sequences of **PhP1** and **5-PhP1** shows that the inclusion of a 5-phenylpyrimidine core results in the loss of N and SmC phases, and the formation of a broader SmA temperature ranges from 10 K to 33K.[34] A

recent report by Cowlings *et al.* also showed that the inclusion of a terminal halogen atom in the side-chain of a calamitic mesogen promotes the formation of a SmA phase.[35] In 2008, Goodby and coworkers showed the chloro end-group is a strong SmA promoter based on the comparison of the compound **1.11a** with the chloro-terminated analogue **1.11b**.[35]

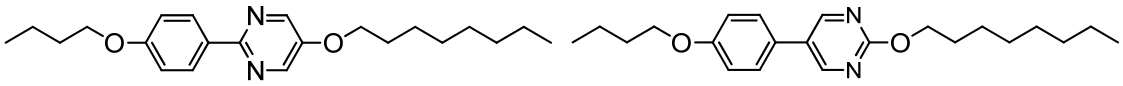

PhP1: Cr 58 SmC 85 SmA 95 N 98 I

5-PhP1: Cr 84 SmA 117 I

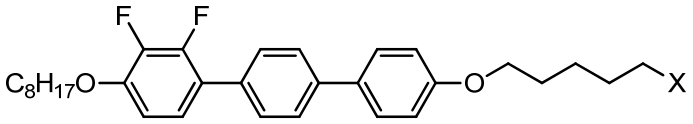

1.11a: X=H, Cr 93.5 SmC 144 SmA 148 N 159 I

1.11b: X=Cl, Cr 80.2 SmA 154.9 I

1.5.2 The Design Hypothesis for "de Vries-like" Materials

Previous work in the Lemieux group has shown that combining a trisiloxane-terminated alkyl chain, which is a SmC promoting element, and a chloro-terminated side chain, which is a SmA promoting element, in a liquid crystal molecule (**1.12a**) with a 2-phenylpyrimidine core results in a maximum layer contraction of only 1.6%.[31] This layer contraction is much smaller than that of its parent compound **PhP1** (7.1%) and led to the hypothesis that combining SmA and SmC phase promoters in the same molecule

could increase the de Vries character. To validate this hypothesis, Jeff Roberts synthesized and characterized the mesogen **1.12b** with a trisiloxane-terminated alkyl side-chain (SmC promoter) and 5-phenylpyrimidine core (SmA promoter).[36] The result showed that the layer contraction of **1.12b** is much smaller than that of its parent compound **PhP1**. By comparison to the parent compound, the large difference between *R* and f for **1.12a** and **1.12b** suggest that their de Vries-like behavior may be attributed in part to a significant negative thermal expansion in the SmA phase that persists in the SmC phase. This behavior was also observed with the de Vries-like material **3M8422**.

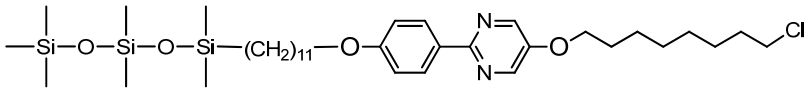

1.12a Cr 48 SmC 89 SmA 98 I

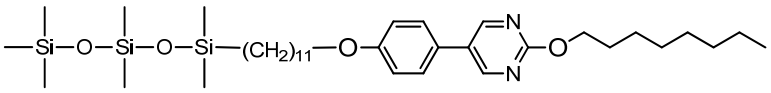

1.12b Cr 66 SmC 76 SmA 80 I

Table 1-1: Smectic layer spacings and figures of merit *R* and *f* at $T-T_{AC} = -10$ K.

Compounds	d_C(Å)	d_A(Å)	$d(T_{AC})$(Å)	*R*	*f*
PhP1[37]	24.8	26.0	25.9	0.80	0.83
1.12a[31]	47.7	49.4	48.5	0.43	0.63
1.12b[36]	40.8	43.1	41.2	0.23	0.54
3M 8422[24]	31.7	32.3	31.8	0.18	0.44

1.6 Project Outline

The aim of this project is to further test the design strategy for the purpose of developing liquid crystals with more "de Vries-like" properties by studying homologous series of the trisiloxane-terminated mesogens **1.13a~e** and **1.14a~e** with 2-phenylpyrimidine cores and chloro terminated side chains, and test the hypothesis that *R* should decrease with a broadening of the SmA range. Another aspect of this project is to prepare two trisiloxane-terminated mesogens **1.15** and **1.16** with chloro-terminated chiral epoxy side-chains to look at effect of a Cl terminal group in chiral mesogens.

The first section of this thesis describes the synthesis of two homologous series of liquid crystals and their characterization by polarized microscopy, DSC and Small angle X-ray Scattering (SAXS). The second section describes the synthesis of chiral compounds **1.15** and **1.16**, their characterization by polarized microscopy, DSC and SAXS, and measurement of their ferroelectric properties.

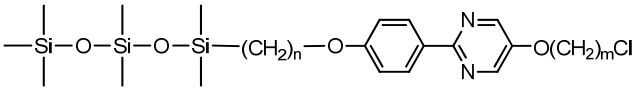

1.13, n=11: **a**, m=4; **b**, m=5; **c**, m=6; **d**, m=7; **e**, m=10
1.14, n=6 : **a**, m=4; **b**, m=5; **c**, m=6; **d**, m=7; **e**, m=10

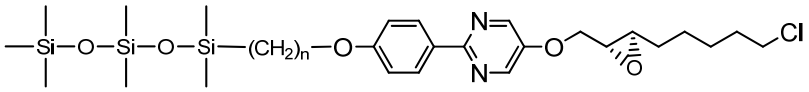

1.15: n=11; **1.16:** n=6

1.7 References

(1) Reinitzer, F. *Monatsh. Chem.* **1888**, *9*, 421.

(2) Link, D. R.; Natale, G.; Shao, R.; Maclennan, J. E.; Clark, N. A.; Korblova, E.; Walba, D. M. *Science (Washington, D. C.)* **1997**, *278*, 1924-1927.

(3) Gray, G. W.; Goodby, J. W. *Smectic Liquid Crystals: Textures and Structures*, 1984.

(4) McMillan, W. L. *Phys. Rev. A* **1973**, *8*, 1921-1929.

(5) Goodby, J. W.; Gray, G. W.; McDonnell, D. G. *Mol. Cryst. Liq. Cryst.* **1977**, *34*, 183-188.

(6) Wulf, A. *Phys. Rev. A* **1975**, *11*, 365-375.

(7) Bartolino, R.; Doucet, J.; Durand, G. *Ann. Phys. (Paris)* **1978**, *3*, 389-395.

(8) Jang, W. G.; Glaser, M. A.; Park, C. S.; Kim, K. H.; Lansac, Y.; Clark, N. A. *Phys. Rev. E: Stat., Nonlinear, Soft Matter Phys.* **2001**, *64*, 051712/1-051712/12.

(9) Tschierske, C. *J. Mater. Chem.* **1998**, *8*, 1485-1508.

(10) Meyer, R. B.; Liebert, L.; Strzelecki, L.; Keller, P. *J. Phys. (Paris), Lett.* **1975**, *36*, L69-L71.

(11) Clark, N. A.; Lagerwall, S. T. *Appl. Phys. Lett.* **1980**, *36*, 899-901.

(12) Kuczynski, W.; Stegemeyer, H. *Chem. Phys. Lett.* **1980**, *70*, 123-126.

(13) Siemensmeyer, K.; Stegemeyer, H. *Chem. Phys. Lett.* **1988**, *148*, 409-412.

(14) Walba, D. M.; Slater, S. C.; Thurmes, W. N.; Clark, N. A.; Handschy, M. A.; Supon, F. *J. Am. Chem. Soc.* **1986**, *108*, 5210-5221.

(15) Walba, D. M. *Adv. Synth. React. Solids* **1991**, *1*, 173-235.

(16) Samulski, E. T.; Dong, R. Y. *J. Chem. Phys.* **1982**, *77*, 5090-5096.

(17) Samulski, E. T. *Isr. J. Chem.* **1983**, *23*, 329-339.

(18) Bryan, R. F.; Leadbetter, A. J.; Mehta, A. I.; Tucker, P. A. *Mol. Cryst. Liq. Cryst.* **1984**, *104*, 257-264.

(19) Wand, M. D.; Vohra, R.; Walba, D. M.; Clark, N. A.; Shao, R. *Mol. Cryst. Liq. Cryst.* **1991**, *202*, 183-192.

(20) Rieker, T. P.; Clark, N. A.; Smith, G. S.; Parmer, D. S.; Sirota, E. B.; Safinya, C. R. *Phys. Rev. Lett.* **1987**, *59*, 2658-2661.

(21) Lagerwall, J. P. F.; Giesselmann, F. *ChemPhysChem* **2006**, *7*, 20-45.

(22) de Vries, A. *J. Chem. Phys.* **1979**, *70*, 2705-2709.

(23) de Vries, A. *Mol. Cryst. Liq. Cryst.* **1977**, *41*, 27-31.

(24) Radcliffe, M. D.; Brostrom, M. L.; Epstein, K. A.; Rappaport, A. G.; Thomas, B. N.; Shao, R.; Clark, N. A. *Liq. Cryst.* **1999**, *26*, 789-794.

(25) Takanishi, Y.; Ouchi, Y.; Takezoe, H.; Fukuda, A.; Mochizuki, A.; Nakatsuka, M. *Jpn. J. Appl. Phys., Part 2* **1990**, *29*, L984-L986.

(26) Gorkunov, M. V.; Osipov, M. A.; Lagerwall, J. P. F.; Giesselmann, F. *Phys. Rev. E: Stat., Nonlinear, Soft Matter Phys.* **2007**, *76*, 051706/1-051706/16.

(27) Gorkunov, M. V.; Giesselmann, F.; Lagerwall, J. P. F.; Sluckin, T. J.; Osipov, M. A. *Phys. Rev. E: Stat., Nonlinear, Soft Matter Phys.* **2007**, *75*, 060701/1-060701/4.

(28) Saunders, K. *Phys. Rev. E: Stat., Nonlinear, Soft Matter Phys.* **2008**, *77*, 061708/1-061708/13.

(29) Saunders, K.; Hernandez, D.; Pearson, S.; Toner, J. *Phys. Rev. Lett.* **2007**, *98*, 197801/1-197801/4.

(30) Shoosmith, D.; Carboni, C.; Perkins, S.; Meyer, S.; Coles, H. J. *Mol. Cryst. Liq. Cryst. Sci. Technol., Sect. A* **1999**, *331*, 2041-2048.

(31) Li, L.; Jones, C. D.; Magolan, J.; Lemieux, R. P. *J. Mater. Chem.* **2007**, *17*, 2313-2318.

(32) Rieker, T. P.; Janulis, E. P. *Phys. Rev. E: Stat. Phys., Plasmas, Fluids, Relat. Interdiscip. Top.* **1995**, *52*, 2688-2691.

(33) Bezner, S.; Krueger, M.; Hamplova, V.; Glogarova, M.; Giesselmann, F. *J. Chem. Phys.* **2007**, *126*, 054902/1-054902/6.

(34) Hegmann, T.; Meadows, M. R.; Wand, M. D.; Lemieux, R. P. *J. Mater. Chem.* **2004**, *14*, 185-190.

(35) Goodby John, W.; Saez Isabel, M.; Cowling Stephen, J.; Gortz, V.; Draper, M.; Hall Alan, W.; Sia, S.; Cosquer, G.; Lee, S.-E.; Raynes, E. P. *Angew. Chem., Int. Ed.* **2008**, *47*, 2754-2787.

(36) Roberts, J. C.; Kapernaum, N.; Giesselmann, F.; Lemieux, R. P. *J. Am. Chem. Soc.* **2008**, *130*, 13842-13843.

(37) Hartley, C. S.; Kapernaum, N.; Roberts, J. C.; Giesselmann, F.; Lemieux, R. P. *J. Mater. Chem.* **2006**, *16*, 2329-2337.

(38) Spector, M. S.; Heiney, P. A.; Naciri, J.; Weslowski, B. T.; Holt, D. B.; Shashidhar, R. *Phys. Rev. E* **2000**, *61*, 1579-1584.

Chapter 2. Siloxane-terminated 2-Phenylpyrimidine Liquid Crystal Hosts with Chloro End-groups

2.1 Syntheses

All siloxane-terminated phenylpyrimidine liquid crystals were prepared by sequential alkylations of 2-(4-hydroxyphenyl)-5-pyrimidinol (**2.3**). As shown in Scheme 2-1, the siloxane-terminated alcohols **2.1** and **2.2** were prepared from 10-undecen-1-ol and 5-hexen-1-ol, respectively, via a platinum-catalyzed hydrosilation reaction using 1,1,1,3,3,5,5-heptamethyltrisiloxane and Karstedt's catalyst in 70-75% yield. The synthesis of compounds **1.13a~e** and **1.14a~e** began with the selective alkylation of **2.3** with chloro-terminated alcohols via a Mitsunobu reaction to give the 2-(4-hydroxyphenyl)-5-chloroalkoxy-pyrimidine precursors **2.4a~e** in 47-54% yield, and then combined with **2.1** or **2.2** via another Mitsunobu reaction to give **1.13a~e** and **1.14a~e** in yields ranging from 45 to 50% (Scheme 2-2). Prior to characterization of these compounds as liquid crystal materials, they were recrystallized from ethanol three times after filtration through a 0.45 μm PTFE filter.

Scheme 2-1:

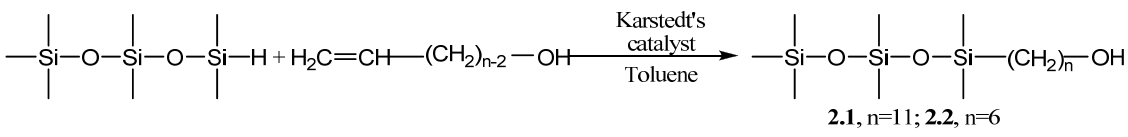

Scheme 2-1[a]**:**

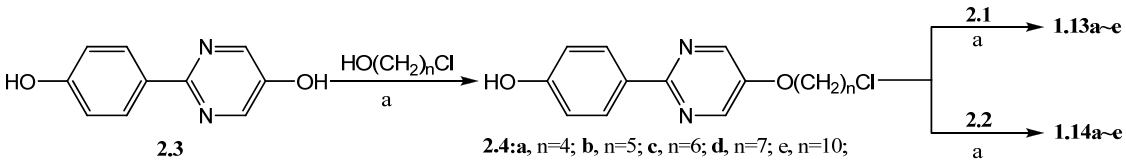

2.3 **2.4:a**, n=4; **b**, n=5; **c**, n=6; **d**, n=7; e, n=10;

Reagent and condition: (a) DIAD, PPh_3, THF, rt., overnight

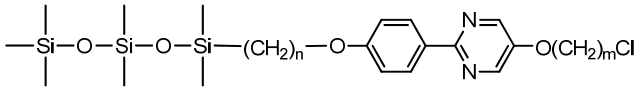

1.13, n=11: **a**, m=4; **b**, m=5; **c**, m=6; **d**, m=7; **e**, m=10
1.14, n=6 : **a**, m=4; **b**, m=5; **c**, m=6; **d**, m=7; **e**, m=10

2.2 Mesophase Characterization

The mesophases formed by compounds **1.13a~e** and **1.14a~e** were characterized by polarized optical microscopy (POM) and differential scanning calorimetry (DSC). All compounds in series **1.13a~e** and **1.14a~e** form SmA and SmC phases on heating and cooling (Figure 2-1), as shown by the characteristic fan and homeotropic textures of the SmA phase that turn into the broken fan and Schlieren textures of the SmC phase, respectively. We also observed significant changes in interference colors in the fan/broken fan textures of these compounds upon cooling from the SmA to the SmC phase (see Figure 2-2a and Figure 2-2b, for example). These color changes indicate an increase in birefringence due to the increase of orientational order that is expected for de Vries-like materials upon SmA-SmC transition.[1]

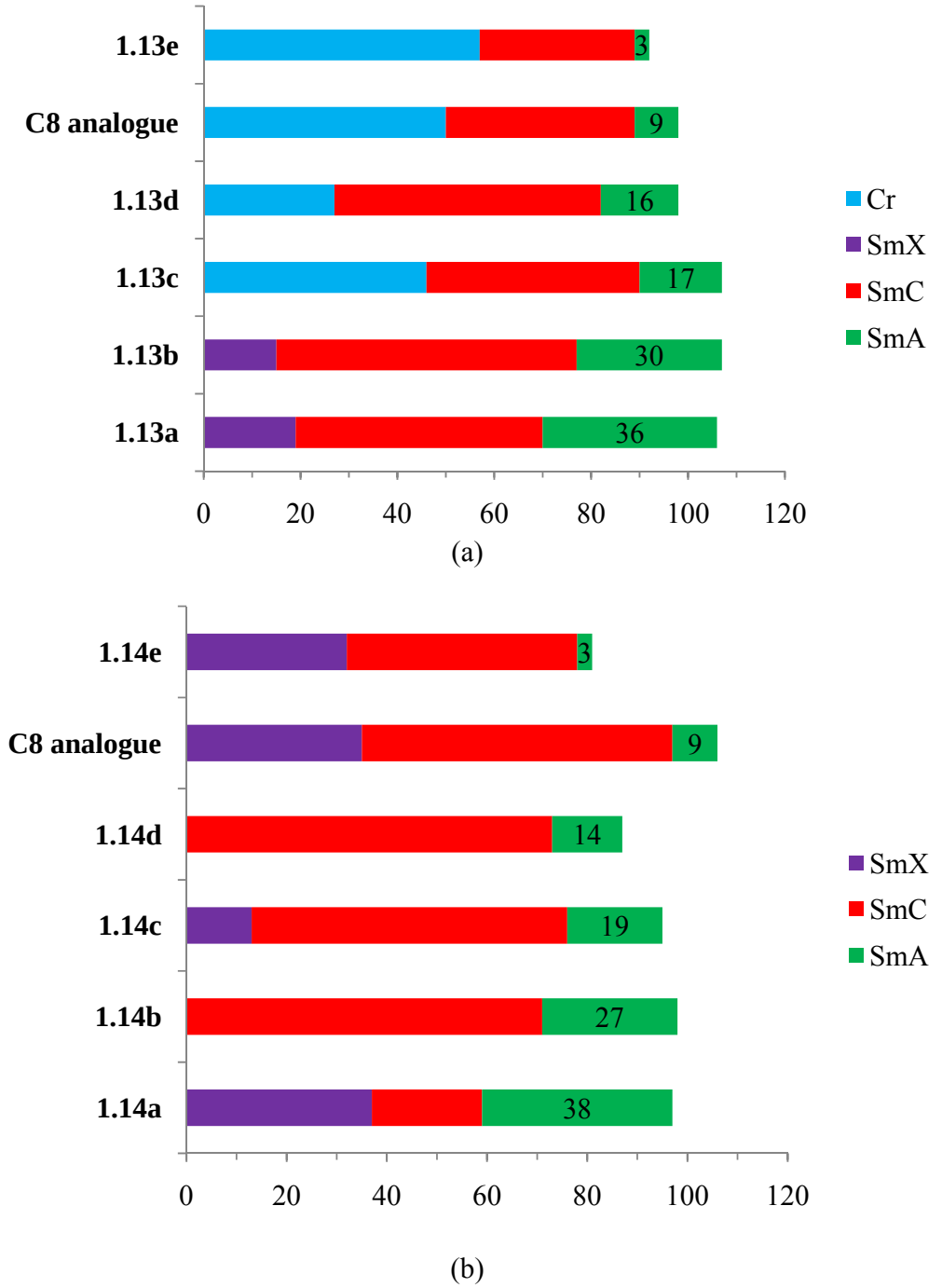

Figure 2-1: Phase transition temperatures for series (a) **1.13** and (b) **1.14** measured by DSC on heating at a rate of 5 K /min (SmA-SmC transition temperatures were measured by POM). Light blue: Cr; purple: SmX; red: SmC; green: SmA. The data for the C_8 analogue are taken from ref. 2 and the number on the bar is the temperature range of SmA phase.

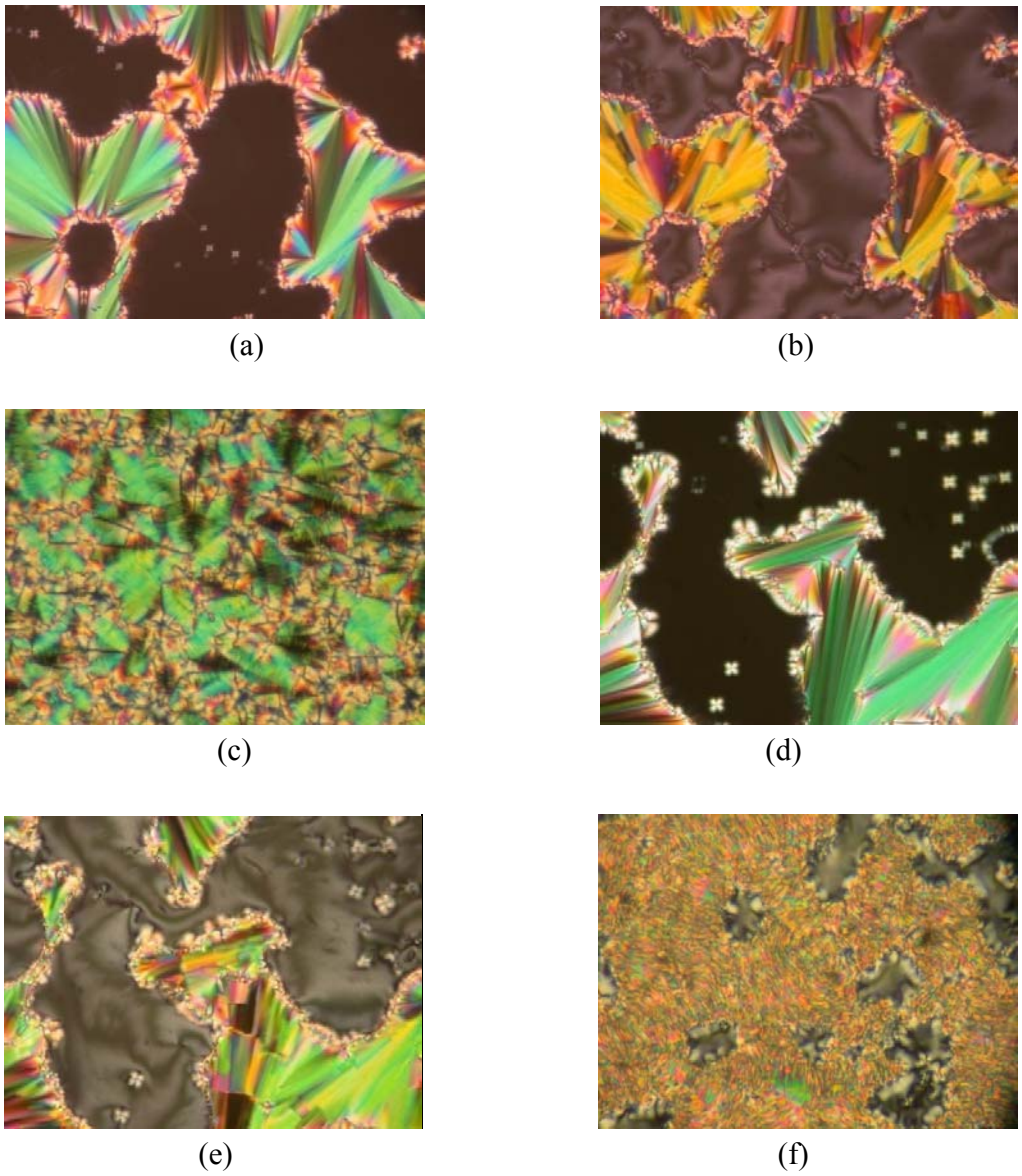

Figure 2-2: Polarized photomicrographs of compounds **1.13c** and **1.14c** between untreated glass slide and cover slip (500×) (a) compound **1.13c** in the SmA phase at T -T_{AC}=5 K, (b) compound **1.13c** in the SmC phase at T -T_{AC}=-5 K, (c) compound **1.13c** in the Cr phase (d) compound **1.14c** in the SmA phase at T -T_{AC}=5 K and (e) compound **1.14c** in the SmC phase at T -T_{AC}=-5 K, (f) compound **1.14c** in the SmX phase.

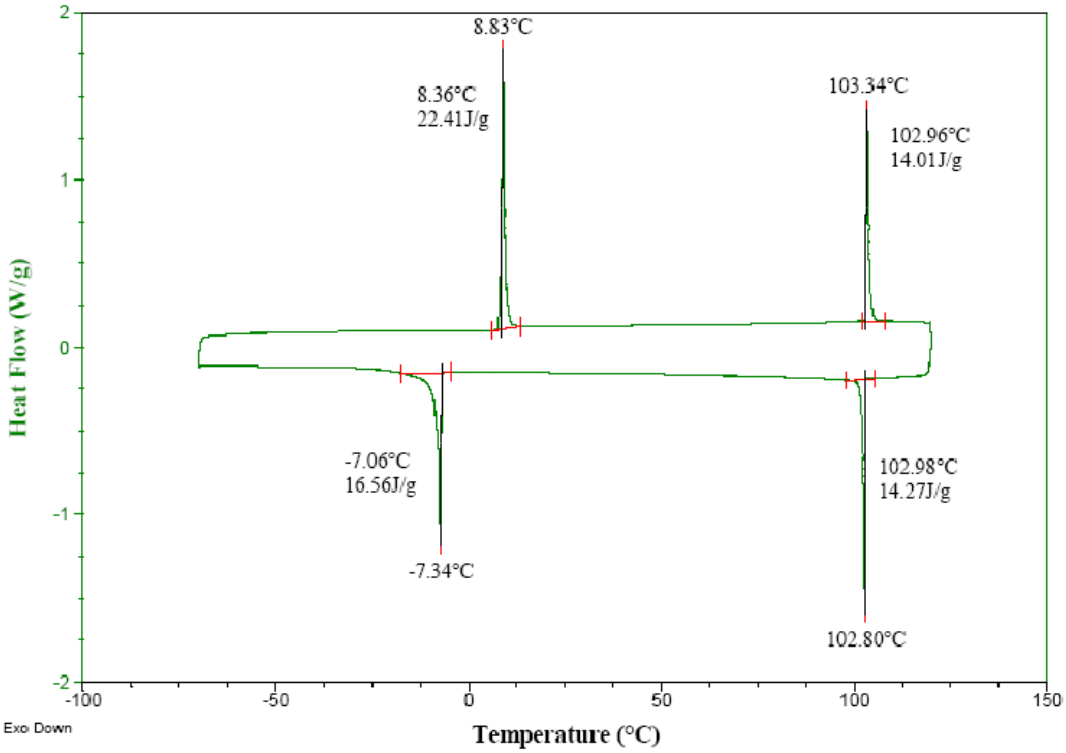

Figure 2-3: DSC profile for compound **1.13b** taken at a scan rate of 5K/min.

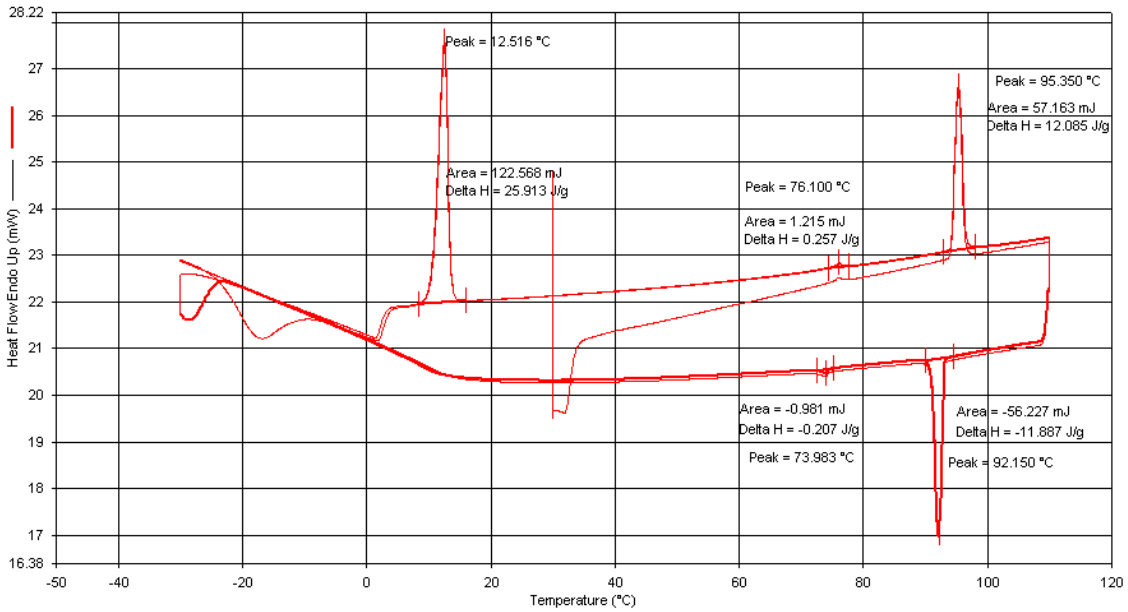

Figure 2-4: DSC profile for compound **1.14c** taken at a scan rate of 5K/min

In addition, DSC and POM analyses suggest that compounds **1.13a**~**b** and **1.14** form an unidentified higher order SmX phase below the SmC phase, and do not crystallize at temperatures as low as –80 °C. The assignment of a SmX phase is based on the low enthalpies of the SmX-SmC transitions for **1.14a~e, 1.13a** and **1.13b** (11-21 kJ/mol) relative to those of the Cr-SmC transitions for the higher homologues (37-62 kJ/mol), and the observation of recrystallization exotherms on heating the higher homologues before the Cr-SmC transitions. As shown in Figure 2-1, increasing the length of the non-siloxane side-chain in **1.13a~e** and **1.14a~e** results in a gradual decrease of the SmA temperature range (from 36 to 3 K in **1.13a~e** and from 37 to 3 K in **1.14a~e**), which is consistent with normally observed trends.[3] Furthermore, the Cr/SmX-SmC transition point shows the expected odd-even effect in **1.13a~e** and **1.14a~e**. The liquid crystal temperature ranges are generally same in series **1.13a~e** and **1.14a~e** with the same length of the non-siloxane side-chain, and the homologues **1.13a~b** and **1.14a~d** are mesogenic in the SmC phase at room temperature.

As shown in Table 2-1, in both series, the increase in enthalpy change for the SmA-SmC phase transition (ΔH_{AC}) increase with increasing alkoxy chain length (from < 0.1 kJ/mol to 0.5 kJ/mol in **1.13a~e** and from <0.1 kJ/mol to 0.29 kJ/mol in **1.14a~e**). The SmA-SmC phase transition is undetectable by DSC except for some homologues **1.13e**, **1.14c**, **1.14d** and **1.14e**, and the corresponding peak temperature in those cases does not show any significant hysteresis, which is inconsistent with a first-order transition.

Table 2-1: Transition temperatures (^{o}C) and enthalpies of transitions ΔH^{0} (kJ/mol, in parentheses) for compounds **1.13** and **1.14**.

Cpd	Cr(●)/SmX(▲)		SmC		SmA		I
1.13a	▲	19(11.4)	●	69(<0.1)	●	105(7.4)	●
1.13b	▲	9(14.9)	●	77(<0.1)	●	103(9.3)	●
1.13c	●	47(53.2)	●	84(<0.1)	●	107(9.4)	●
1.13d	●	26(36.9)	●	84(<0.1)	●	98(9.1)	●
1.13e	●	57(61.6)	●	89(0.5)	●	92(10.4)	●
1.14a	▲	37(15.6)	●	58(<0.1)	●	97(5.3)	●
1.14b	▲	0(13.5)	●	71(<0.1)	●	98(6.5)	●
1.14c	▲	13(15.7)	●	76(0.13)	●	95(7.36)	●
1.14d	▲	4(19.1)	●	69(0.18)	●	88(7.26)	●
1.14e	▲	32(21.3)	●	78(0.29)	●	81(9.94)	●

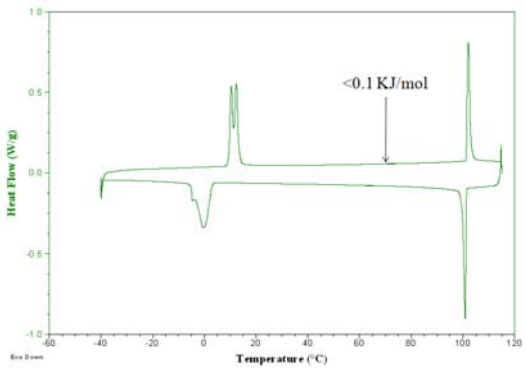

1.13a

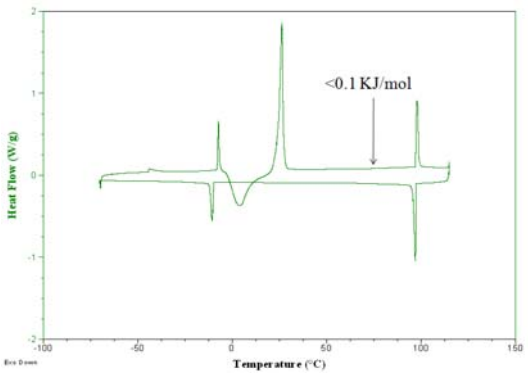

1.13d

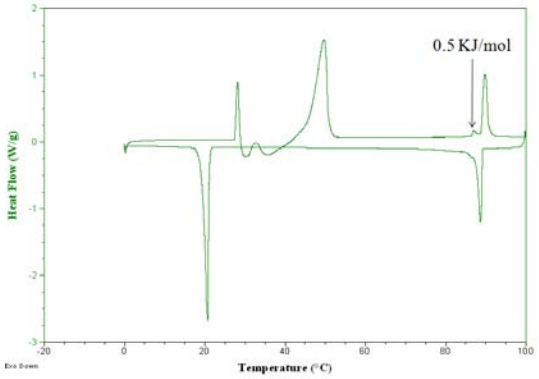

1.13e

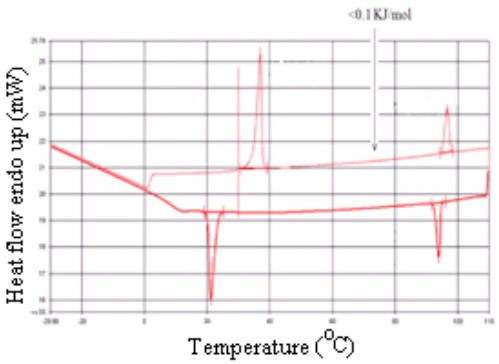

1.14a

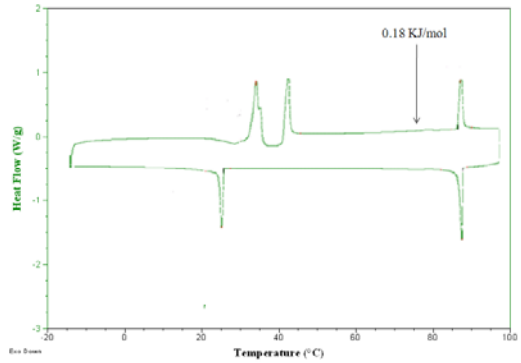

1.14d

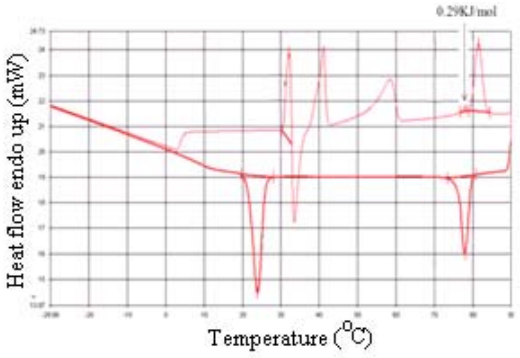

1.14e

Figure 2-5: DSC traces of compounds **1.13a, 1.13d, 1.13e, 1.14a, 1.14d** and **1.14e** showing the SmC-SmA and SmA-I phase transitions on heating and cooling, and the enthalpy change for the SmA-SmC phase transition (ΔH_{AC}) in kJ/mol.

2.3 Optical tilt angle measurements

Optical tilt angles (θ_{opt}) in the SmC phase were measured as a function of reduced temperature by POM by applying a field of 10V across surface-stabilized FLC films (4 μm) in ITO glass cells with rubbed Nylon alignment layers using liquid crystal samples doped with the chiral additive **2.5** (1-2 mol%).[4] In both series **1.13** and **1.14**, the optical tilt angle increases with the length of the non-siloxane side-chain, which is also consistent with normally observed trends.[3] At $T–T_{AC} = –10$ K, θ_{opt} increases from 14° to 24° for **1.13**, and from 23° to 43° for **1.14** (Figure 2-6). Since the tilt angle is the primary

order parameter describing the SmA-SmC phase transition, the temperature variation of θ is described according to the power law:

$$\theta \propto | T–T_{AC} |^{\beta} \qquad \text{(eq. 2-1)}$$

where β is the order parameter exponent related to the nature of the phase transition.[5] According to the generalized mean-field theory of phase transitions (Landau theory), a β value of 0.5 is expected in the case of a pure second-order transition, whereas a β value of 0.25 is expected in the case of a second-order transition approaching the crossover (tricritical) point from second- to first-order transition.[6,7] The plots of θ_{opt} vs $| T–T_{AC} |$ for two groups, as shown as Figure 2-7, are compared to the best fits to eq. 2-1. These fits give β values of 0.21, 0.22 and 0.14 in series **1.13** and 0.21, 0.19 and 0.17 in series **1.14**, respectively, which are consistent with the ΔH_{AC} measurements and suggest that the SmA-SmC phase transitions in this series are tricritical but do not crossover to a first-order transition.

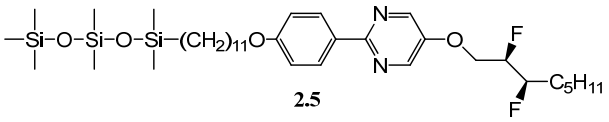

2.5

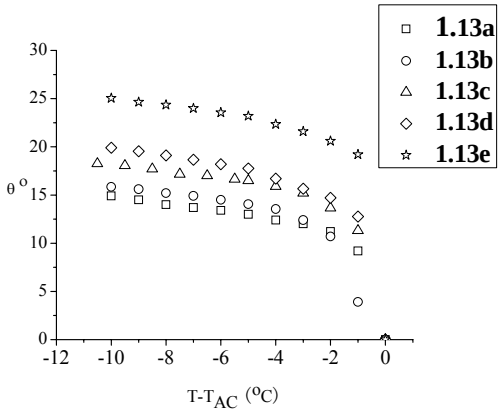

(a)

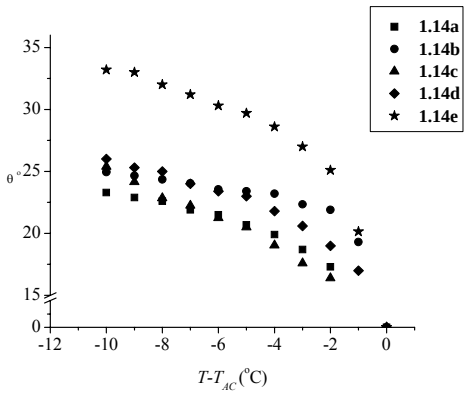

(b)

Figure 2-6: Optical tilt angle θ versus $T - T_C$ of **1.13**(a) and **1.14**(b).

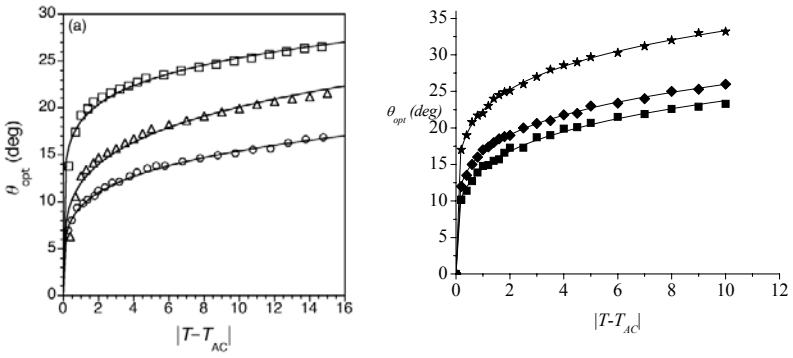

(a) (b)

Figure 2-7: Optical tilt angles (θ_{opt}) vs reduced temperature for (a) compounds **1.13a** (○), **1.13d** (△) and **1.13e** (□) (b) compounds **1.14a** (■), **1.14d** (◆) and **1.14e** (★)

2.4 'de Vries' Character

Accurate measurements of smectic layer spacings (d) as a function of temperature were carried out by small-angle X-ray scattering (SAXS). As shown in Figure 2-8a, the d/d_{AC} vs $T–T_{AC}$ profiles for series **1.13** are qualitatively similar and show a negative thermal expansion in the SmA phase that persists in the SmC phase to such an extent that the layer spacing in the SmC phase (d_C) exceeds the spacing at the SmA-SmC transition (d_{AC})

at reduced temperatures as high as –20 K. The maximum layer contraction increases with the length of the chloroalkoxy side-chain, from 0.5% for **1.13a** to 1.5% for **1.13e**, which correlates with the increase in θ_{opt}. The d/d_{AC} vs $T–T_{AC}$ profiles for series **1.14** show a negative thermal expansion in the SmA but not in the SmC phase (Figure 2-8b). The profiles in the SmC phase for the lower homologues **1.14a** show a maximum layer contraction of 1.7%, which progressively increases with increasing alkoxy chain length to 3.4% with **1.14e**. Although the maximum layer contractions measured for the **1.14** series upon SmA-SmC phase transition are much bigger than those of **1.13**, this difference can be accounted for, to some extent, by the higher tilt angles formed by **1.14**. This is reflected by a smaller difference in R values. As shown in Table 2-2, the R values in series **1.13** range from 0.34 to 0.47 at $T–T_{AC} = –10$ K, whereas the R values in series **1.14** range from 0.44 to 0.53.

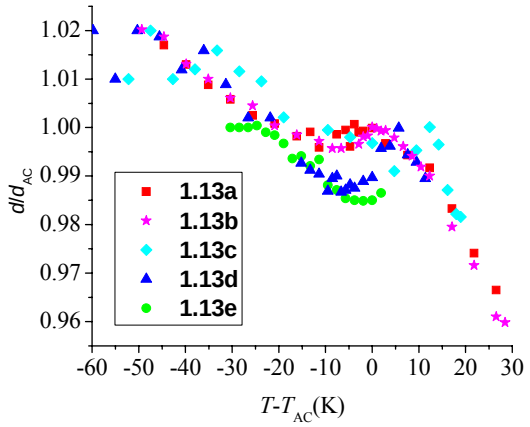

(a)

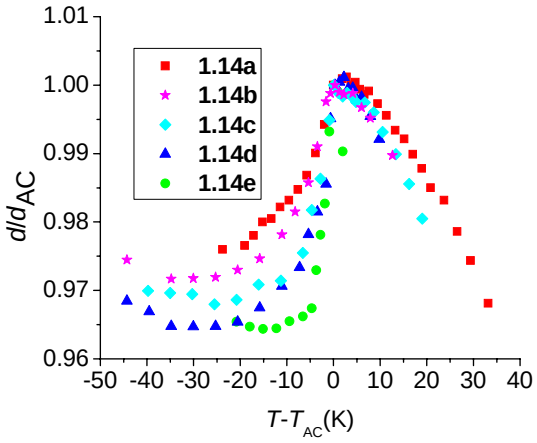

(b)

Figure 2-8: Normalized smectic layer spacing d/d_{AC} versus reduced temperature $T\text{-}T_{AC}$ for compound **1.13** and **1.14**

Table 2-2: Liquid crystal smectic layer spacings at the SmA*–SmC* transition ($d(T_{AC})$) and in the SmC* phase at T-T_{AC}=-10 K (d_C), tilt angles, and figures of merit R at T-T_{AC}=-10 K.

Cpd	$d(T_{AC})$/Å[a]	d_C/Å[a]	Maximum Layer Contraction	θ_{opt}/deg	R	SmA Temperature range (K)
1.13a	44.7	44.5	0.50%	15	0.38	36
1.13b	44.8	44.6	0.50%	16	0.36	30
1.13c	45.0	44.6	0.90%	18	0.43	17
1.13d	45.3	44.7	1.30%	20	0.46	16
1.13e	47.3	44.6	1.50%	25	0.40	3
1.14a	37.6	36.9	1.78%	23	0.47	38
1.14b	38.2	37.4	2.17%	25	0.48	27
1.14c	38.5	37.4	2.85%	25	0.54	19
1.14d	38.8	37.6	2.94%	26	0.52	14
1.14e	40.8	39.4	3.41%	33	0.48	3

[a] Error is ±0.1Å

2.5 Conclusions

In both series of liquid crystal materials, shortening the length of the alkyl chain linker between the terminal chloro group and the phenylpyrimidine core resulted in a broader SmA phase range. As shown in Table 2-2, the increase in SmA temperature range does correlate with a decrease in maximum layer contraction, as was observed by Giesselmann *et al.* for the homologous series **nHL**. However, tilt angle measurements and corresponding *R* values indicate that there is no correlation between SmA temperature range and de Vries-like behavior. Indeed, the increase in layer contraction can be accounted for by the increase in tilt angle. Nevertheless, the *R* values for both series are smaller than that of the parent compound **PhP1**, which supports our design strategies based on combining SmA and SmC-promoting elements. Evidence provided by DSC and tilt angle measurements also suggest that the SmA-SmC frustration in both series is near the crossover point between second order and first order, which is consistent with the expected behavior of mesogens with high lamellar order and low orientational order,[8] a requirement for de Vries-like behavior. However, neither series may be considered true de Vries-like with *R* values typically no more than 0.20.

2.6 References

(1) Lagerwall, J. P. F.; Giesselmann, F. *ChemPhysChem.* **2006**, *7*, 20-45.

(2) Li, L.; Jones, C. D.; Magolan, J.; Lemieux, R. P. *J. Mater. Chem.* **2007**, *17*, 2313-2318.

(3) Hartley, C. S.; Kapernaum, N.; Roberts, J. C.; Giesselmann, F.; Lemieux, R. P. *J. Mater. Chem.* **2006**, *16*, 2329.

(4) Roberts, J. C.; Kapernaum, N.; Giesselmann, F.; Wand, M. D.; Lemieux, R. P. *J. Mater. Chem.* **2008**, *18*, 5301-5306.

(5) Chandrasekhar, S. *Liquid Crystals*; 2nd ed.; Cambridge University Press: Cambridge, 1992.

(6) Birgeneau, R. J.; Garland, C. W.; Kortan, A. R.; Litster, J. D.; Meichle, M.; Ocko, B. M.; Rosenblatt, C.; Yu, L. J.; Goodby, J. *Phys. Rev. A* **1983**, *27*, 1251.

(7) Landau, L. D. *Statistical Physics*; 3rd ed.; Pergamon Press: Oxford, 1980.

(8) Saunders, K.; Hernandez, D.; Pearson, S.; Toner, J. *Phys. Rev. Lett.* **2007**, *98*, 197801/1-197801/4.

Chapter 3. Chiral Siloxane-Terminated 2-Phenylpyrimidine Dopants

As mentioned in Chapter 2, the addition of a chloro end-group on the side chain of an achiral 2-phenylpyrimidine mesogen notably reduces layer contraction upon transition from the SmA to the SmC phase, and that layer contraction may be tuned by changing the alkyl chain length. In the best case (**1.13b**), the maximum layer contraction upon SmA-SmC phase transition is only 0.4%, which is comparable to that achieved with other 'de Vries-like' materials.[1] However, it should be noted that the achiral liquid crystals in series **1.13** and **1.14** are not ferroelectric. In order to formulate ferroelectric SmC* mixtures using these new organosiloxane host materials and to test the effect of a chloro end-group on de Vries-like properties of chiral mesogens, the chiral 2-phenylpyrimidine trisiloxane materials with a (*R, R*)-2, 3-epoxy-8-chlorooctyloxy side-chain (**1.15** and **1.16**) were synthesized, characterized and compared to the non-chloro terminated analogues **E11** and **E6**.

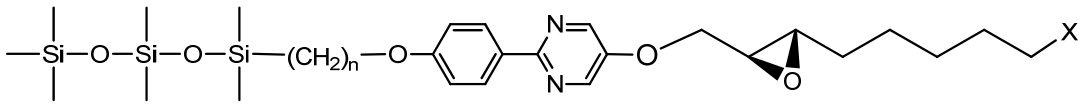

1.15: x=Cl, n=11
1.16: x=Cl, n=6
E11: x=H, n=11;
E6: x=H, n=6

3.1 Syntheses

3.1.1 Methods

The synthesis of the two chloro-terminated mesogens **1.15** and **1.16** is shown as Scheme 3-1. The synthesis of the chiral side chain begins with 6-chloro-1-hexanol (**3.1**), which is commercially available. In the first step, the alcohol is oxidized with pyridinium chlorochromate (PCC) to 6-chloro-1-hexanol (**3.2**), and then converted to (*E*)-ethyl 8-chlorooct-2-enoate (**3.3**)[2] in 50% overall yield via a Wittig reaction. The unsaturated ester is then reduced with DIBAL to give (*E*)-8-chlorooct-2-en-1-ol (**3.4**)[3] in 88% yield. The following key step of this synthesis is the Sharpless epoxidation, which is used to convert the double bond to the epoxide enantioselectively in ca. 60% yield using tert-butyl hydroperoxide (TBHP) as oxidant and *D*-(-)-DET (diethyl tartrate) and titanium(IV) isopropoxide as catalyst. The resulting product ((*2R,3R*)-3-(5-chloropentyl) oxiran-2-yl)methanol (**3.5**) is then condensed with 2-(4-hydroxyphenyl)-5-pyrimidinol (**2.3**) via a Mitsunobu reaction to give the 5-(((*E*)-(*2R,3R*)-3-(5-chloropentyl) oxiran-2-yl)methoxy)-2-(4-hydroxyphenol)pyrimidine (**3.6**) in 67% yield. Condensation of **3.6** with either siloxane-termianted alcohol **2.1** or **2.2** via another Mitsunobu reaction gave **1.15** and **1.16** in yields ranging from 45 to 50%. Prior to characterization, the final compounds were recrystallized from ethanol three times after filtration through a 0.45 um PTFE filter. Because this synthesis is modified from a literature procedure, the configuration of the major product in the enantioelective reaction is assumed to be the

same as that reported in the literature[4].

Scheme 3-1[a]:

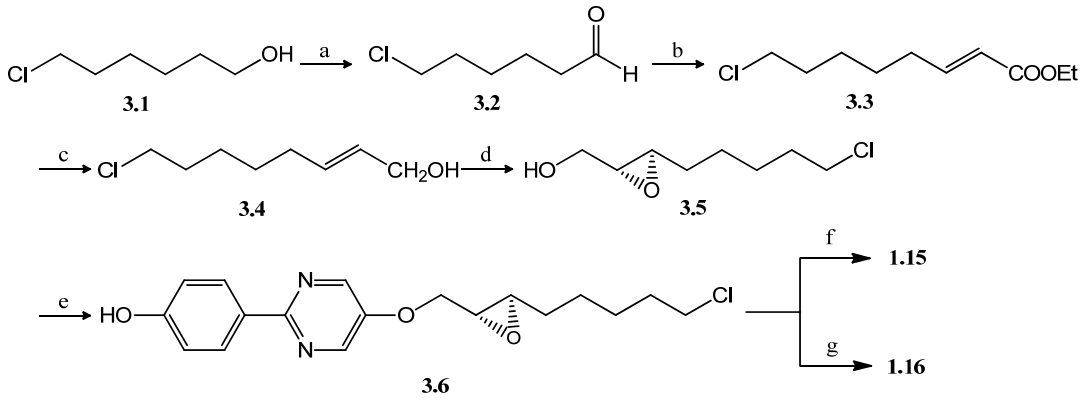

[a] *Reagents and conditions*: (a) (i) Pyridinium chlorochromate, CH_2Cl_2,3h, rt., (ii) Et_2O,2h, rt.; (b) THF, Ph_3P=CHCOOEt, overnight, rt.; (c)CH_2Cl_2, DIBAL, -70^oC;

(d) *D*-(-)-DET, Ti (O-^{i}Pr)$_4$, 4Å Sieves, TBHP, CH_2Cl_2, -20^oC; (e) **2.3**, DIAD, PPh_3, THF, rt. overnight; (f) **2.1**, DIAD, PPh_3, THF, rt. overnight; (g) **2.2**, DIAD, PPh_3, THF, rt. overnight;

3.1.2 Determination of Optical Purity

In developing the synthetic route shown in Scheme 3-1, a sample of **3.5** prepared using impure *L*-(+)-DET was used to first prepare **3.6**. Analysis of this sample using supercritical CO_2 chiral phase HPLC (Daicel chiralcd OD column, 20% MeOH/ supercritical CO_2, 2 mL/min, 200 bar) suggested that its optical purity was 50% ee (*S,S*), as shown in Figure 3.1a. Analysis of a sample of **3.6** derived from **3.5** prepared with fresh *D*-(-)-DET confirmed this assignment and indicated that the sample of **3.6** used in the synthesis of the final compounds **1.15** and **1.16** was 92% ee (*R, R*).

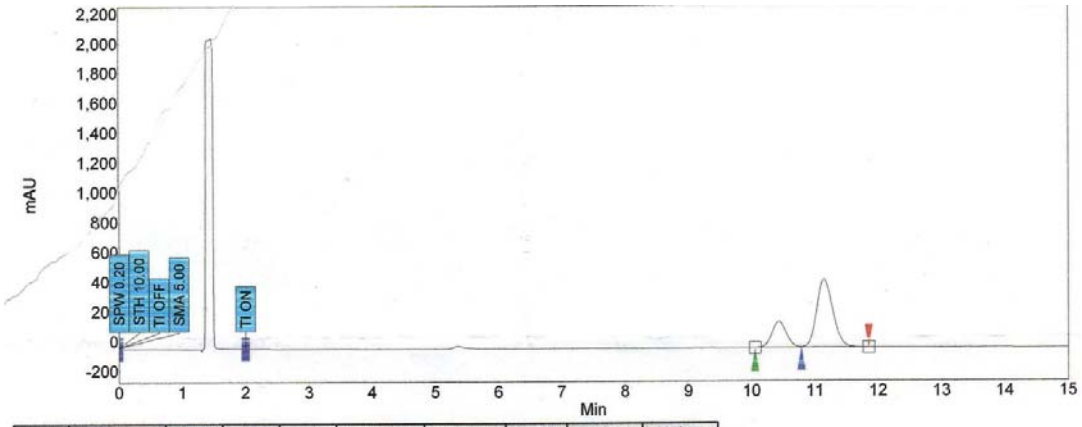

Index	Name	Start	Time	End	RT Offset	Quantity	Height	Area	Area
		[Min]	[Min]	[Min]	[Min]	[% Area]	[µV]	[µV.Min]	[%]
1	UNKNOWN	10.05	10.43	10.79	0.00	25.56	175.9	46.7	25.555
2	UNKNOWN	10.79	11.14	11.85	0.00	74.44	459.1	136.1	74.445
Total						100.00	635.0	182.8	100.000

(a)

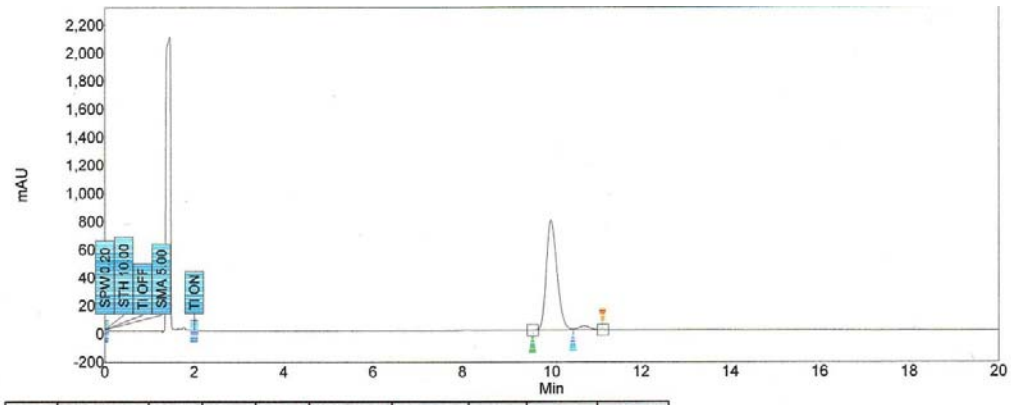

Index	Name	Start	Time	End	RT Offset	Quantity	Height	Area	Area
		[Min]	[Min]	[Min]	[Min]	[% Area]	[µV]	[µV.Min]	[%]
1	UNKNOWN	9.57	9.98	10.48	0.00	96.19	781.9	216.3	96.187
2	UNKNOWN	10.48	10.73	11.15	0.00	3.81	27.9	8.6	3.813
Total						100.00	809.8	224.8	100.000

(b)

Figure 3-1: Chiral phase HPLC trace of (a) a **3.6** derived from **3.5** prepared with impure *L*-(+)-DET and (b) **3.6** derived from **3.5** prepared with fresh *D*-(-)-DET (OD column, 20% MeOH, 2 mL/min, 200 bar)

3.2 Mesophase Characterization

The mesophases formed by compounds **1.15** and **1.16** were characterized by polarized optical microscopy (POM) and differential scanning calorimetry (DSC). Both mesogens form chiral SmA* phase and chiral SmC* on heating and cooling. The SmC*-SmA* transition temperatures were determined by POM observation of the characteristic homeotropic and fan textures (SmA*) turning to broken fan and Schlieren textures (SmC*), as shown in Fgure 3-2. We also observed significant changes in interference colours in the fan/broken fan textures of both liquid crystals on cooling from the SmA* to the SmC* phase (Figure 3-2), which is consistent with an increase in orientational order. Interestingly, the broken fan texture of **1.16** in the SmC* phase also shows the periodic fringe pattern characteristic of the SmC* helical structure. The fact that these are not observed with **1.15** suggests that the helical pitch of **1.16** is significant shorter than that of **1.15**.

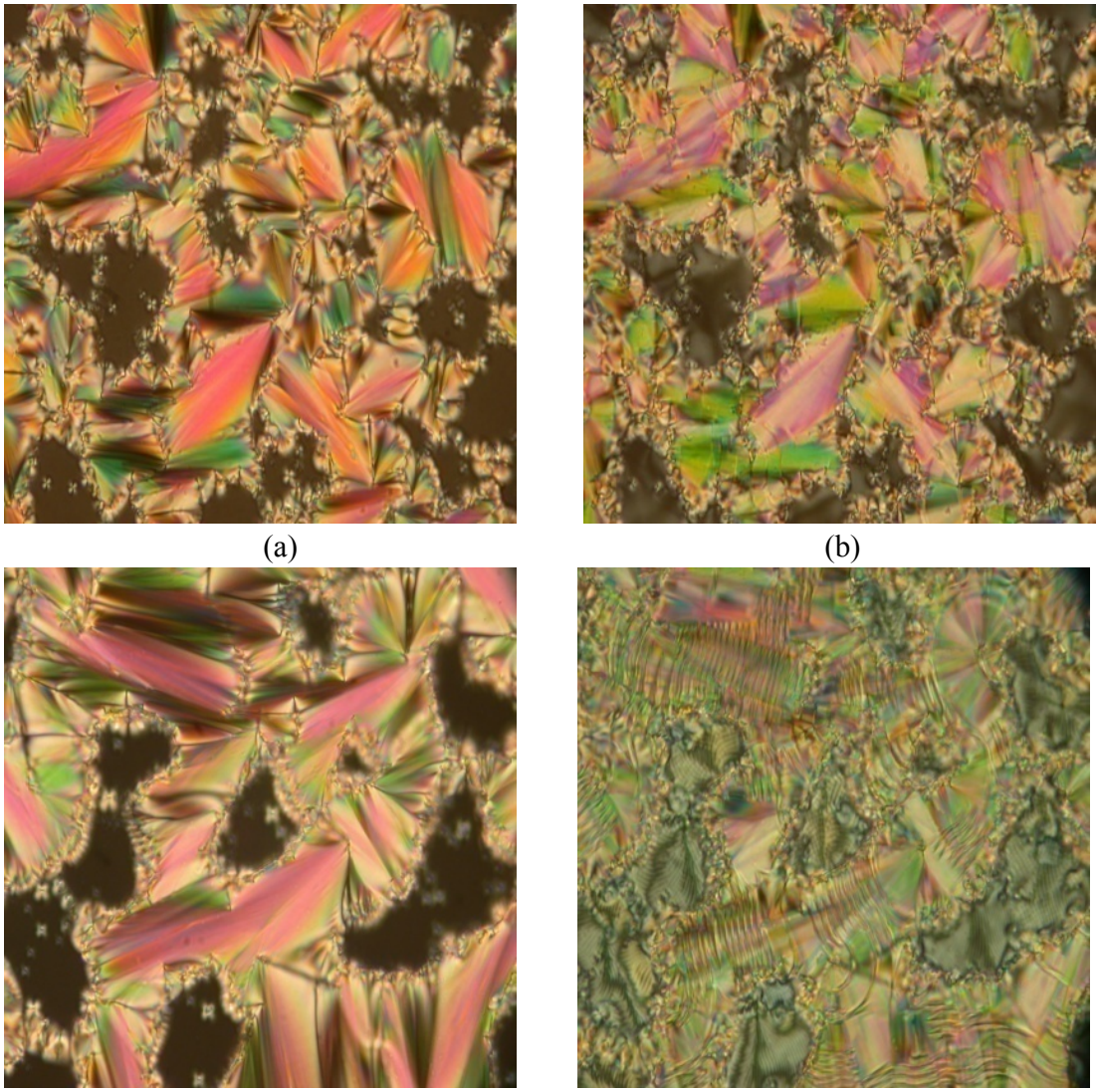

Figure 3- 2: Polarized photomicrographs of compounds **1.15** and **1.16** between untreated glass slide and cover slip (500×) (a) compound **1.15** in the SmA* phase at T -T_{AC} =5 K, (b) compound **1.15** in the SmC* phase at T -T_{AC} =-5 K, (c) compound **1.16** in the SmA* phase at T -T_{AC} =5 K and (d) compound **1.16** in the SmC* phase at T -T_{AC} =-5 K.

As shown in Figure 3-3, the inclusion of a terminal chloro substituent resulted in broader SmA* phases in both cases, which is consistent with the previous result in the non-chiral siloxane-terminated mesogens series.[5] It is normally difficult to detect the transition from SmC* phase to SmA* phase by DSC because it is normally second order. However, in

the case of **1.15** and **1.16**, the SmA-SmC transition is detectable, as shown by small peaks (ΔH^0=0.1-0.4 kJ/mol) on heating and cooling cycles of the DSC (Figure 3-4).

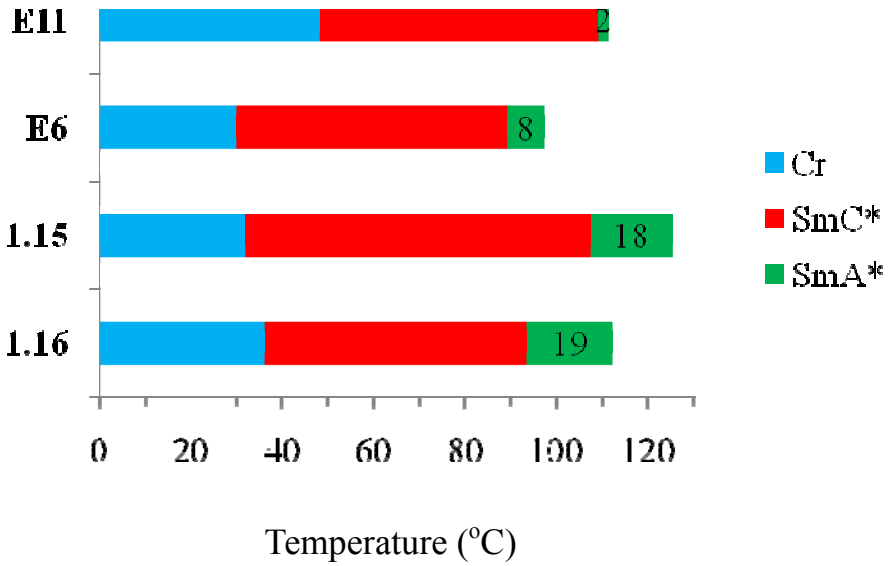

Figure 3-3: Phase transition temperatures for compounds **E11, E6, 1.15** and **1.16** measured by DSC on heating at a rate of 5 K /min(SmA-SmC transition temperatures were measured by POM). Light blue: Cr; red: SmC*; green: SmA*. The number on the bar is the temperature range of SmA phase.

Table 3-1: Transition temperatures (°C) and enthalpies of transitions ΔH^0(kJ/mol, in parentheses) for compounds **E11**, **E6**, **1.15** and **1.16**

Cpd	Cr(●)/SmX(▲)		SmC		SmA		I
E11	●	38(11.7)	●	110(1.0)	●	113(8.3)	●
E6	●	30(20.9)	●	89(0.3)	●	97(8.4)	●
1.15	▲	32(13.9)	●	107(<0.1)	●	125(10.4)	●
1.16	▲	36(6.9)	●	93(0.6)	●	112(7.2)	●

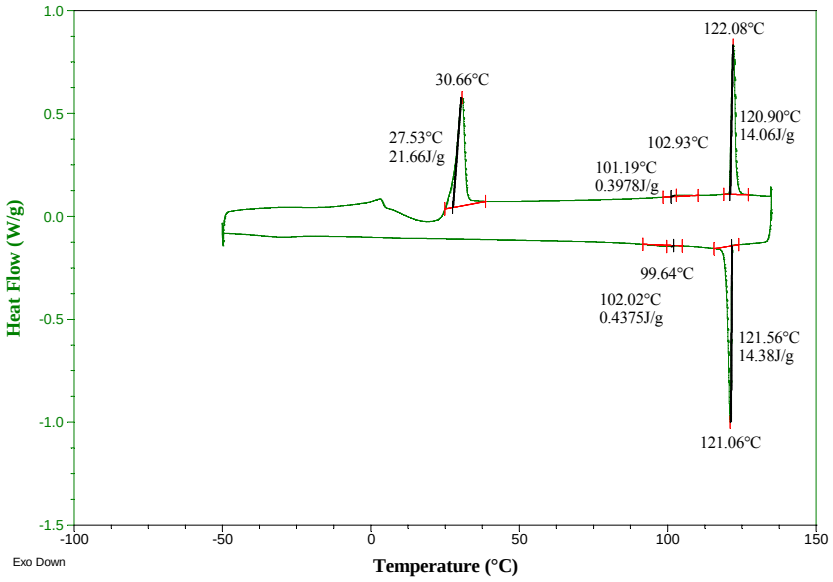

(a)

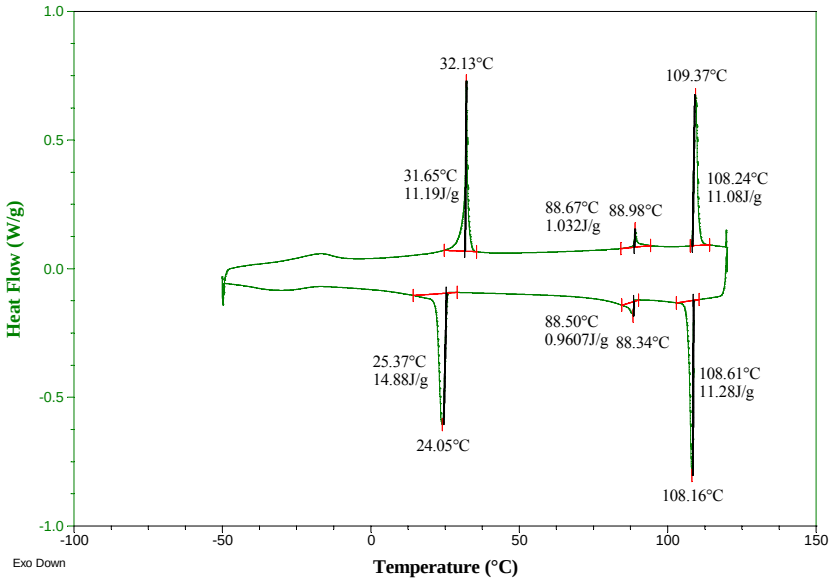

(b)

Figure 3-4: Differential scanning calorimetry (DSC) trace for (a) compound **1.15** and (b) **1.16** taken at a scan rate of 5K/min.

3.3 Ferroelectric properties

Attempt were made to produce uniformly aligned surface-stabilized ferroelectric liquid crystal (SSFLC) films of **1.15** and **1.16** using commercial ITO glass cells with alignment layers consisting of either rubbed polyimide (4 μm spacing) or rubbed nylon (4.0 μm spacing). However, a uniform alignment could not be achieved by cooling from the isotropic liquid phase to SmC* phase at 2K/min in either case. Recently, Roberts *et al.* reported that a uniform alignment could be achieved for a related class of chiral siloxane mesogens by applying a triangular wave ac field of 12 V μm^{-1} for 10 to 30 min after the mesogens were cooled into SmC* phase.[6] Therefore, we used this method to align **1.15** in rubbed nylon cell and obtained a somewhat better alignment but not completely uniform.

Spontaneous polarizations P_S and optical tilt angles θ_{opt} were measured as a function of temperature for **1.15** and **1.16** in rubbed nylon cells. As shown as Figure 3-5, the spontaneous polarization of **1.16** is ca. twice those of **E11**, **E6** and **1.15**, but the optical tilt angles of these compounds are quite different (Figure 3-6). In order to normalize for differences in tilt angle, the reduced polarizations were calculated (eq. 3-1). As seen previously with the achiral organosiloxane series, the addition of a chloro end-group has the effect of reducing the tilt angle in the SmC phase, which is consistent with its SmA stabilizing effect. As shown in Figure 3-7, the reduced polarization of the compound with the shorter spacer (**1.16**) is *ca.* twice that of the compound with the longer spacer (**1.15**), which is opposite to the trend observed with the series without chloro end-groups.

$$P_0 = P_S / \sin\theta \qquad \text{(eq. 3-1)}$$

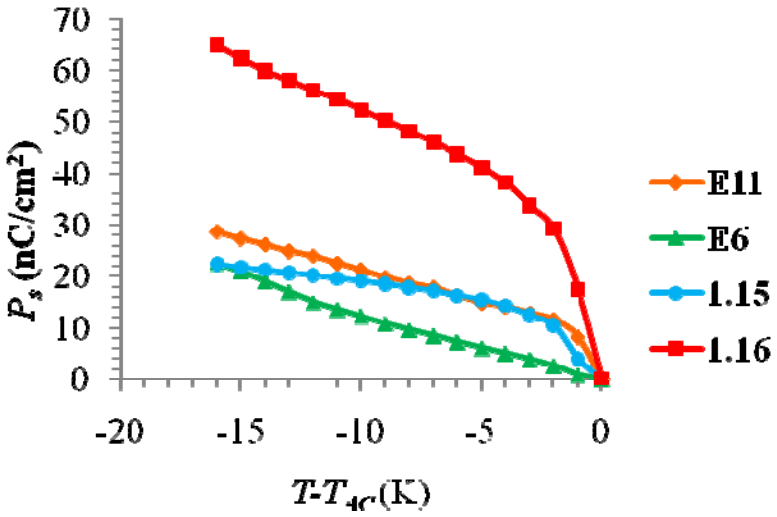

Figure 3-5: Spontaneous polarization P_S versus $T - T_{AC}$ of dopants **E11**(◆), **E6**(▲), **1.15**(●) and **1.16**(■).

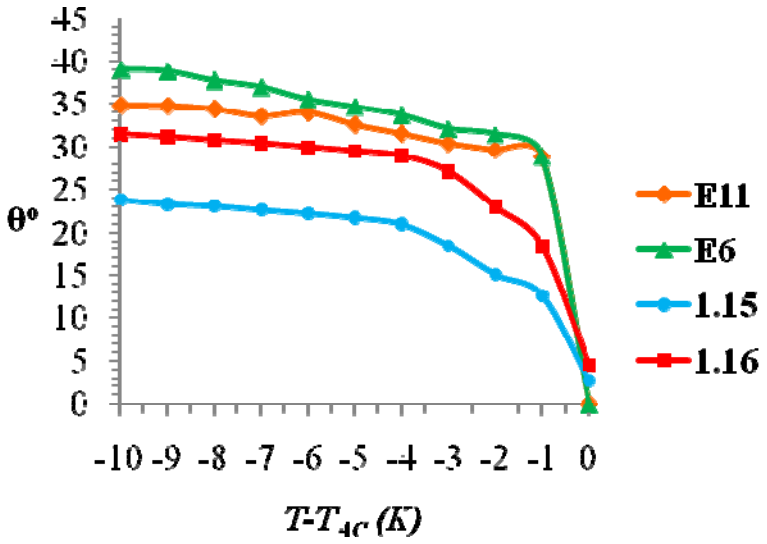

Figure 3-6: Optical tilt angle θ_{opt} versus $T - T_{AC}$ of dopants **E11** (◆), **E6** (▲), **1.15**(●) and **1.16**(■).

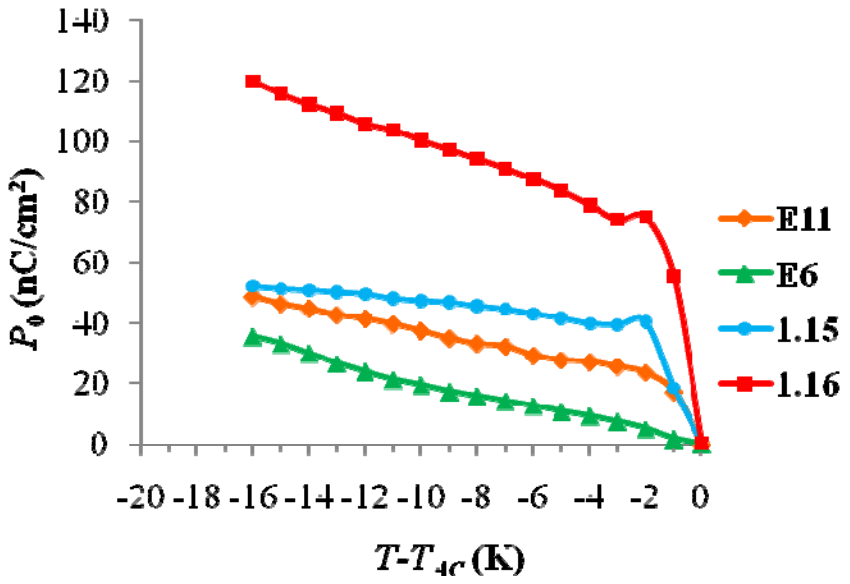

Figure 3-7: Reduced polarization P_0 versus $T - T_{AC}$ of dopants **E11** (◆), **E6** (▲), **1.15**(●) and **1.16**(■).

3.4 'de Vries' Character

Layer spacings (d) as a function of temperature were measured accurately by small angle X-ray scattering (SAXS) and the resulting profiles for **1.15** and **1.16** are shown in Figure 3-8, together with the previous results of **E11** and **E6**. In the cases of **1.15** and **1.16**, the layer spacing in the SmA* phase increases with decreasing temperature (Figure 3-8), which is likely due to an increase in orientational order, and in effective molecular length as the alkyl chains become more extended at lower temperatures.[7] Other "de Vries-like" materials have been reported to show a similar negative thermal expansion in their $d(T)$ profiles.[1] This is consistent with the profile of **E6**, whereas the SmA temperature range of **E11** is too narrow to allow for comparison.

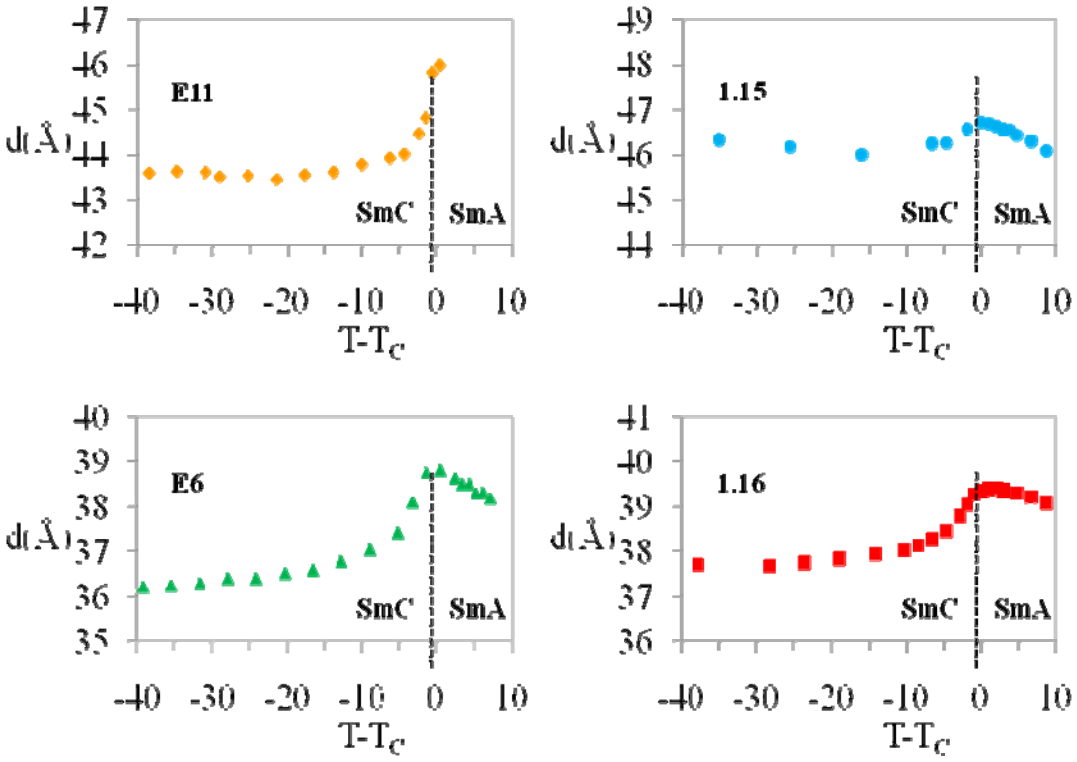

Figure 3-8: Smectic layer spacing *d* versus reduced temperature $T\text{-}T_C$ for compound **E11** (◆), **E6** (▲), **1.15**(●) and **1.16**(■).

The maximum layer constractions of compounds **E11, E6**, **1.15** and **1.16** are 4.7%, 5.2%, 1.5% and 3.4%, respectively. Except for **1.15**, the other three compounds may not be considered 'de Vries-like' because of the relatively large layer contractions[1]. Nevertheless, compounds **E6** and **1.16** may exhibit more de Vries-like character than conventional non-siloxane phenylpyrimidine mesogens such as **PhP1** due to their large tilt angles in the SmC* phase. Compound **1.15** may be considered 'de Vries-like' since its layer contraction is similar to that reported for a 'de Vries-like' 5-phenylpyrimidine

organosiloxane material.[8] However, because of its smaller tilt angle in the SmC* phase, this compound has significantly less de Vries character than the 5-phenylpyrimidine mesogen **1.12**. As mentioned in Chapter 1, the reduction factor *R* is given by equation 1-6 as the ratio of the tilt angle δ (*T*) required to give the layer contraction according to a classic rigid-rod model over the optical tilt angle $\theta_{opt}(T)$ measured by POM. At $T - T_{AC} = -10$ K, the *R* values for **E11**, **E6**, **1.15** and **1.16** are 0.51, 0.48, 0.41 and 0.48, respectively (Table 3-1). The fact that the *R* value of **1.15** is somewhat smaller than that of **E11** suggests that its de Vries-like character has been enhanced by inclusion of the chloro terminated group. But in the case of the short spacer case (**E6** and **1.16**), the *R* values are almost the same despite the difference in layer contraction because the tilt angle of **1.16** is smaller than that of **E6**. This is consistent with what we observed in the case of C_6/C_{11} chloro *vs* non-chloro 2-phenylpyrimidine series **1.13** and **1.14**. As shown as Figure 3-8, the C11 chloro/non-chloro series (**E11** and **1.15**) show negative thermal expansion persisting in the SmC phase, whereas the C_6 chloro/non-chloro series (**E6** and **1.16**) do not. This is consistent with the concept of SmC/SmA frustration, with the C_{11} siloxane side-chain being a stronger SmC promoter than the C_6 siloxane side-chain.

Table 3-2: Liquid crystal smectic layer spacings at the SmA*–SmC* transition ($d(T_{AC})$) and in the SmC* phase at T-T_{AC}=-10 K (d_C), tilt angles, and figures of merit *R* at T-T_{AC}=-10 K.

Cpd	$d(T_{AC})$/Å[a]	d_C/Å[a]	Layer Contraction	Tilt Angle (deg)	*R*	SmA Temperature range(K)
1.15	46.7	46	1.5%	24	0.41	18
1.16	39.3	38	3.4%	31	0.48	19
E11	46.1	43.9	4.7%	35	0.51	2
E6	39.1	37.1	5.2%	39	0.48	8

[a] Error is ±0.1Å .

3.5 Conclusions

Two new chiral 2-phenylpyrimidine mesogens with chloro end-groups that form SmA* and SmC* liquid crystal phases were synthesized and their ferroelectric properties as SSFLC films were investigated. The temperature range of the SmA* phase is broadened by the addition of a terminal chloro substituent. The spontaneous polarization of **1.16** is *ca*. twice those of **E11**, **E6** and **1.15**. A comparison of between SAXS profiles shows that the non-chloro analogous **E11** and **E6** undergo SmA-SmC frustration with higher % layer contraction than the chloro-terminated analogous **1.15** and **1.16** (Table 3-2), which can be explained in large part to higher tilt angles in the SmC phase. As a result, the *R* values for **1.15** and **1.16** are not significant smaller than those of **E11** and **E6,** and are certainly not in the range of de Vries-like materials ($R \leq 0.20$). Furthermore, those results also indicate, as in series **1.13** and **1.14,** that there is no apparent correlation between de Vries-like character and the temperature range of SmA phase.

3.6 References

(1) Lagerwall, J. P. F.; Giesselmann, F. *ChemPhysChem* **2006**, *7*, 20-45.

(2) Fischer, C.; Smith, S. W.; Powell, D. A.; Fu, G. C. *J. Am. Chem. Soc.* **2006**, *128*, 1472-1473.

(3) Wilson, R. M.; Jen, W. S.; MacMillan, D. W. C. *J. Am. Chem. Soc.* **2005**, *127*, 11616-11617.

(4) Gao, Y.; Klunder, J. M.; Hanson, R. M.; Masamune, H.; Ko, S. Y.; Sharpless, K. B. *J. Am. Chem. Soc.* **1987**, *109*, 5765-5780.

(5) Li, L.; Jones, C. D.; Magolan, J.; Lemieux, R. P. *J. Mater. Chem.* **2007**, *17*, 2313-2318.

(6) Roberts, J. C.; Kapernaum, N.; Giesselmann, F.; Wand, M. D.; Lemieux, R. P. *J. Mater. Chem.* **2008**, *18*, 5301-5306.

(7) Radcliffe, M. D.; Brostrom, M. L.; Epstein, K. A.; Rappaport, A. G.; Thomas, B. N.; Shao, R.; Clark, N. A. *Liq. Cryst.* **1999**, *26*, 789-794.

(8) Roberts J, C.; Kapernaum, N.; Giesselmann, F.; Lemieux R, P. *J. Am. Chem. Soc.* **2008**, *130*, 13842-13843.

Chapter 4. Experimental

4.1. Syntheses and characterization

4.1.1. General

^{1}H and ^{13}C NMR spectra were recorded on Bruker Avance 300, 400 or 500 MHz spectrometers using deuterated chloroform or deuterated methanol as solvent. Chemical shifts are reported in δ (ppm) relative to chloroform as internal standard. Low resolution EI mass spectra were recorded on an Applied Biosystems/MDS Sciex QSTAR XL QqTOF mass spectrometer; Peaks are reported as *m/z* (% intensity relative to base peak). High resolution EI mass spectra were recorded on a Waters/Micromass GCT mass spectrometer, and high resolution ESI mass spectra were recorded on an AppliedBiosystems/MDS Sciex QSTAR XL QqTOF mass spectrometer. Melting points were obtained on a Fisher-Johns melting point apparatus and are uncorrected. Flash chromatography was performed on 60 Å silica gel (Silicycle Inc., Quebec).

4.1.2 Materials

All solvents and reagents were obtained from commercial sources and used without further purification unless otherwise noted. Anhydrous CH_2Cl_2 was distilled over P_2O_5 under an argon atmosphere. Anhydrous THF, hexane, ether, DMF and toluene were

obtained from a Solv-Tek, Inc. solvent purification system. 2-(4-Hydroxyphenyl)-5-pyrimidinol was purchased from Aldrich and purified by flash chromatography on silica gel (50%EtOAc/hexanes). (E)-Ethyl 9-chloronon-2-enoate,[1] (E)-9-chloronon-2-en-1-ol[2] and the trisiloxane-terminated alcohols 11-(1,1,1,3,3,5,5-heptamethyltrisiloxanyl)undecanol (**2.1**) and 6-(1,1,1,3,3,5,5-heptamethyltrisiloxanyl)hexanol (**2.2**) were prepared by a literature procedure and shown by ^{1}H NMR to be free of impurities.[3] 7-Chloro-1-heptanol was prepared by a modified literature procedure.[1,2,4]

4.1.3 Synthesis of 7-chloro-1-heptanol

(*E*)-Ethyl-7-chlorohept-2-enoate A flask was charged with pyridinium chlorochromate (PCC) (2.17 g, 10 mmol), and flushed with argon. To the orange solid was added CH_2Cl_2 (50 mL) and 5-chloro-1-pentanol (1 g, 8 mmol). The resulting dark-brown reaction mixture was stirred for 3 h at rt., and then Et_2O (50 mL) was added, leading to the precipitation of a brown solid. The mixture was allowed to stir at rt. for 2 h, and then it was filtered through a plug of silica gel (washed with Et_2O). The solvent was removed and the residue was transferred to a 100 mL flask under argon. THF (50 mL) and (thoxycarbonylmethylene) triphenylphosphorane (3.83 g, 11 mmol) were added, and the resulting reaction mixture was stirred at r.t overnight. The reaction mixture was absorbed onto silica gel and the crude product was purified by flash chromatography on silica gel

(6.25% EtOAc/hexanes) to give 0.78 g (50%) of **(*E*)-ethyl-7-chlorohept-2-enoate** as a clear oil.

(*E*)-7-Chlorohept-2-en-1-ol To a solution of (*E*)-ethyl-7-chlorohept-2-enoate (0.78 g, 4 mmol) in 25 mL $CHCl_2$, cooled to -78 ^oC, DIBAl (1.71g, 12mmol) was added slowly. The reaction was allowed to warm to 25 ^oC, then quenched with MeOH (10 mL), and stirred with 15 mL of Rochelle's salt solution (sat) for 8 hours. The layers were separated and the aqueous layer was extracted with CH_2Cl_2 (3 x 20 mL). The combined organic layers were washed with brine (20 mL), dried ($MgSO_4$) and concentrated to afford 0.52 g (88%) of **(*E*)-7-chlorohept-2-en-1-ol** as a clear oil; ^1H NMR (400 MHz, $CDCl_3$) δ 5.72-5.55 (m, 2H), 4.20 (d, *J* = 6.6 Hz, 2H), 3.54 (t, *J* = 6.7 Hz, 2H), 2.13-2.05 (m, 2H), 1.82-1.75 (m, 2H), 1.61-1.37 (m, 2H).

7-Chloro-1-heptanol A mixture of **(*E*)-7-Chlorohept-2-en-1-ol** (0.52g, 3.5mmol), Pd/C catalyst (10%, 0.052 g) and Ph_2S (6.3 mg, 0.035 mmol) in EtOH (30 mL) was stirred at r.t. under atmospheric H_2 pressure (balloon) for 24 h. The reaction mixture was then filtered through a plug of silica gel (washed with EtOH) and the solvent was removed in vacuo to give 0.5 g (95%) of **7-chloro-1-heptanol** as a clear oil. ^1H NMR (400 MHz, $CDCl_3$) δ 3.65 (t, *J* = 6.3 Hz ,2H), 3.54 (t, *J* = 6.4 Hz, 2H), 1.73 (m, 2H), 1.58 (m, 2H), 1.49-1.32 (m, 6H);

4.1.4 Syntheses of liquid crystal materials

5-(4-chlorobutyloxy)-2-(4-hydroxyphenol)pyrimidine (2.3) Under an argon atmosphere, DIAD (482 mg, 0.4 mmol) was added to a solution of 2-(4-hydroxyphenyl)-5-pyrimidinol (0.40 g, 2.13 mmol), 4-chloro-1-butanol (0.23 g, 2.13 mmol) and triphenylphosphine (0.67 g, 2.56 mmol) in dry THF (15 mL). The yellow solution was stirred overnight at room temperature, then concentrated and purified by flash chromatography on silica gel (20% EOAc/hexanes) to give **2.3** (0.36 g, 60%) as a white solid contaminated with traces of DIAD. This compound was used in the next step without further purification: ^{1}H NMR (400 MHz, $CDCl_3$) δ 8.44 (s, 2H), 8.25 (d, *J* = 8.7 Hz, 2H), 6.92 (d, *J* = 8.7 Hz, 2H), 5.33 (s, 1H), 4.14 (t, *J* = 6.3 Hz, 2H), 3.60 (t, *J* = 6.4 Hz, 2H), 1.99 (m, 4H);

5-(4-Chlorobutyloxy)-2-(4-(11-(1,1,1,3,3,5,5-heptamethyltrisiloxanyl)undecyloxy)-phenyl)pyrimidine (1.13a) The procedure used for the preparation of **2.3** was repeated with **2.3** (0.15 g, 0.54 mmol) and 11-(1,1,1,3,3,5,5-heptamethyltrisiloxanyl)undecanol (0.24 g, 0.61 mmol). The crude product was purified by flash chromatography on silica gel (10% EtOAc/hexanes) to give 0.20 g (56%) of **1.13a** as white solid. Prior to analysis by POM and DSC, the material was recrystallized three times from HPLC-grade ethanol: ^{1}H NMR (500 MHz, $CDCl_3$) δ 8.45 (s, 2H), 8.30 (d, *J* = 8.7 Hz, 2H), 6.99 (d, *J* = 8.7 Hz,

2H), 4.16 (t, *J* = 5.0 Hz, 2H), 4.04 (t, *J* = 6.7 Hz, 2H), 3.67 (t, *J* = 5.0 Hz, 2H), 1.83 (m, 2H), 1.81-1.30 (m, 22H), 0.55 (t, *J* = 7.2 Hz, 2H), 0.11 (s, 9H), 0.08 (s, 6H), 0.04 (s, 6H); ^{13}C NMR (125MHz, $CDCl_3$) δ 161.2, 158.4, 151.3, 144.2, 130.4 129.5, 114.9, 69.1, 68.5, 44.9, 33.8, 30.1-29.4 (several overlapping peaks), 27.0, 26.5, 25.4, 23.6, 18.7, 2.2, 1.7, 0.6; LRMS (EI) *m/z* 652 (M^+,95), 637 (28), 616 (1), 498 (3), 483 (4), 431 (3), 393 (1), 291 (3), 278 (11), 223 (6), 222 (15), 221 (100), 188 (18), 159 (3), 119 (2), 91 (8), 73 (13); HRMS (EI) *m/z* m/z calcd for $C_{32}H_{57}{}^{35}ClN_2O_4Si_3$ 652.3315, found 652.3310.

5-(4-Chlorobutyloxy)-2-(4-(6-(1,1,1,3,3,5,5-Heptamethyltrisiloxanyl)hexyloxy)-phenyl)pyrimidine (1.14a) The procedure used for the preparation of **2.3** was repeated with **2.3** (0.15 g, 0.54 mmol) and 6-(1,1,1,3,3,5,5-heptamethyltrisiloxanyl)hexanol (0.19 g, 0.60 mmol). The crude product was purified by flash chromatography on silica gel (10% EtOAc/hexanes) to give 0.17 g (55%) of **1.14a** as a white solid. Prior to analysis by POM and DSC, the material was recrystallized three times from HPLC-grade ethanol; ^{1}H NMR (400 MHz, $CDCl_3$) δ 8.44 (s, 2H), 8.29 (d, *J* = 8.9 Hz, 2H), 6.99 (d, *J* = 8.9 Hz, 2H), 4.16 (t, *J* = 5.0 Hz, 2H), 4.04 (t, *J* = 6.6 Hz, 2H), 3.67 (t, *J* = 6.6 Hz, 2H), 1.83 (m, 2H), 1.59-1.37 (m, 12H), 0.58 (t, *J* = 7.7 Hz, 2H), 0.11 (s, 9H), 0.09 (s, 6H), 0.05 (s, 6H); ^{13}C NMR (100 MHz, $CDCl_3$) δ 161.2, 158.4, 151.3, 144.2, 130.4, 129.4, 114.9, 68.5, 68.4, 45.0, 33.6, 29.6, 29.5, 27.0, 26.2, 23.6, 18.7, 2.3, 1.7, 0.6; LRMS (EI) *m/z* 582 (M^+,28), 579 (11), 546 (2), 502 (9), 483 (13), 481 (7), 414 (7), 361 (2), 278 (9), 264 (24),

221 (100), 219 (63), 218 (25), 188 (22), 149 (28), 131 (60), 73 (32), 70 (48), 69 (70); HRMS (EI) *m/z* calcd for $C_{27}H_{47}{}^{35}ClN_2O_4Si_3$ 582.2532, found 582.2533.

5-(5-Chloropentyloxy)-2-(4-hydroxyphenol) pyrimidine (2.4) The procedure used for the preparation of **2.3** was repeated with 5-chloro-1-heptanol (0.26 g, 2.13 mmol) and 2-(4-hydroxyphenyl)-5-pyrimidinol (0.40 g, 2.13 mmol). The crude product was purified by flash chromatography on silica gel (25% EtOAc/hexanes) to give 0.35 g (56%) of **2.4** as white solid contaminated with traces of DIAD. This compound was used in the next step without further purification; ^{1}HNMR (400 MHz, $CDCl_3$) δ 8.43 (s, 2H), 8.25 (d, *J* = 8.7 Hz, 2H), 6.90 (d, *J* = 8.7 Hz, 2H), 5.30 (s,1H), 4.15 (t, *J* = 6.4 Hz, 2H), 3.59 (t, *J* = 6.5 Hz, 2H), 2.01 (m, 4H), 1.60 (m, 2H);

5-(5-Chloropentyloxy)-2-(4-(11-(1,1,1,3,3,5,5-Heptamethyltrisiloxanyl)undecyloxy)-phenyl)pyrimidine (1.13b) The procedure used for the preparation of **2.3** was repeated with **2.4** (0.15 g, 0.51 mmol) and 11-(1,1,1,3,3,5,5-heptamethyltrisiloxanyl)undecanol (0.24 g, 0.60 mmol). The crude product was purified by flash chromatography on silica gel (10% EtOAc/hexanes) to give 0.16 g (48%) of **1.13b** as white solid. Prior to analysis by POM and DSC, the material was recrystallized three times from HPLC-grade ethanol; ^{1}H NMR (400 MHz, $CDCl_3$) δ 8.42 (s, 2H), 8.27 (d, *J* = 8.9 Hz, 2H), 6.98 (d, *J* = 8.9 Hz, 2H), 4.11 (t, *J* = 6.3 Hz, 2H), 4.02 (t, *J* = 6.6 Hz, 2H), 3.60 (t, *J* = 6.5 Hz, 2H), 1.85 (m,

6H), 1.67 (m, 2H), 1.51-1.29 (m, 16H), 0.53 (t, *J* = 7.3 Hz, 2H), 0.09 (s, 9H), 0.06 (s, 6H), 0.03 (s, 6H); ^{13}C NMR (100 MHz, $CDCl_3$) δ 159.0, 156.1, 149.1, 142.0, 128.2, 127.2, 112.6, 66.8, 66.3, 42.9, 31.6, 30.4, 27.8-27.5 (several overlapping peaks), 26.7, 24.3, 21.6, 21.4, 16.5, 0.0, -0.5, -1.6; LRMS (EI) *m/z* 666 (M^+,7), 662 (8), 630 (9), 615 (2), 292 (1), 223 (4), 222 (10), 221 (100), 220 (70), 188 (22), 187 (15), 133 (2), 73 (7); HRMS (EI) *m/z* calcd for $C_{33}H_{59}{}^{35}ClN_2O_4Si_3$ 666.3471, found 666.3475.

5-(5-Chloropentyloxy)-2-(4-(6-(1,1,1,3,3,5,5-Heptamethyltrisiloxanyl)hexyloxy)-phenyl)pyrimidine (1.14b) The procedure used for the preparation of **2.3** was repeated with **2.4** (0.15 g, 0.51 mmol) and 6-(1,1,1,3,3,5,5-heptamethyltrisiloxanyl)hexanol (0.19 g, 0.60 mmol). The crude product was purified by flash chromatography on silica gel (10% EtOAc/hexanes) to give 0.18 g (60%) of **1.14b** as a white solid. Prior to analysis by POM and DSC, the material was recrystallized three times from HPLC-grade ethanol; ^{1}H NMR (400 MHz, $CDCl_3$) δ 8.42 (s, 2H), 8.28 (d, *J* = 8.8 Hz, 2H), 6.98 (d, *J* = 8.8 Hz, 2H), 4.11 (t, *J* = 6.2 Hz, 2H), 4.03 (t, *J* = 6.6 Hz, 2H), 3.60 (t, *J* = 6.6 Hz, 2H), 1.86 (m, 6H), 1.69 (m, 2H), 1.51-1.37 (m, 6H), 0.56 (t, *J* = 7.9 Hz, 2H), 0.09 (s, 9H), 0.07 (s, 6H), 0.03 (s, 6H); ^{13}C NMR (100 MHz, $CDCl_3$) δ 158.9, 156.1, 149.1, 142.0, 128.2, 127.2, 112.6, 66.7, 66.3, 42.9, 31.3, 30.4, 27.4, 26.7, 24.0, 21.6, 21.4, 16.4, 0.0, -0.5, -1.6; LRMS (EI) *m/z* 596 (M^+,32), 592 (25), 560 (10), 512 (2), 497 (10), 494 (6), 461 (3), 393 (1),292 (3), 223

(3), 222 (10), 221 (100), 220 (62), 188 (13), 187 (9), 159 (1), 119(1), 73 (18); HRMS (EI) *m/z* calcd for $C_{28}H_{49}{}^{35}ClN_2O_4Si_3$ 596.2689, found 596.2686.

5-(6-Chlorohexyloxy)-2-(4-hydroxyphenol)pyrimidine (2.5) The procedure used for the preparation of **2.3** was repeated with 6-chloro-1-hexanol (0.29 g, 2.13 mmol) and 2-(4-hydroxyphenyl)-5-pyrimidinol (0.40 g, 2.13 mmol). The crude product was purified by flash chromatography on silica gel (20% EtOAc/hexanes) to give 0.40 g (61%) of **2.4** as white solid: mp.100-102^{o}C; ^{1}H NMR (500 MHz, $CDCl_3$) δ 8.44 (s, 2H), 8.26 (d, *J* = 8.8 Hz, 2H), 6.93 (d, *J* = 8.8 Hz, 2H), 5.28 (s,1H), 4.11 (t, *J* = 6.4 Hz, 2H), 3.59 (t, *J* = 6.6 Hz, 2H), 1.86 (m, 4H), 1.63-1.54 (m, 4H); ^{13}C NMR (100 MHz, $CDCl_3$) δ 158.0, 157.7, 151.5, 144.2, 130.9, 129.7, 115.8, 69.1, 45.3, 32.8, 29.4, 27.0, 25.7; LRMS (EI) *m/z* 306 (M^+,24), 237 (3), 232 (9), 231 (12), 189 (15), 188 (100), 165 (10), 133 (14), 119 (24), 117 (27), 115 (30), 105 (39), 57 (40), 55 (44); HRMS (EI) *m/z* calcd for $C_{16}H_{19}{}^{35}ClN_2O_2$ 306.1135, found 306.1124.

5-(6-Chlorohexyloxy)-2-(4-(11-(1,1,1,3,3,5,5-heptamethyltrisiloxanyl)undecyloxy)-phenyl)pyrimidine (1.13c) The procedure used for the preparation of **2.3** was repeated with **2.5** (0.20 g, 0.65 mmol) and 11-(1,1,1,3,3,5,5-heptamethyltrisiloxanyl)undecanol (0.28g, 0.71mmol). The crude product was purified by flash chromatography on silica gel (10% EtOAc/hexanes) to give 0.23 g (51%) of **1.13c** as white solid. Prior to analysis by

POM and DSC, the material was recrystallized three times from HPLC-grade ethanol; ^{1}H NMR (400 MHz, $CDCl_3$) δ 8.42 (s, 2H), 8.27 (d, *J* = 8.7 Hz, 2H), 6.98 (d, *J* = 8.7 Hz, 2H), 4.10 (t, *J* = 6.3 Hz, 2H), 4.02 (t, *J* = 6.5 Hz, 2H), 3.58 (t, *J* = 6.6 Hz, 2H), 1.85 (m, 6H), 1.56-1.25 (m, 20H), 0.53 (t, *J* = 7.8 Hz, 2H), 0.09 (s, 9H), 0.06 (s, 6H), 0.03 (s, 6H); ^{13}C NMR (125MHz, $CDCl_3$) δ 161.1, 158.2, 151.4, 144.2, 130.4, 129.4, 114.8, 69.1, 68.5, 45.3, 33.9, 32.8, 30.1, 30.0-29.4 (several overlapping peaks), 27.0, 26.5, 25.7, 23.6, 18.7, 2.2, 1.7, 0.6; LRMS (EI) *m/z* 680 (M^+,65), 665 (10), 646 (6), 631 (1), 527 (2), 459 (3), 393(1), 308 (3), 306 (9), 272 (1), 223 (6), 222 (12), 221 (100), 188 (35), 159 (4), 119(3), 73(11); HRMS (EI) *m/z* calcd for $C_{34}H_{61}{}^{35}ClN_2O_4Si_3$ 680.3628, found 680.3602.

5-(6-Chlorohexyloxy)-2-(4-(6-(1,1,1,3,3,5,5-heptamethyltrisiloxanyl)hexyloxy)-phenyl)pyrimidine (1.14c) The procedure used for the preparation of **2.3** was repeated with **2.5** (0.20 g, 0.65 mmol) and 6-(1,1,1,3,3,5,5-heptamethyltrisiloxanyl)hexanol (0.23 g, 0.71 mmol). The crude product was purified by flash chromatography on silica gel (10% EtOAc/hexanes) to give 0.19 g (48%) of **1.14c** as a white solid. Prior to analysis by POM and DSC, the material was recrystallized three times from HPLC-grade ethanol; ^{1}H NMR (400 MHz, $CDCl_3$) δ 8.44 (s, 2H), 8.29 (d, *J* = 8.8 Hz, 2H), 6.99 (d, *J* = 8.8 Hz, 2H), 4.11 (t, *J* = 6.4 Hz, 2H), 4.04 (t, *J* = 6.6 Hz, 2H), 3.59 (t, *J* = 6.6 Hz, 2H), 1.85 (m, 6H), 1.61-1.36 (m, 10H), 0.58 (t, *J* = 7.87 Hz, 2H), 0.11 (s, 9H), 0.09 (s, 6H), 0.05 (s, 6H); ^{13}C NMR (100 MHz, $CDCl_3$) δ 161.2, 158.2, 151.4, 144.2, 130.4, 129.4, 114.9, 69.1, 68.5,

45.3, 33.6, 32.8, 29.6, 29.4, 27.0, 26.2, 25.7, 23.6, 18.6, 2.2, 1.7, 0.6; LRMS (EI) *m/z* 610 (M^+,38), 574 (60), 511 (5), 475 (11), 394 (1), 393 (5), 361 (2), 306 (4), 270 (3), 223 (5), 222 (11), 221 (100), 188 (17), 187 (4), 119 (2), 73 (13); HRMS (EI) *m/z* calcd for $C_{29}H_{51}{}^{35}ClN_2O_4Si_3$ 610.2845, found 610.2822.

5-(7-Chloroheptyloxy)-2-(4-hydroxyphenol)pyrimidine (2.6) The procedure used for the preparation of **2.3** was repeated with 7-chloro-1-heptanol (0.32 g, 2.13 mmol) and 2-(4-hydroxyphenyl)-5-pyrimidinol (0.40g, 2.13mmol). The crude product was purified by flash chromatography on silica gel (25% EtOAc/hexanes) to give 0.34 g (50%) of **2.6** as white solid: mp. 127-129^oC; ^1H NMR (300 MHz, $CDCl_3$) δ 8.43 (s, 2H), 8.26 (d, *J* = 8.6 Hz, 2H), 6.93 (d, *J* = 8.6 Hz, 2H), 6.33 (s,1H), 4.10 (t, *J* = 6.3 Hz, 2H), 3.57 (t, *J* = 6.6 Hz, 2H), 1.83 (m, 4H), 1.54-1.41 (m, 6H); ^{13}C NMR (100MHz, $CDCl_3$) δ 158.0, 157.6, 151.7, 144.3, 142.4, 129.8, 115.9, 69.3, 45.4, 32.9, 29.4, 29.0, 27.1, 26.1; LRMS (EI) *m/z* 320 (M^+,8), 284 (8), 229(1), 189 (6), 188 (100), 163(3), 159(6), 133 (2), 132(12), 119 (15), 105(24), 91(5), 77 (12), 55(18); HRMS (EI) *m/z* calcd for $C_{17}H_{21}{}^{35}ClN_2O_2$ 320.1292, found 320.1305.

5-(7-Chloroheptyloxy)-2-(4-(11-(1,1,1,3,3,5,5-heptamethyltrisiloxanyl)undecyloxy)-phenyl)pyrimidine (1.13d) The procedure used for the preparation of **2.3** was repeated with **2.6** (0.15 g, 0.47 mmol) and 11-(1,1,1,3,3,5,5-heptamethyltrisiloxanyl)undecanol (0.20g, 0.52mmol). The crude product was purified by flash chromatography on silica gel (10% EtOAc/hexanes) to give 0.17 g (52%) of **1.13d** as white semi-solid. Prior to analysis by POM and DSC, the material was recrystallized three times from HPLC-grade ethanol; ^{1}H NMR (400 MHz, $CDCl_3$) δ 8.42 (s, 2H), 8.28 (d, *J* = 9.0 Hz, 2H), 6.98 (d, *J* = 9.0 Hz, 2H), 4.09 (t, *J* = 6.4 Hz, 2H), 4.03 (t, *J* = 6.6 Hz, 2H), 3. 56 (t, *J* = 6.7 Hz, 2H), 1.82 (m, 6H), 1.54-1.29 (m, 22H), 0.54 (t, *J* = 7.6 Hz, 2H), 0.10 (s, 9H), 0.07 (s, 6H), 0.03 (s, 6H); ^{13}C NMR (100 MHz, $CDCl_3$) δ 158.9, 156.0, 149.2, 142.0, 128.3, 127.2, 112.6, 67.0, 66.3, 43.2, 31.6, 30.7, 27.8-27.6 (several overlapping peaks), 27.5, 27.2, 26.8, 24.9, 24.3, 23.9, 21.4, 16.5, 0.0, -0.5, -1.6; LRMS (EI) *m/z* 694 (M^+,37), 662 (64), 658 (76), 643 (12), 437(1), 395(1), 321(3), 285 (8), 223 (18), 222 (100), 221 (82), 189 (70), 188 (55), 160 (2), 133 (2), 73 (40); HRMS (EI) *m/z* calcd for $C_{35}H_{63}{}^{35}ClN_2O_4Si_3$ 694.3784, found 694.3768.

5-(7-Chloroheptyloxy)-2-(4-(6-(1,1,1,3,3,5,5-heptamethyltrisiloxanyl)hexyloxy)-phenyl)pyrimidine (1.14d) The procedure used for the preparation of **2.3** was repeated with **2.6** (0.15 g, 0.47 mmol) and 6-(1,1,1,3,3,5,5-heptamethyltrisiloxanyl)hexanol (0.17 g, 0.52 mmol). The crude product was purified by flash chromatography on silica gel (10%

EtOAc/hexanes) to give 0.13 g (46%) of **1.14d** as a white semi-solid. Prior to analysis by POM and DSC, the material was recrystallized three times from HPLC-grade ethanol; ^{1}H NMR (300 MHz, $CDCl_3$) δ 8.43 (s, 2H), 8.29 (d, *J* = 8.9 Hz, 2H), 6.99 (d, *J* = 8.9 Hz, 2H), 4.10 (t, *J* = 6.5 Hz, 2H), 4.04 (t, *J* = 6.5 Hz, 2H), 3. 57 (t, *J* = 6.6 Hz, 2H), 1.83 (m, 6H), 1.54-1.29 (m, 14H), 0.57 (t, *J* = 7.8 Hz, 2H), 0.11 (s, 9H), 0.09 (s, 6H), 0.04 (s, 6H); ^{13}C NMR (100MHz, $CDCl_3$) δ 158.9, 156.0, 149.2, 142.0, 128.3, 127.2, 112.6, 67.0, 66.3, 43.2, 31.6, 30.7, 27.6, 27.3, 26.8, 24.9, 24.3, 23.9, 21.4, 16.5, 0.0, -0.5, -1.6; LRMS (EI) *m/z* 624 (M^+,35), 622 (22), 588 (12), 586 (10), 525(2), 488(1), 393(4), 377(1), 320(8), 284 (4), 238(6), 223 (12), 222 (20), 221 (100), 188 (32), 187(6), 133 (12), 95 (10), 73 (70); HRMS (EI) *m/z* calcd for $C_{30}H_{53}{}^{35}ClN_2O_4Si_3$ 624.3002, found 624.3002.

5-(10-Chlorodecyloxy)-2-(4-hydroxyphenol)pyrimidine (2.7) The procedure used for the preparation of **2.3** was repeated with 10-chloro-1-decanol (0.41 g, 2.13 mmol) and 2-(4-hydroxyphenyl)-5-pyrimidinol (0.40 g, 2.13 mmol). The crude product was purified by flash chromatography on silica gel (25% EtOAc/hexanes) to give 0.40 g (52%) of **2.7** as white solid: mp. 79-81^{o}C; ^{1}H NMR (400 MHz, $CDCl_3$) δ 8.35 (s, 2H), 8.12 (d, *J* = 8.7 Hz, 2H), 6.80 (d, *J* = 8.7 Hz, 2H), 6.56 (s,1H), 4.00 (t, *J* = 6.5 Hz, 2H), 3.46 (t, *J* = 6.7 Hz, 2H), 1.72 (m, 4H), 1.40-1.24 (m, 12H); ^{13}C NMR (100MHz, $CDCl_3$) δ 157.8, 157.6, 151.2, 143.9, 130.0, 129.3, 115.6, 69.0, 45.2, 32.6, 31.0, 29.4, 29.3, 29.1, 28.9, 26.9, 23.8;

LRMS (EI) *m/z* 362 (M^+,38), 327 (2), 189 (7), 188 (100), 132 (7), 119 (8), 69 (2), 55(5); HRMS (EI) *m/z* calcd for $C_{20}H_{27}{}^{35}ClN_2O_2$ 362.1761, found 362.1756.

5-(10-Chlorodecyloxy)-2-(4-(11-(1,1,1,3,3,5,5-heptamethyltrisiloxanyl)undecyloxy)-phenyl)pyrimidine (1.13e) The procedure used for the preparation of **2.3** was repeated with **2.7** (0.15 g, 0.41 mmol) and 11-(1,1,1,3,3,5,5-heptamethyltrisiloxanyl)undecanol (0.18g ,0.45mmol). The crude product was purified by flash chromatography on silica gel (10% EtOAc/hexanes) to give 0.16 g (53%) of **1.13e** as white solid. Prior to analysis by POM and DSC, the material was recrystallized three times from HPLC-grade ethanol;^{1}H NMR (500 MHz, $CDCl_3$) δ 8.44 (s, 2H), 8.29 (d, *J* = 8.8 Hz, 2H), 6.99 (d, *J* = 8.8 Hz, 2H), 4.10 (t, *J* = 6.5 Hz, 2H), 4.04 (t, *J* = 6.6 Hz, 2H), 3.56 (t, *J* = 6.8 Hz, 2H), 1.81 (m, 6H), 1.52-1.30 (m, 28H), 0.55 (t, *J* = 7.6 Hz, 2H), 0.11 (s, 9H), 0.08 (s, 6H), 0.04 (s, 6H); ^{13}C NMR (125MHz, $CDCl_3$) δ 161.1, 158.1, 151.5, 144.2, 130.4, 129.4, 114.8, 69.3, 68.5, 45.6, 33.9, 33.0, 30.1-29.3 (several overlapping peaks), 27.3, 26.5, 26.3 23.6, 18.7, 2.2,1.7 0.6; LRMS (EI) *m/z* 736 (M^+,42), 721 (6), 700 (2), 515 (6), 375 (3), 371 (6), 362 (11), 293 (4), 231 (8), 223 (13), 222 (23), 221 (100), 188 (54), 123 (8), 119 (15), 117 (19), 73 (19), 55(30); HRMS (EI) *m/z* calcd for $C_{38}H_{69}{}^{35}ClN_2O_4Si_3$ 736.4254, found 736.4227.

5-(10-Chlorodecyloxy)-2-(4-(6-(1,1,1,3,3,5,5-heptamethyltrisiloxanyl)hexyloxy)-phenyl)pyrimidine (1.14e) The procedure used for the preparation of **2.3** was repeated with **2.7** (0.20 g, 0.55 mmol) and 6-(1,1,1,3,3,5,5-heptamethyltrisiloxanyl)hexanol (0.20 g, 0.61 mmol). The crude product was purified by flash chromatography on silica gel (10% EtOAc/hexanes) to give 0.19 g (51%) of **1.14e** as a white solid. Prior to analysis by POM and DSC, the material was recrystallized three times from HPLC-grade ethanol; ^{1}H NMR (400 MHz, $CDCl_3$) δ 8.33 (s, 2H), 8.18 (d, *J* = 8.9 Hz, 2H), 6.88 (d, *J* = 8.9 Hz, 2H), 3.99 (t, *J* = 6.5 Hz, 2H), 3.93 (t, *J* = 6.6 Hz, 2H), 3.45 (t, *J* = 6.7 Hz, 2H), 1.85 (m, 6H), 1.39-1.23 (m, 18H), 0.47 (t, *J* = 7.9 Hz, 2H), 0.00 (s, 9H), -0.02 (s, 6H), -0.07 (s, 6H); ^{13}C NMR (100 MHz, $CDCl_3$) δ 158.9, 155.9, 149.3, 142.0, 128.2, 127.1, 112.6, 67.1, 66.3, 43.3, 31.3, 30.8, 27.6, 27.5, 27.4, 27.3, 27.0, 25.0, 24.0, 23.9, 21.3, 16.4, -0.0, -0.6, -1.6; LRMS (EI) *m/z* 666 (M^+,53), 567 (7), 531 (2), 501 (2), 393 (3), 362 (7), 326 (2), 264 (7), 223 (11), 222 (18), 221 (100), 188 (27), 149 (32), 105 (32), 73 (24); HRMS (EI) *m/z* calcd for $C_{33}H_{59}{}^{35}ClN_2O_4Si_3$ 666.3471, found 666.3480.

((*E*)-(*2R,3R*)-3-(5-Chloropentyl)oxiran-2-yl)methanol (3.5) In a flame-dried 200mL 3-necked flask under an argon atmosphere, a solution of *tert*-butyl hydroperoxide solution (~5.5 M in decane, 6.7 mL, 36.9 mmol) was added by syringe over 5 min to a solution of *D*-(-)-diethyl tartrate (0.23 g, 0.19 mL, 1.1 mmol) and titanium(IV)

isopropoxide (0.26 g, 0.27 mL, 0.92 mmol) in dry CH_2Cl_2 (80 mL) stirred over 0.7 g of powered 4Å molecular sieves and cooled to -20 ^oC.

The solution was stirred at -20^oC for 30 min , then a solution of (*E*)-9-chloronon-2-en-1-ol (2.9 g, 17.8 mmol) in dry CH_2Cl_2 (12 mL) previously dried over molecular sieves under argon for 30 min was added over 20min while keeping the temperature between -15 ^oC to -20 ^oC. After stirring at -20 ^oC for 3.5 h, the mixture was warmed to -10 ^oC and a solution of $FeSO_4 \cdot 7H_2O$ (5.94 g, 21.4 mmol) and citric acid (2.05 g, 10.7 mmol) in H_2O (30 mL) was added. After stirring for 5 minutes, the organic layer was separated and the aqueous layer was extracted with ether (2×25 mL). To the combined organic layer was added a cold solution of 30% NaOH in brine, the mixture was stirred for 2 hours at 0^oC and H_2O was added (25 mL). The organic layer was separated and the aqueous layer was extracted with ether (2×25 mL). The combined organic layers were dried ($MgSO_4$), concentrated and the residue was purified by flash chromatography on silica gel (33% EtOAc/hexanes) to give a clear oil. Recrystallization from CH_2Cl_2/Hexane gave **3.5** (1.95 g, 61%) as a white solid. Analysis by SCF (supercritical fluid) chiral HPLC (Daicd chiraled OD Column, 20% MeOH, 2 mL/min, 200 bar) showed the alcohol to be 92% ee: mp 23-25 ^oC; ^1H NMR (400 MHz, $CDCl_3$) δ 3.91 (m, 1H), 3.58 (m, 1H), 3.52 (t, *J* = 6.6 Hz, 2H), 3.00-2.76 (m, 2H), 1.77-1.23 (m, 8H); ^{13}C NMR (100 MHz, $CDCl_3$) δ 61.9, 58.6, 56.0, 45.2, 32.7, 31.7, 26.9, 25.6; LR MS (ES)

m/z 201 ([M+Na]$^+$, 100), 192(10), 181(28), 180(12), 162(26), 143(6), 121(12); HRMS (ES) *m/z* calcd for $C_8H_{15}O_2Na^{35}Cl$([M+Na]$^+$): 201.0658, found 201.0653.

5-(((*E*)-(*2R,3R*)-3-(5-Chloropentyl)oxiran-2-yl)methoxy)-2-(4-hydroxyphenol)-pyrimidine (3.6) The procedure used for the preparation of **2.3** was repeated with **3.5** (0.34 g, 1.7 mmol) and 2-(4-hydroxyphenyl)-5-pyrimidinol (0.32 g, 1.7 mmol). The crude product was purified by flash chromatography on silica gel (20% EtOAc/hexanes) to give 0.42 g (67%) of **3.6** as a white solid: mp. 129-131^{o}C; ^{1}H NMR (400 MHz, $CDCl_3$) δ 8.47 (s, 2H), 8.27 (d, *J* = 8.7 Hz, 2H), 6.93 (d, *J* = 8.7 Hz, 2H), 4.97 (s, 1H), 4.37 (dd, *J* = 11.0, 3.0 Hz, 1H), 4.10 (dd, *J* = 11.0, 5.7 Hz, 1H), 3.57 (t, *J* = 6.6 Hz, 2H), 3.17 (m, 1H), 3.03 (m, 1H), 1.84-1.26 (m, 6H); ^{13}C NMR (100 MHz, $CDCl_3$) δ 158.2, 157.9, 150.7, 144.2, 129.8, 129.5, 115.6, 69.2, 56.3, 55.7, 44.9, 32.4, 31.3, 26.6, 25.2; LRMS (EI) *m/z* 348 (M$^+$,90), 214 (4), 189 (12), 188(100), 159 (28), 132 (43), 119 (48), 81 (43); HRMS (EI) *m/z* calcd for $C_{18}H_{21}{}^{35}ClN_2O_3$ 348.1241, found 348.1246.

5-(((*E*)-(*2R,3R*)-3-(5-Chloropentyl)oxiran-2-yl)methoxy)-2-(4-(11-(1,1,1,3,3,5,5-heptamethyltrisiloxanyl)undecyloxy)phenyl)pyrimidine (1.15) The procedure used for the preparation of **2.3** was repeated with **3.6** (0.15 g, 0.43 mmol) and 11-(1,1,1,3,3,5,5-heptamethyltrisiloxanyl)undecanol (0.20 g, 0.51 mmol). The crude product was purified by flash chromatography on silica gel (17% EtOAc/hexanes) to give

0.15 g (47%) of **1.15** as white solid. Prior to analysis by POM and DSC, the material was recrystallized three times from HPLC-grade ethanol; ^{1}H NMR (400 MHz, $CDCl_3$) δ 8.47 (s, 2H), 8.30 (d, *J* = 8.5 Hz, 2H), 6.99 (d, *J* = 8.5 Hz, 2H), 4.36 (dd, *J* = 11.3, 3.0 Hz, 2H), 4.10 (dd, *J* = 11.3, 5.50 Hz, 2H), 4.04 (t, *J* = 6.3 Hz, 2H), 3.58 (m, 2H), 3.10 (m, 2H), 1.86-1.30 (m, 24H), 0.55 (t, *J* = 6.8 Hz, 2H), 0.11 (s, 9H), 0.08 (s, 6H), 0.04 (s, 6H); ^{13}C NMR (100 MHz, $CDCl_3$) δ 159.1, 156.6, 148.8, 142.3, 128.1, 127.3, 112.7, 67.4, 66.3, 54.4, 53.8, 43.0, 31.6, 30.6, 29.5, 27.8-27.5 (several overlapping peaks), 24.8, 24.2, 23.4, 21.4, 16.5, 0.0, -0.5, -1.6; LRMS (EI) *m/z* 722 (M^+,11), 707 (2), 562 (2), 348 (2), 223 (4), 222 (9), 221 (100), 207 (9), 159 (3), 81 (2), 73 (9); HRMS (EI) *m/z* calcd for $C_{36}H_{63}{}^{35}ClN_2O_5Si_3$ 722.3733, found 722.3730.

5-(((*E*)-(*2R,3R*)-3-(5-Chloropentyl)oxiran-2-yl)methoxy)-2-(4-(6-(1,1,1,3,3,5,5-heptamethyltrisiloxanyl)hexyloxy)phenyl)pyrimidine (1.16) The procedure used for the preparation of **2.3**was repeated with **3.6** (0.15 g, 0.43 mmol) and 6-(1,1,1,3,3,5,5-heptamethyltrisiloxanyl)hexanol (0.16 g, 0.50 mmol). The crude product was purified by flash chromatography on silica gel (17% EtOAc/hexanes) to give 0.13 g (46%) of **1.16** as a white solid. Prior to analysis by POM and DSC, the material was recrystallized three times from HPLC-grade ethanol; ^{1}H NMR (400 MHz, $CDCl_3$) δ 8.46 (s, 2H), 8.28 (d, *J* = 9.0 Hz, 2H), 6.98 (d, *J* = 9.0 Hz, 2H), 4.34 (dd, *J* = 11.0, 3.1 Hz, 1H), 4.08 (dd, *J* = 11.0, 5.6 Hz, 1H), 4.03 (t, *J* = 6.6 Hz, 2H), 3.15(m, 1H), 3.01 (m, 1H) , 1.81

(m,4H), 1.72-1.27 (m, 14H), 0.57 (t, J = 7.9 Hz, 2H), 0.10 (s, 9H), 0.08 (s, 6H), 0.03 (s, 6H); ^{13}C NMR (100 MHz, $CDCl_3$) δ 159.1, 156.5, 148.8, 142.3, 128.0, 127.3, 112.6, 67.4, 66.3, 54.4, 53.8, 43.0, 31.6, 30.6, 29.5, 27.4, 24.8, 24.2, 23.4, 21.4, 16.5, 0.0, -0.5, -1.6; LRMS (EI) *m/z* 652 (M^+,22), 637 (2), 553 (2), 492 (2), 435 (2), 393 (3), 348(4), 286(2), 241(4), 223 (10), 222 (19), 221 (100), 188 (10), 129 (28), 81(20), 73 (72); HRMS (EI) *m/z* m/z calcd for $C_{31}H_{53}{}^{35}ClN_2O_5Si_3$ 652.2951, found 652.2936.

4.2 Mesophase Characterization

Phase transition temperatures of the liquid crystal materials were determined on heating and cooling by DSC (Perkin-Elmer DSC-7 and TA (Thermal Analysis) DSC Q2000, 5K min^{-1}). The liquid crystal phase assignments were made by texture analysis using polarized optical microscopy on thin films of the samples in ITO glass cells with rubbed Nylon (4.0μm spacing, 0.25 cm^2 addressed area, AWAT PPW, Poland), and on untreated glass slides with a cover slip using a Nikon Eclipse E600 POL polarized microscope fitted with a Nikon Coolpix 995 digital camera, and a Linkam LTS 350 hot stage. The 2nd order SmA (SmA*)-SmC (SmC*) phase transition temperatures were determined based on changes in texture observed between crossed polarizers. Small angle X-ray scattering (SAXS) data from unaligned samples (filled into Mark capillary tubes of 0.7 mm diameter) were obtained using a Kratky compact camera (A. Paar) equipped with a temperature controller (A. Paar) and a one-dimensional electronic detector (M.Braun).

4.3 Ferroelectric and Electro-optical Properties

4.3.1 Sample Preparation

Samples for ferroelectric polarization measurements were prepared by loading the materials in the isotropic phase by capillary action into ITO glass cells with rubbed Nylon (4.0 μm spacing, 0.25 cm^2 addressed area, AWAT PPW, Poland). Cell thicknesses were determined by capacitance measurement of an empty cell using a LC Vision LCAS 1 liquid crystal analysis system. Each cell was heated to the isotropic phase under an AC triangular wave (100 Hz, 6 V/μm), unless otherwise noted, and held until any bubbles in the addressed area disappeared. Alignment was obtained by applying a high frequency AC field (100 Hz) to the filled cells while slowly cooling the mixtures from the isotropic phase to the SmA* phase (2 ^oC /min).

4.3.2 Properties Measurements

The spontaneous polarization was measured as a function of temperature using the triangular wave method (6 V μm^{-1}, 100 Hz)[5] as implemental on the LC Vivian LCAS 1 analysis system, and optical tilt angles (θ_{opt}) were measured by polarized microscopy as half the rotation between the two extinction positions corresponding to opposite signs of the applied field. The sign of P_S along the polar axis was assigned from the relative configuration of the electric field and the switching position of the sample according to

the established convention.[6] Optical rise times were determined using the LCAS 1 system in conjunction with a FLC Electronics photo detector fitted on the polarizing microscope with a 1/4λ optical compensator positioned between the sample and analyzer; $\tau_{10\text{-}90}$ values are reported as the time required for a 10% to 90% change of optical signal in response to a 6 V μm^{-1} square wave ac field. Rotational viscosities were measured using the LCAS1 system according to Escher *et al*.[7]

4.4 References

(1) Fischer, C.; Smith, S. W.; Powell, D. A.; Fu, G. C. *J. Am. Chem. Soc.* **2006**, *128*, 1472-1473.

(2) Wilson, R. M.; Jen, W. S.; MacMillan, D. W. C. *J. Am. Chem. Soc.* **2005**, *127*, 11616-11617.

(3) Li, L.; Jones, C. D.; Magolan, J.; Lemieux, R. P. *J. Mater. Chem.* **2007**, *17*, 2313-2318.

(4) Mori, A.; Miyakawa, Y.; Ohashi, E.; Haga, T.; Maegawa, T.; Sajiki, H. *Org. Lett.* **2006**, *8*, 3279-3281.

(5) K. Miyasato, S. A., H. Takezoe, A. Fukuda and E. Kuze *Jpn. J. Appl. Phys.* **1983**, *22*, L661.

(6) Walba, D. M. *Adv. Synth. React. Solids* **1991**, *1*, 173-235.

(7) Escher, C.; Geelhaar, T.; Böhm, E. *Liq. Cryst.* **1988**, *3*, 467.

Chapter 5. Conclusions and Future Work

The primary goal of this thesis is to investigate the claim made by Giesselmann *et. al.* that a correlation exists between the temperature range of the SmA phase of de Vries-like materials and their de Vries character as defined by the reduction factor *R*. Another goal of this thesis is to further validate the hypothesis that combining structural elements promoting SmA and SmC phases in a single molecule increases de Vries character in order to design “de Vries-like” liquid crystals. The siloxane-terminated side-chain and chloro end-group were chosen as SmC promoter and SmA promoter, respectively.

In the first section, the syntheses and characterization of two homologous series of siloxane-terminated liquid crystals with 2-phenylpyrimidine cores and chloro-terminated side-chains (**1.13** and **1.14**) were achieved. These compounds form a broad SmC phase and a SmA phase with a temperature range that varies with the length of the chloro-terminated alkyl chain. The *R* values in series **1.13** range from 0.34 to 0.47 and in series **1.14**, from 0.44 to 0.53. In both series, the maximum layer contraction decreases with increasing SmA temperature range, which can be accounted for primarily by decreasing tilt angles as the SmA temperature range increases. Overall, there is no apparent correlation between *R* and the SmA temperature range. In general, series **1.13** is more de Vries-like than **1.14** due to the negative thermal expansion in the SmC phase. It is consistent with C_{11} siloxane being stronger SmC promoter than C_6 siloxane.

In the second section, the chiral 2-phenylpyrimidine trisiloxane materials with a (*R*, *R*)-2,3-epoxy-8-chlorooctyloxy side-chain (**1.15** and **1.16**) were synthesized and characterized in order to formulate ferroelectric SmC* mixtures using these new organosiloxane host materials. Compared to the non-chloro terminated compounds (**E11** and **E6**), the SmA temperature ranges of **1.15** and **1.16** are broader and the % maximum layer contraction of **1.15** and **1.16** are much smaller. The reduction of % maximum layer contraction is accounted for by decreasing optical tilt angles. It is consistent with the observations made in achiral series **1.13** and **1.14**. The fact that the *R* values of **1.15** and **1.16** are smaller than that of the parent compound **PhP1** also support the hypothesis of SmC/SmA frustration.

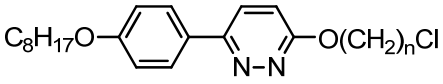

5.1

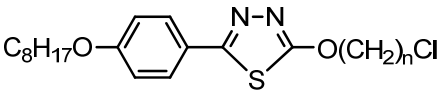

5.2

Further studies on SmC/SmA frustration will focus on the issue of designing more “de Vries-like” materials based on this hypothesis. Hence, the two series of mesogens **5.1** and **5.2** will be investigated, since the 6-phenylpyridazine and 2-phenyl-1,3,4-thiadiazole core are also known as strong SmC-promoting elements. Motivation for going with phenylpyridazine and thiazole was that the SmC-promoting element is not siloxane

end-group, which is problematic in terms of viscosity and alignment.

Appendix 1. ^{1}H NMR Spectra of Novel Compounds

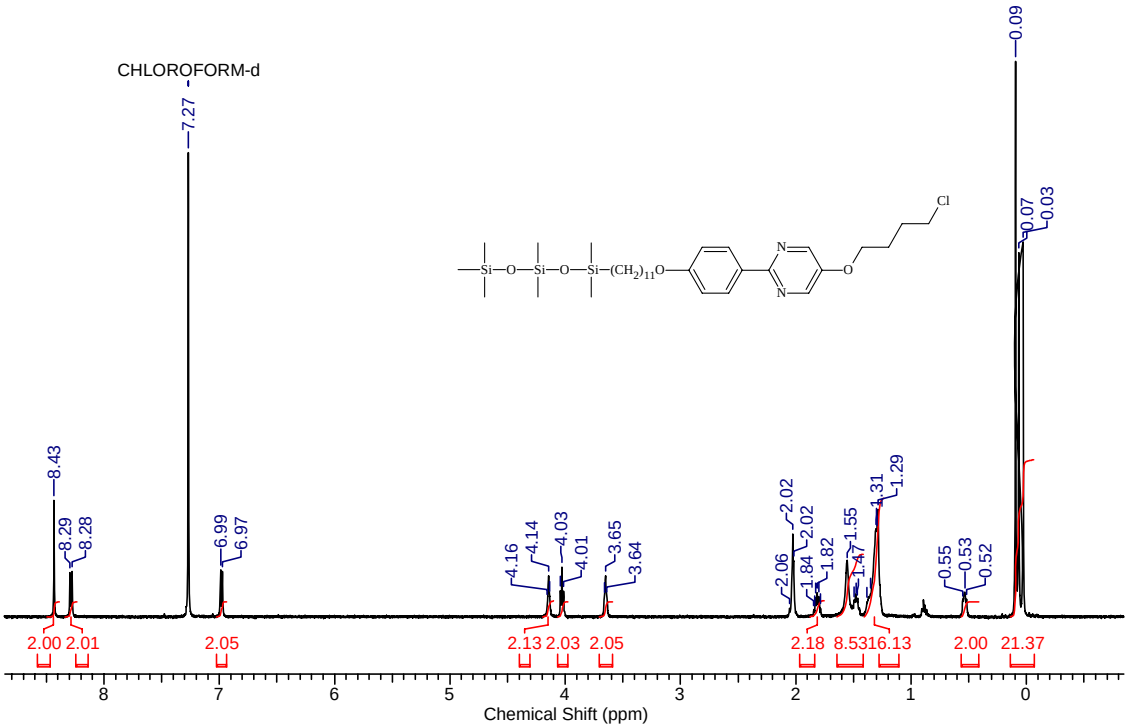

Figure A1-1: 400 MHz ^{1}H NMR spectrum of **1.13a**

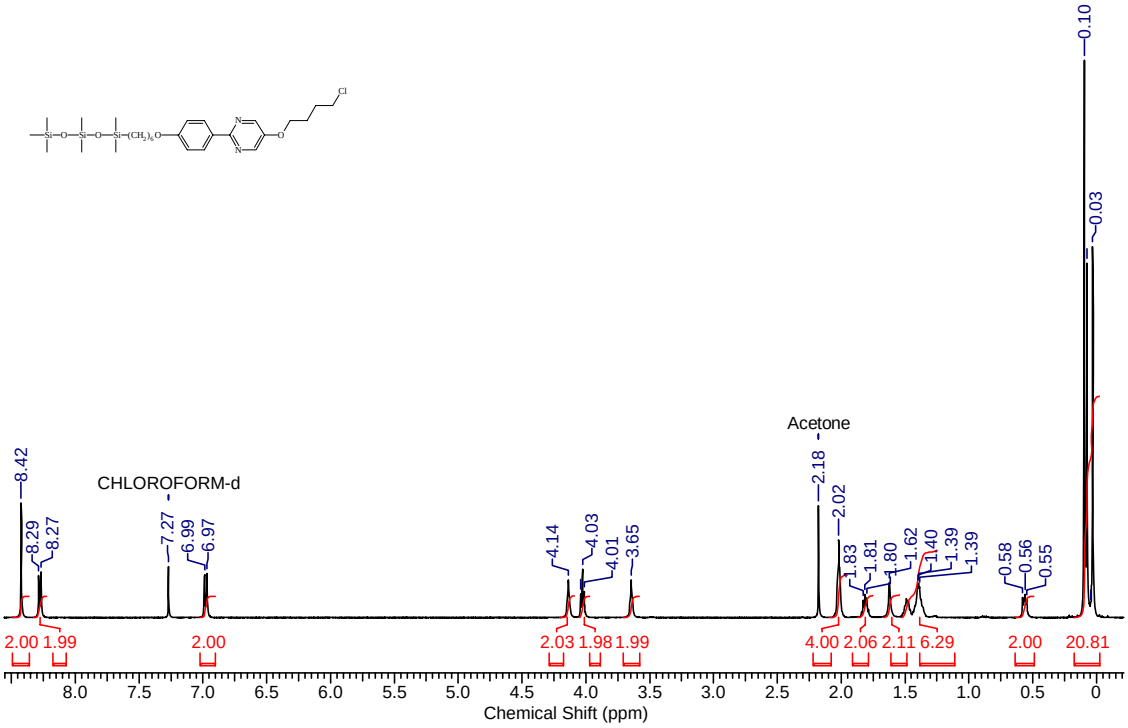

Figure A1-2: 400 MHz ^{1}H NMR spectrum of **1.14a**

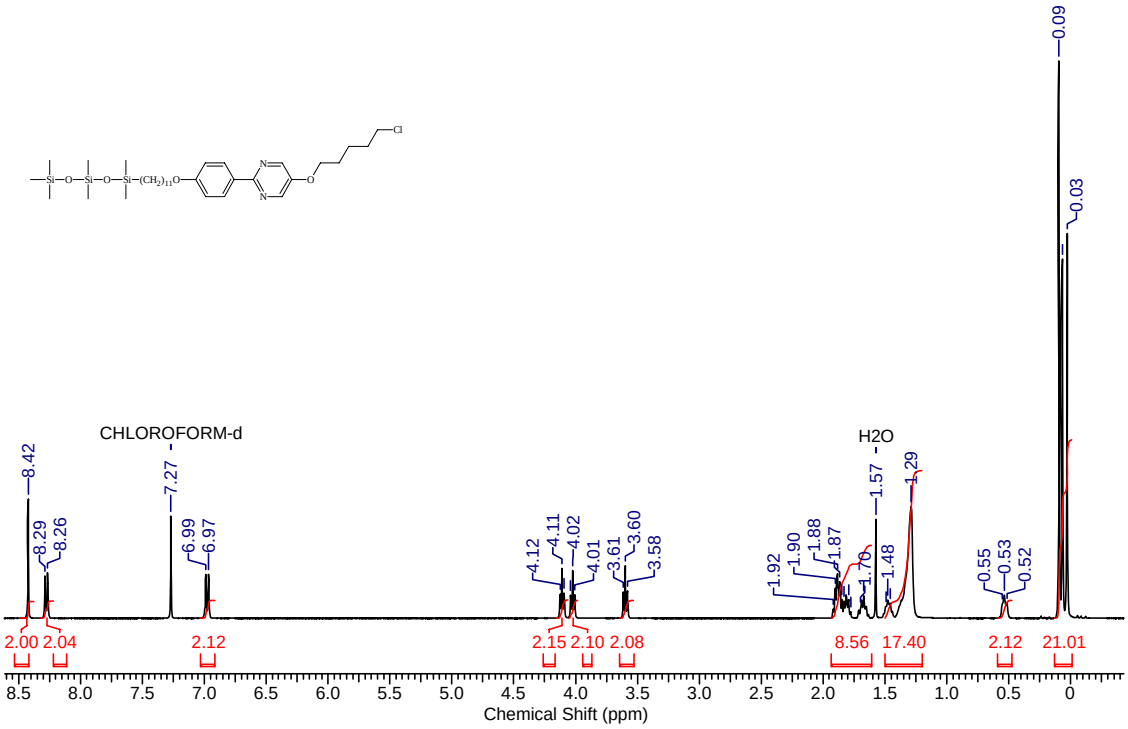

Figure A1- 3: 400 MHz ^{1}H NMR spectrum of **1.13b**

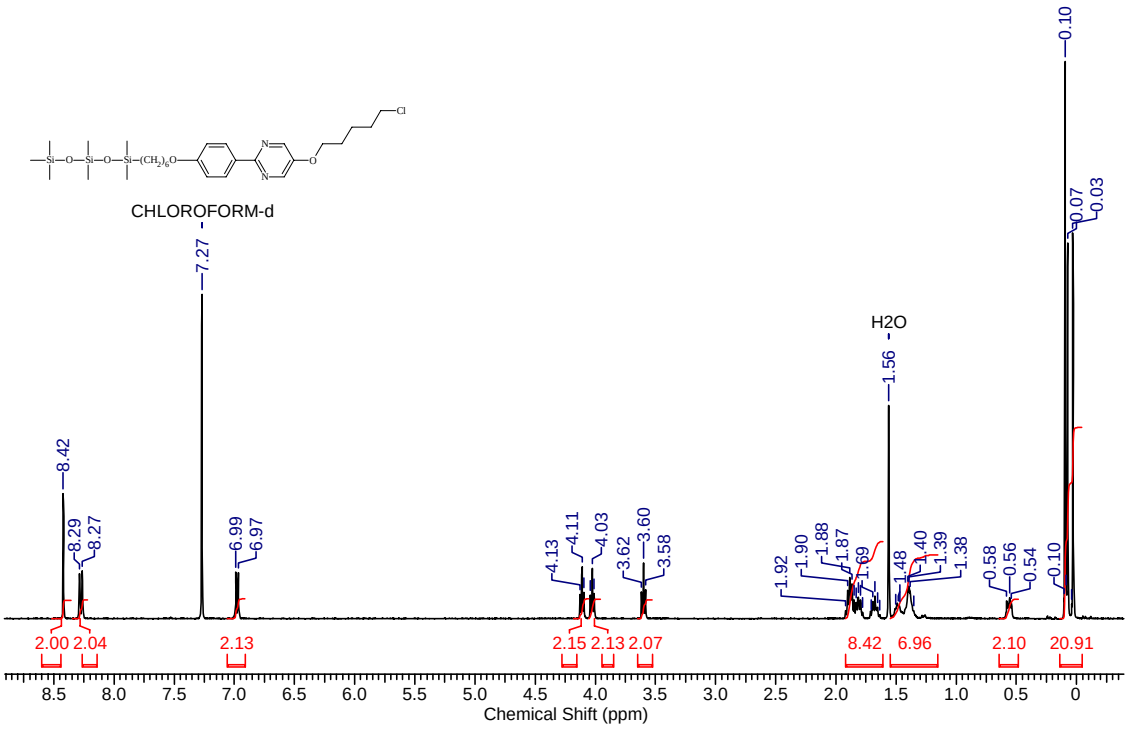

Figure A1-4: 400 MHz ^{1}H NMR spectrum of **1.14b**

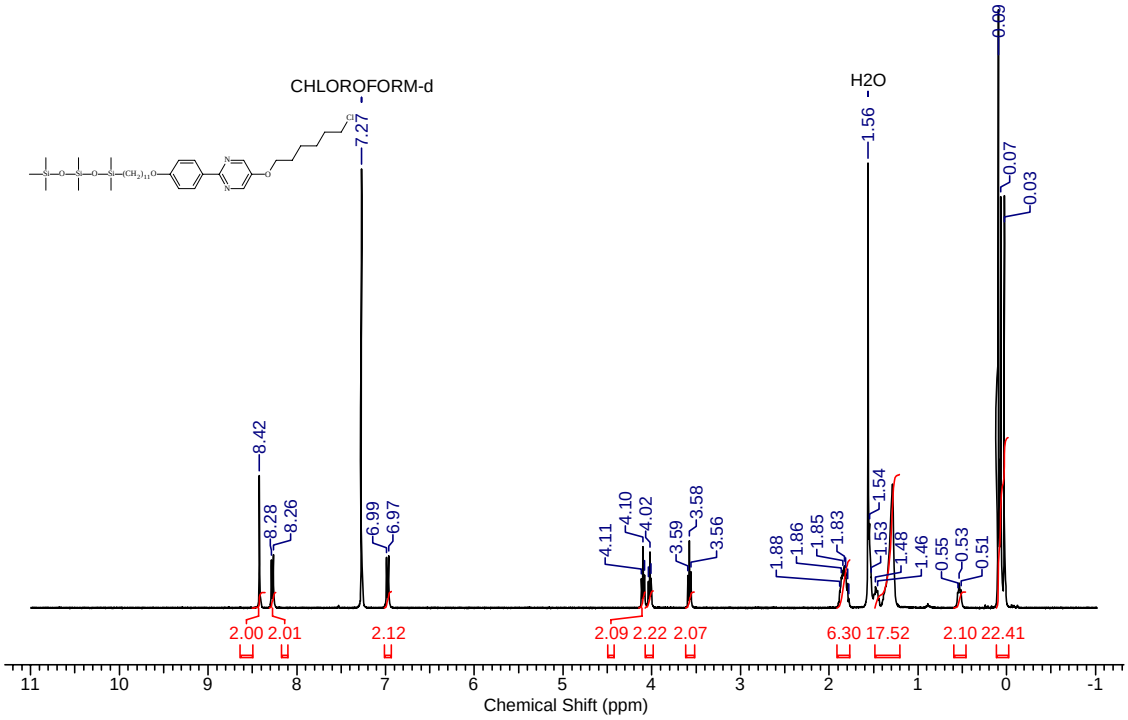

Figure A1-5: 400 MHz ^{1}H NMR spectrum of **1.13c**

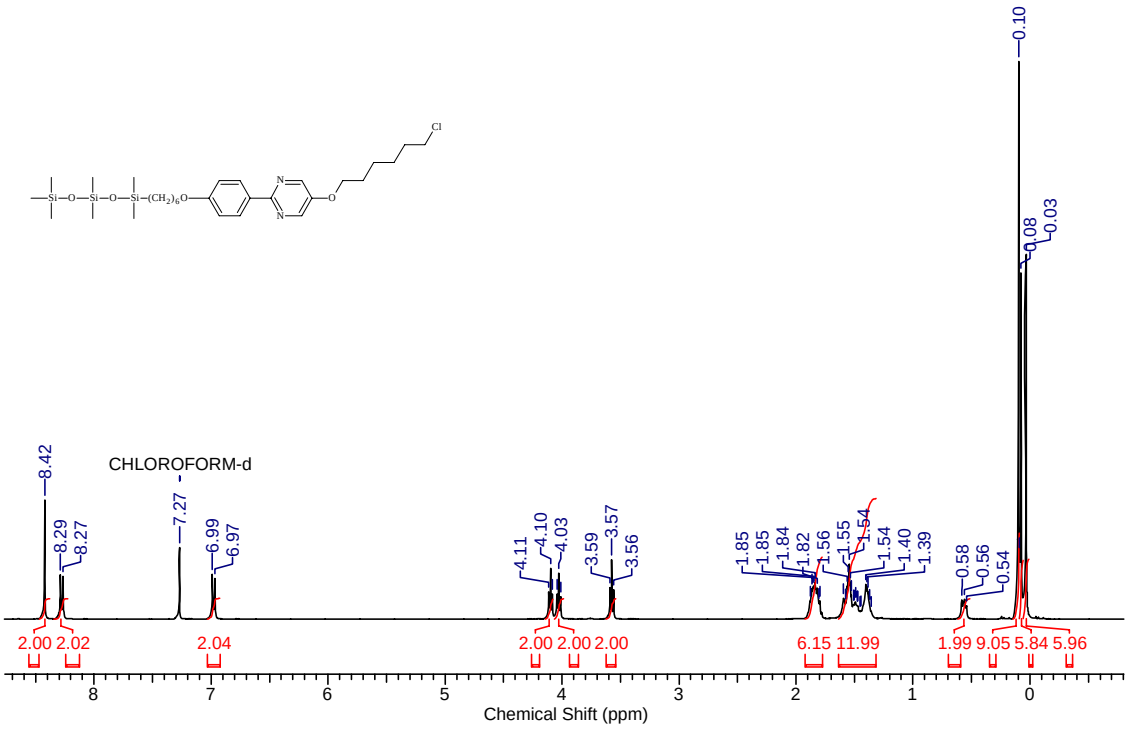

Figure A1-6: 400 MHz ^{1}H NMR spectrum of **1.14c**

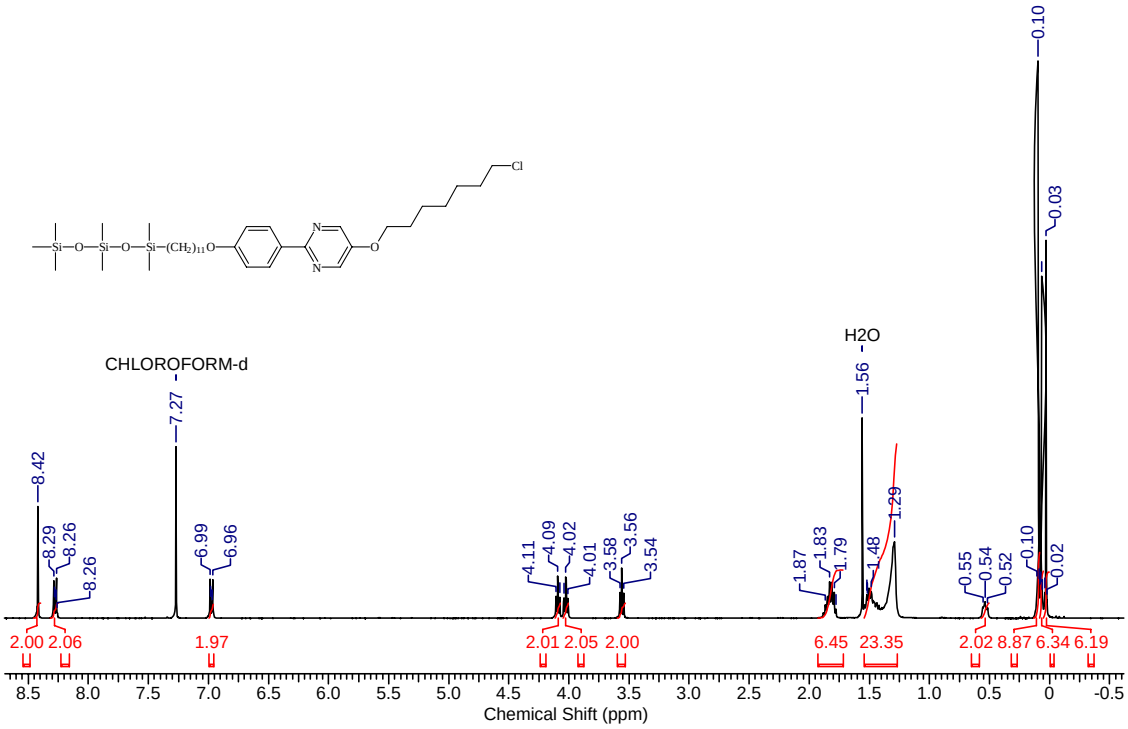

Figure A1-7: 400 MHz ^{1}H NMR spectrum of **1.13d**

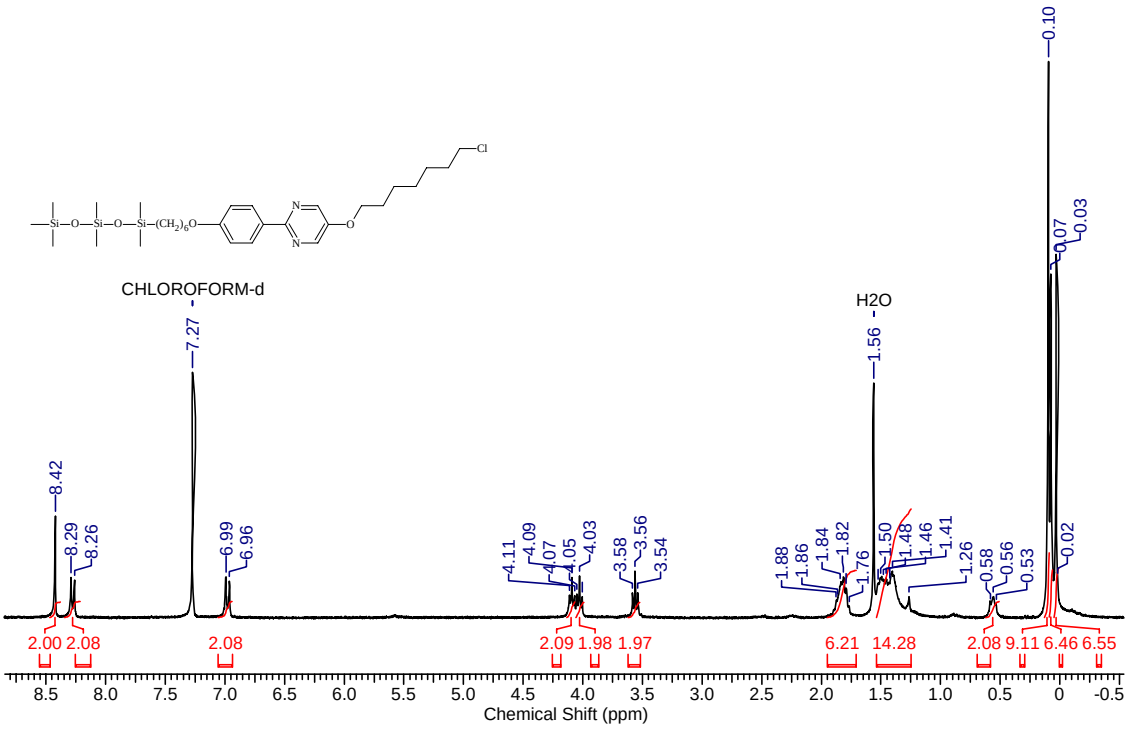

Figure A1-8: 400 MHz ^{1}H NMR spectrum of **1.14d**

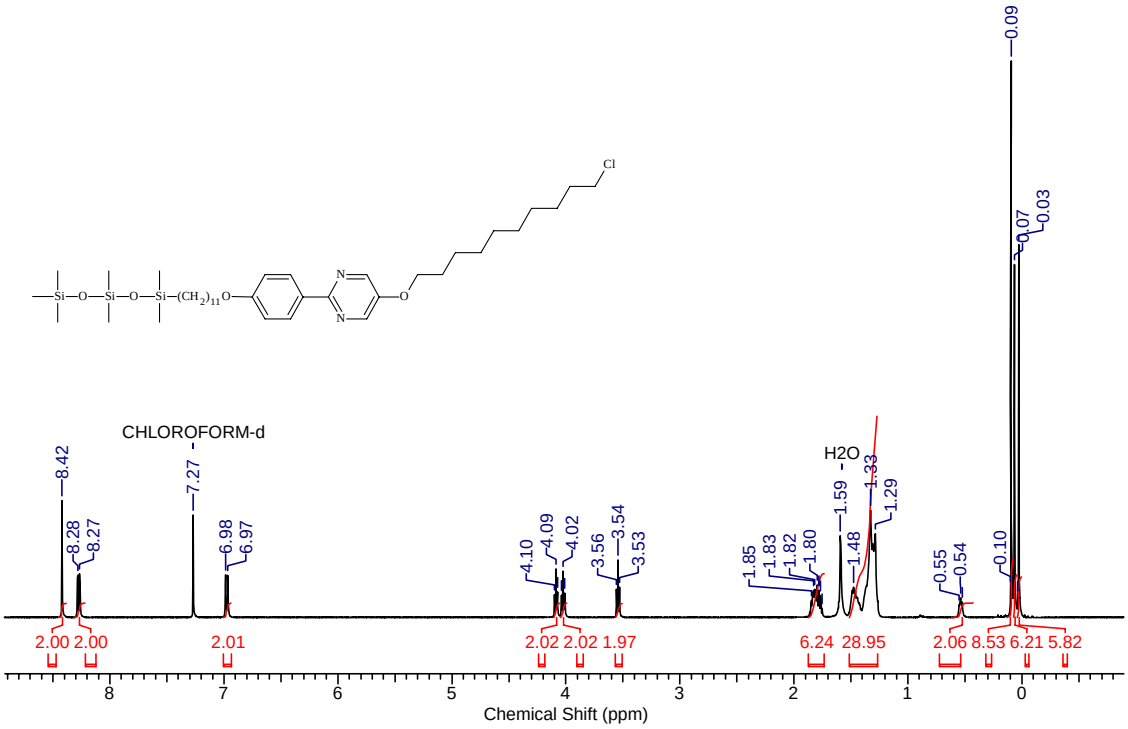

Figure A1-9: 400 MHz ^{1}H NMR spectrum of **1.13e**

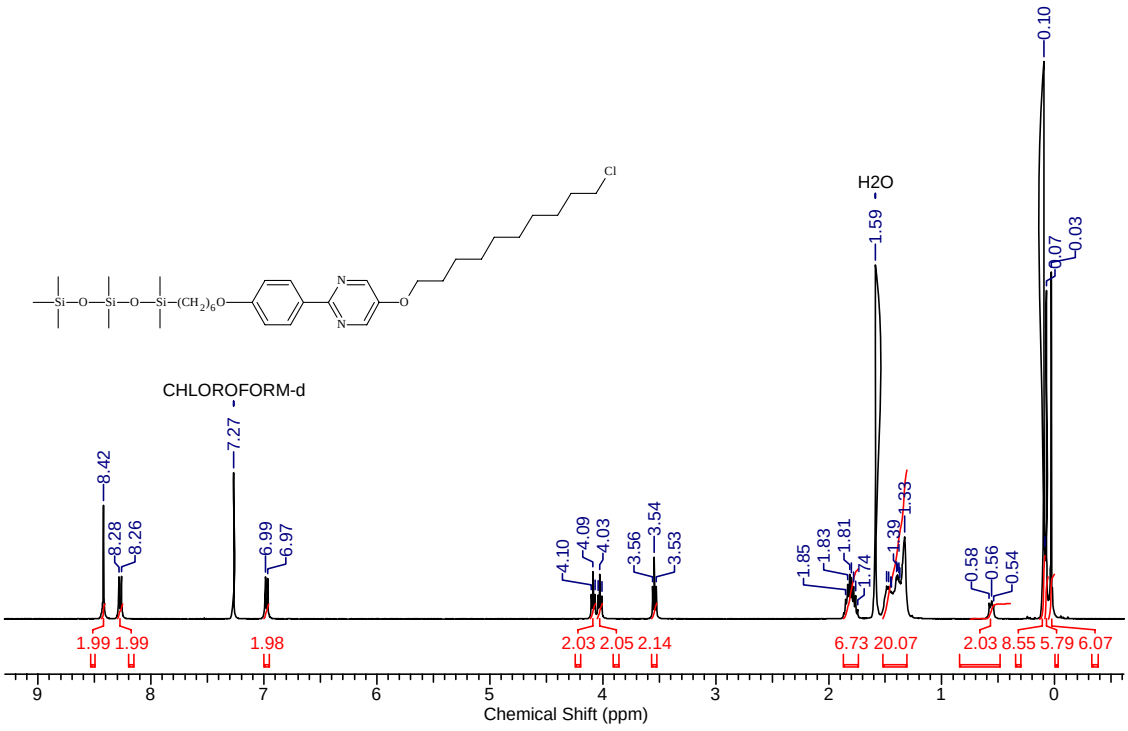

Figure A1-10: 400 MHz ^{1}H NMR spectrum of **1.14e**

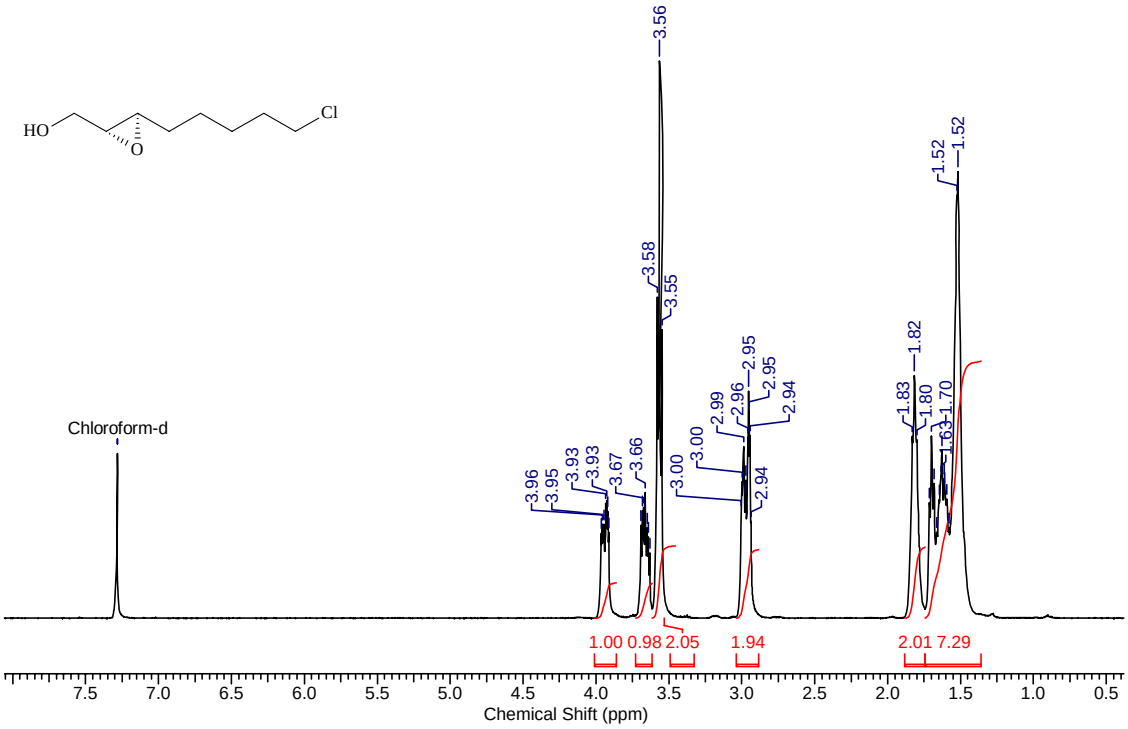

Figure A1-11: 400 MHz ^{1}H NMR spectrum of **3.5**

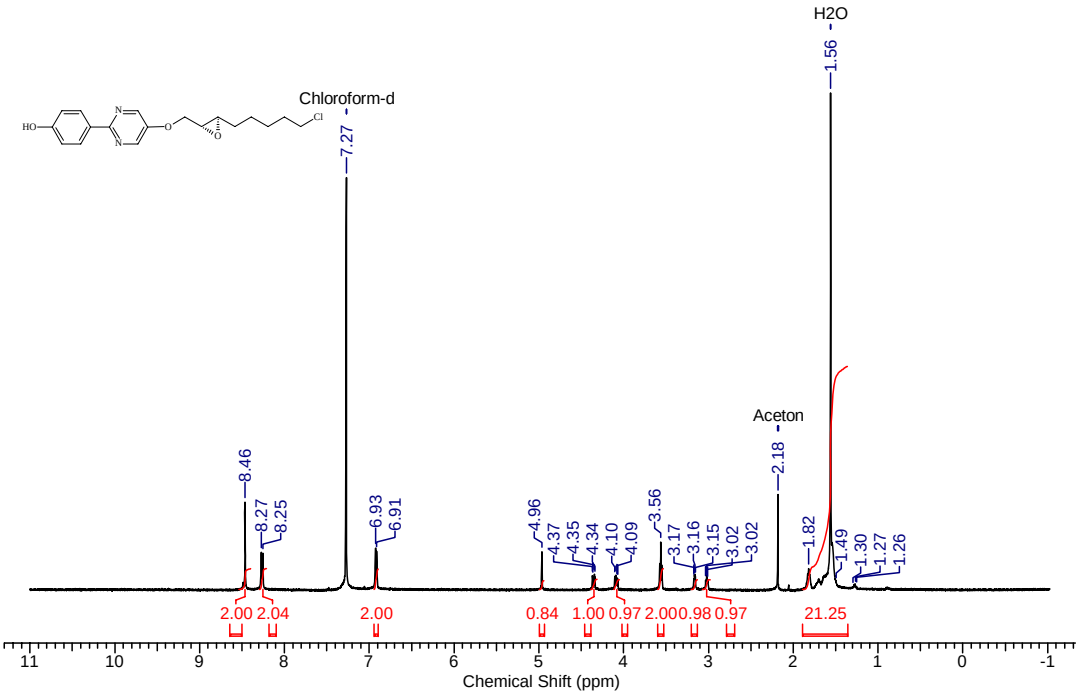

Figure A1-12:400 MHz ^{1}H NMR spectrum of **3.6**

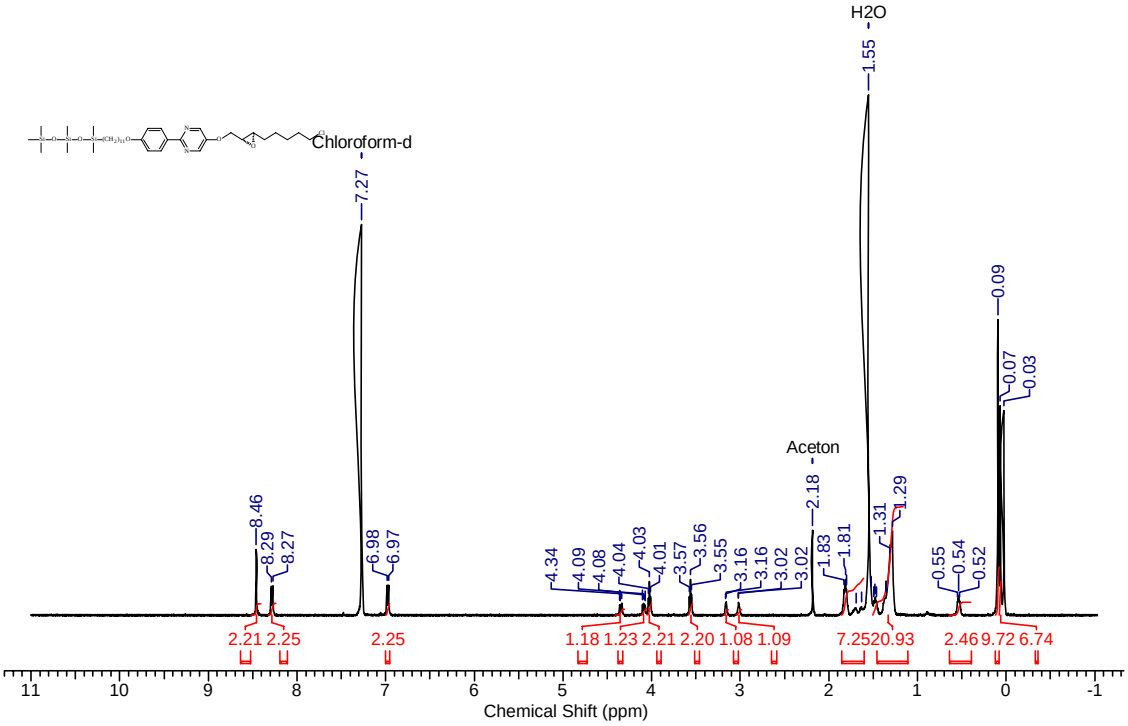

Figure A1-13: 400 MHz ^{1}H NMR spectrum of **1.15**

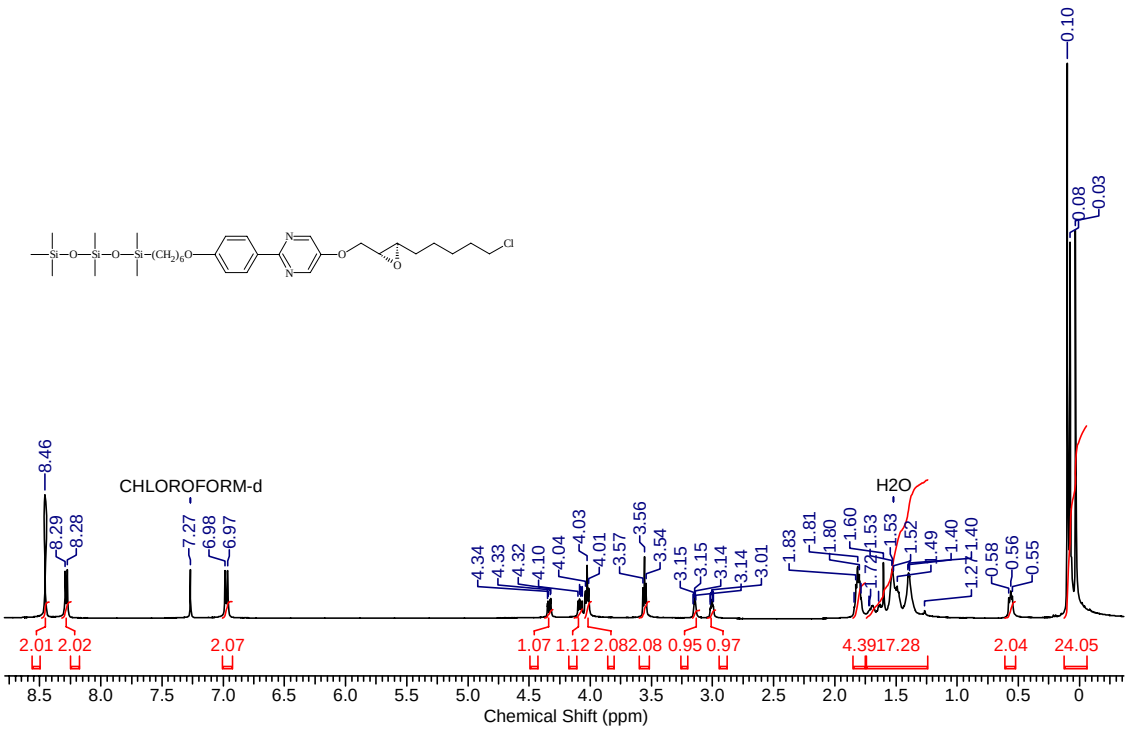

Figure A1-14: 400 MHz ^{1}H NMR spectrum of **1.16**

Appendix 2. DSC Profiles of Liquid Crystals

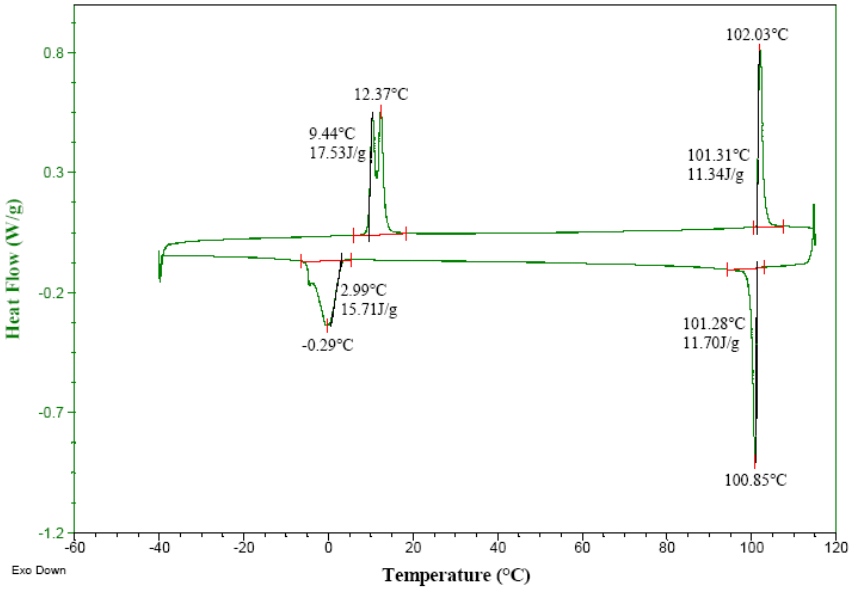

Figure A2-1: DSC profile for compound **1.13a** taken at a scan rate of 5K/min.

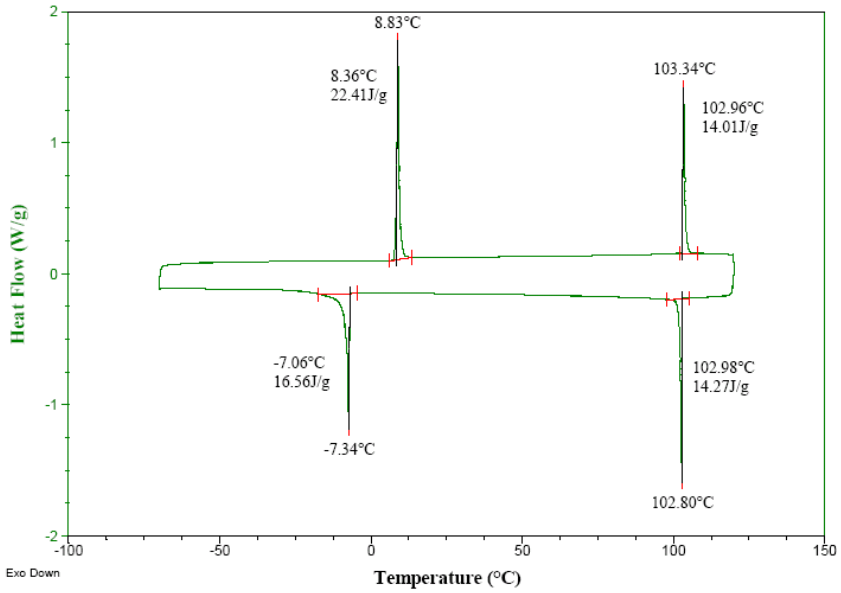

Figure A2-2: DSC profile for compound **1.13b** taken at a scan rate of 5K/min.

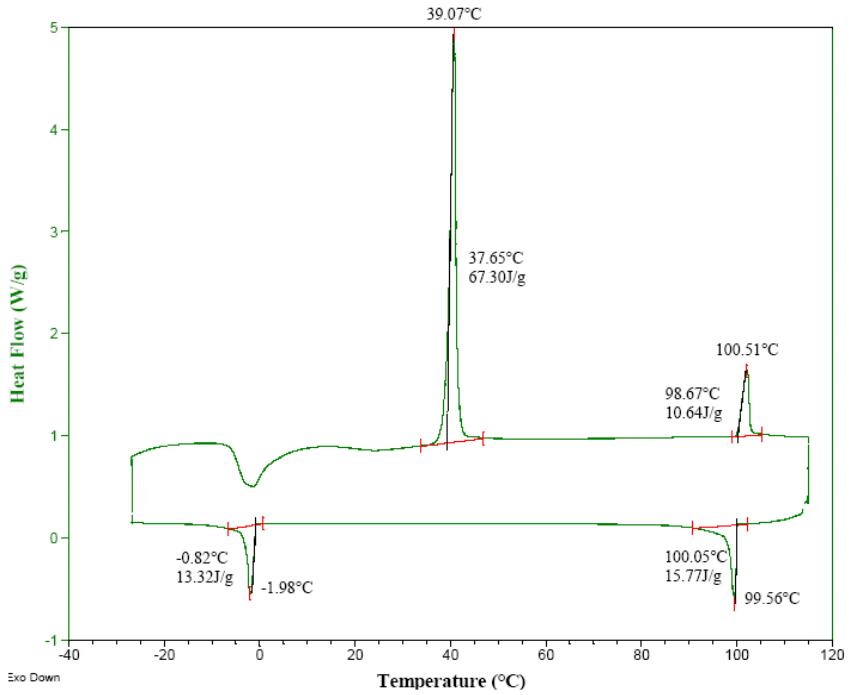

Figure A2-3: DSC profile for compound **1.13c** taken at a scan rate of 5K/min.

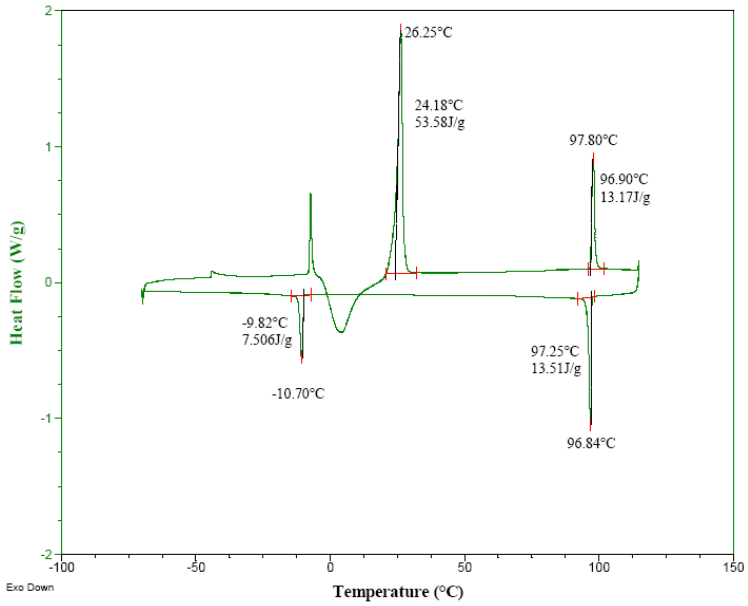

Figure A2-4: DSC profile for compound **1.13d** taken at a scan rate of 5K/min.

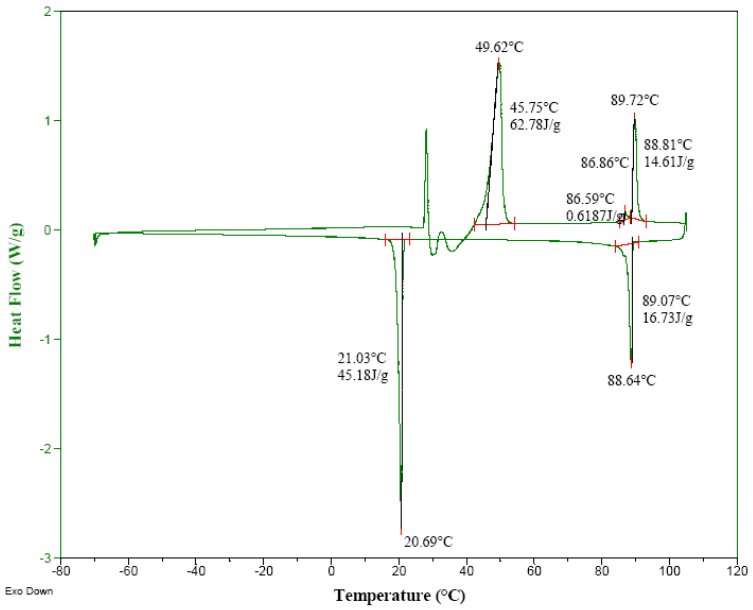

Figure A2-5: DSC profile for compound **1.13e** taken at a scan rate of 5K/min.

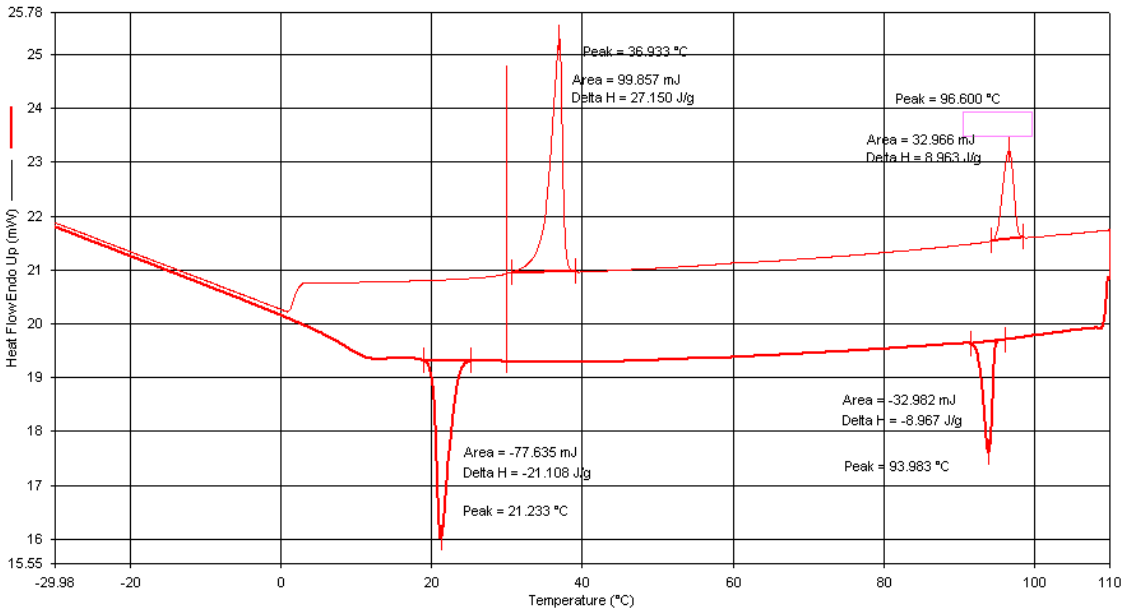

Figure A2-6: DSC profile for compound **1.14a** taken at a scan rate of 5K/min.

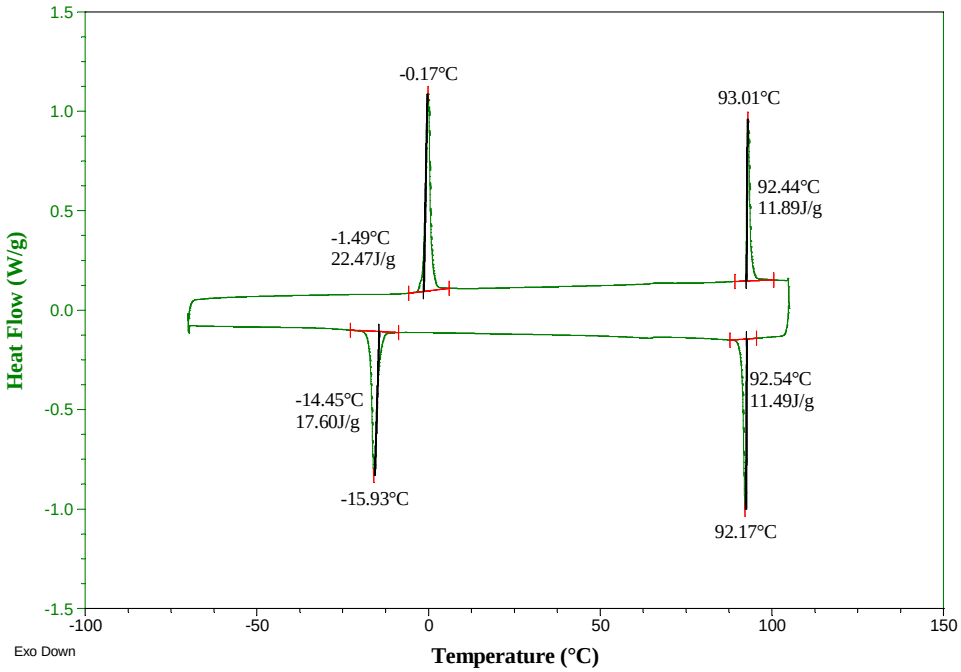

Figure A2-7: DSC profile for compound **1.14b** taken at a scan rate of 5K/min.

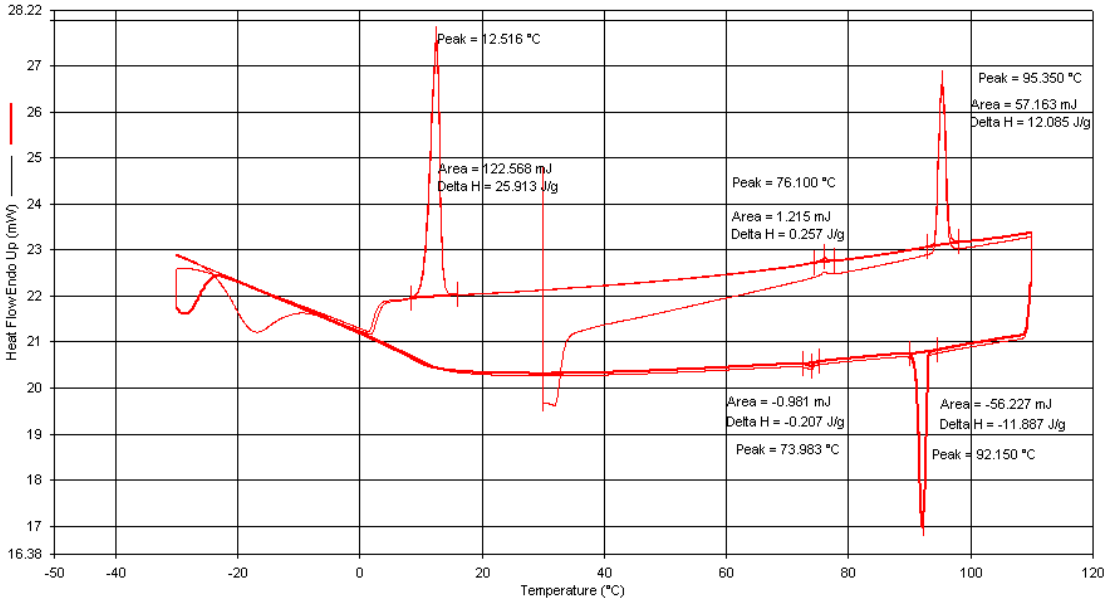

Figure A2-8: DSC profile for compound **1.14c** taken at a scan rate of 5K/min.

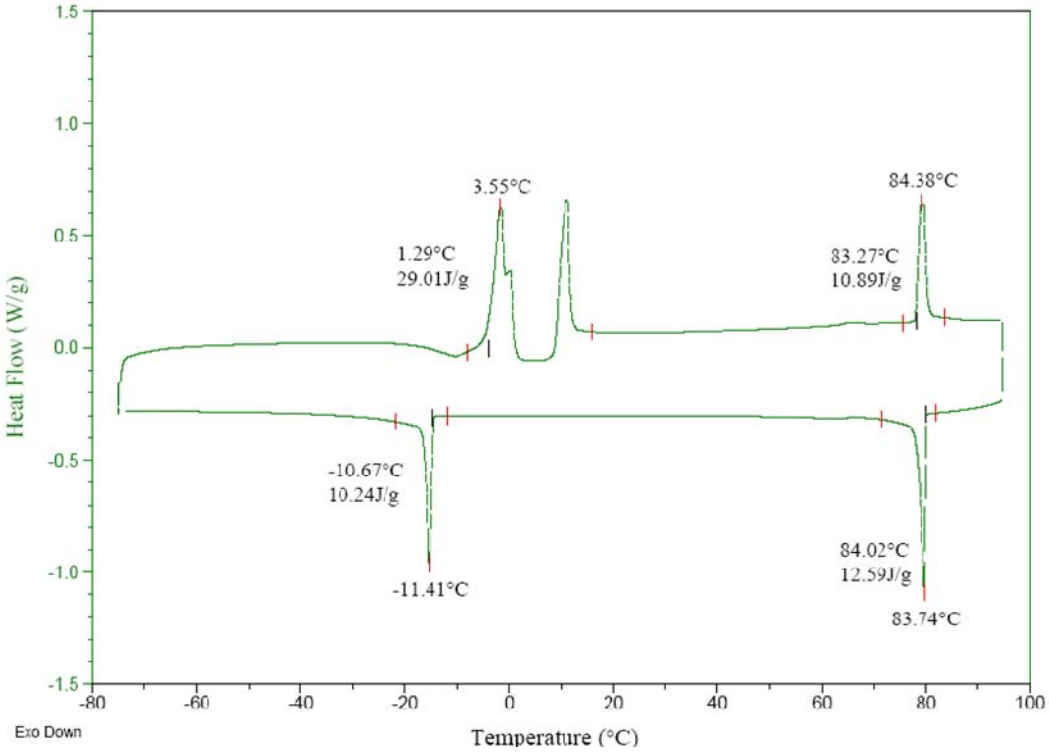

Figure A2-9: DSC profile for compound **1.14d** taken at a scan rate of 5K/min.

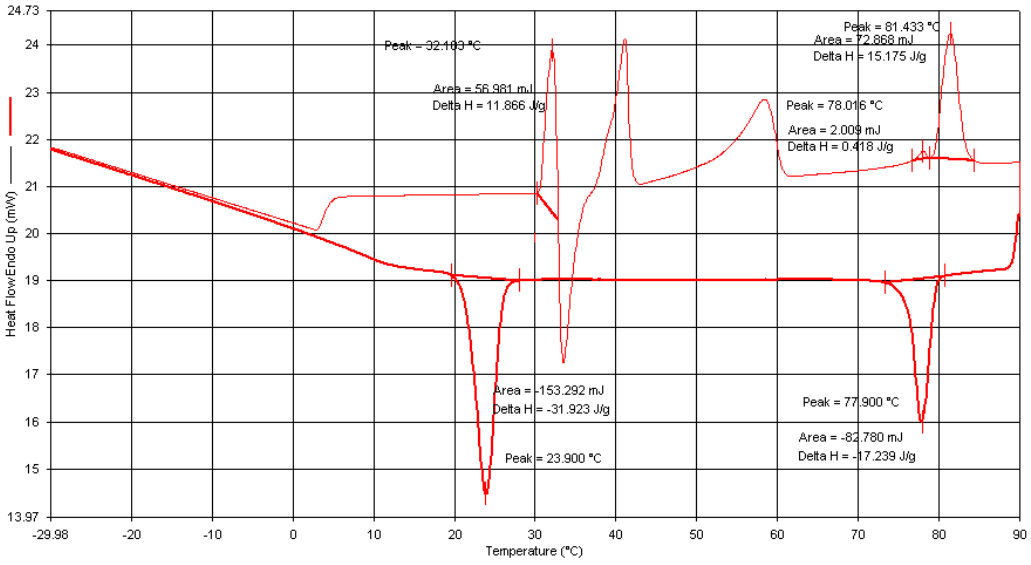

Figure A2-10: DSC profile for compound **1.14e** taken at a scan rate of 5K/min.

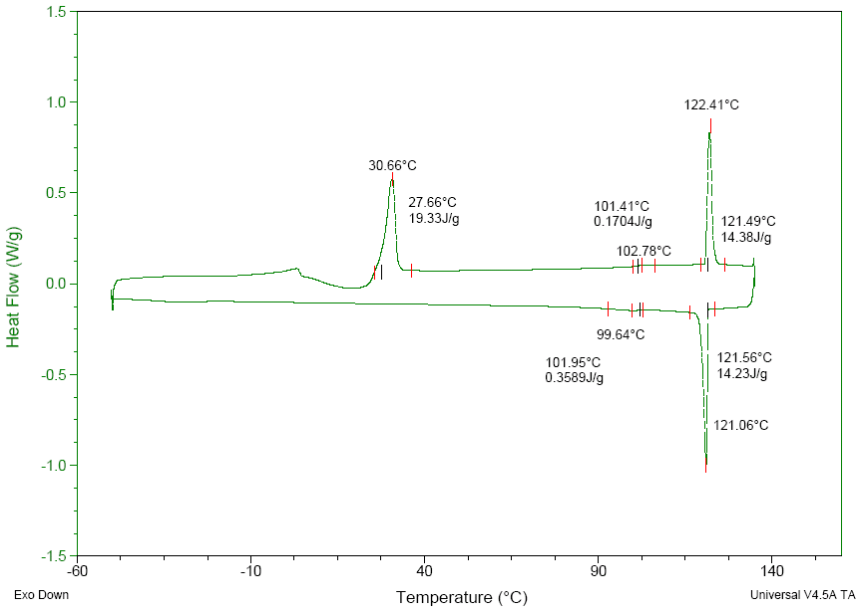

Figure A2-11: DSC profile for compound **1.15** taken at a scan rate of 5K/min.

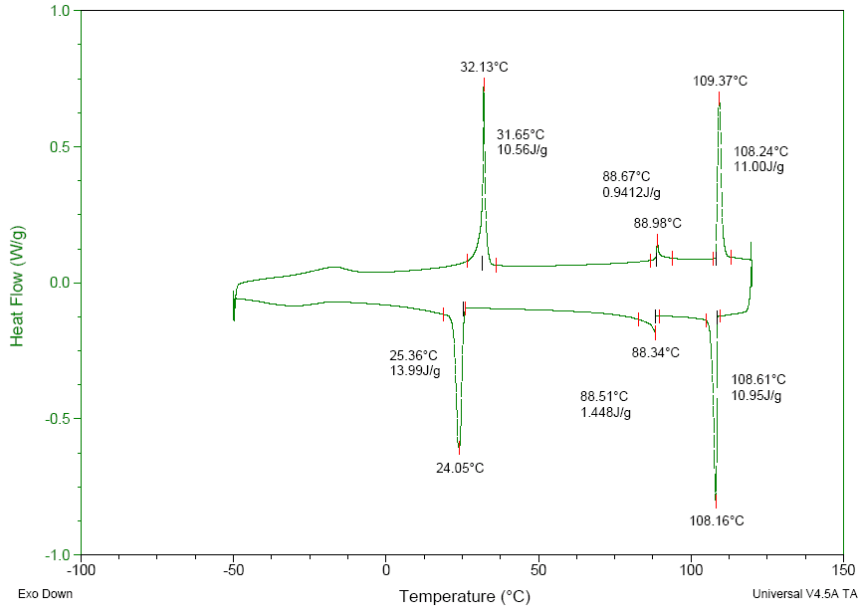

Figure A2- 12: DSC profile for compound **1.16** taken at a scan rate of 5K/min.

Appendix 3. Textures of liquid crystals by polarized microscopy

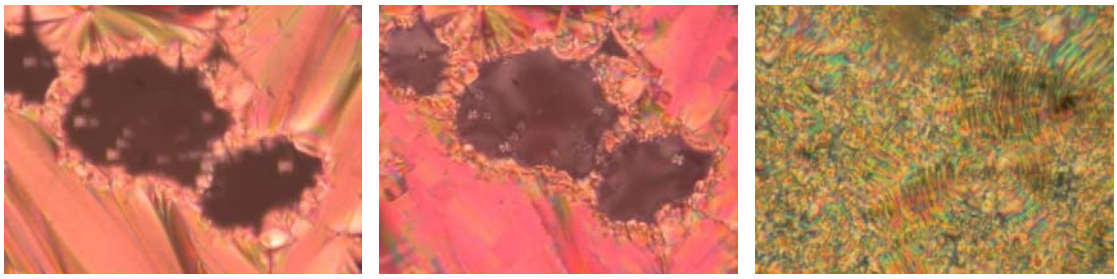

Figure A3-1: Textures of compound **1.13a** observed by polarized microscopy on cooling: in the SmA phase at 71^{o}C (left), in the SmC phase at 67^{o}C (middle) and in the SmX phase at 10^{o}C (right). (500X Magnification)

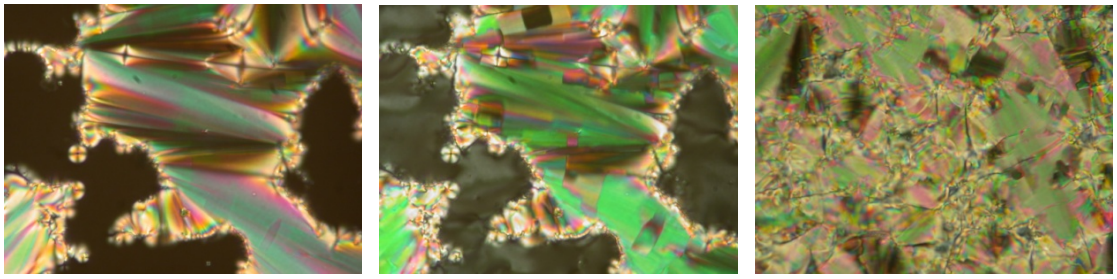

Figure A3-2: Textures of compound **1.13b** observed by polarized microscopy on cooling: in the SmA phase at 80^{o}C (left), in the SmC phase at 75^{o}C (middle) and in the SmX phase at 0^{o}C (right). (500X Magnification)

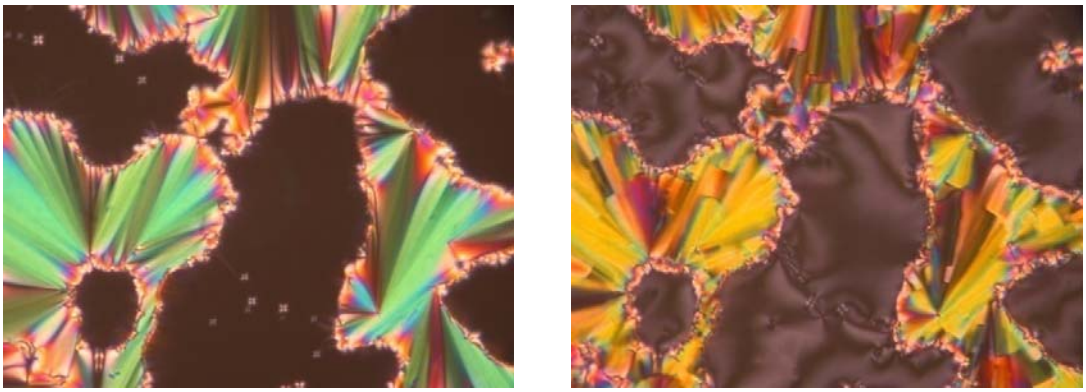

Figure A3-3: Textures of compound **1.13c** observed by polarized microscopy on cooling: in the SmA phase at 83^{o}C (left) and in the SmC phase at 76^{o}C (right). (500X Magnification)

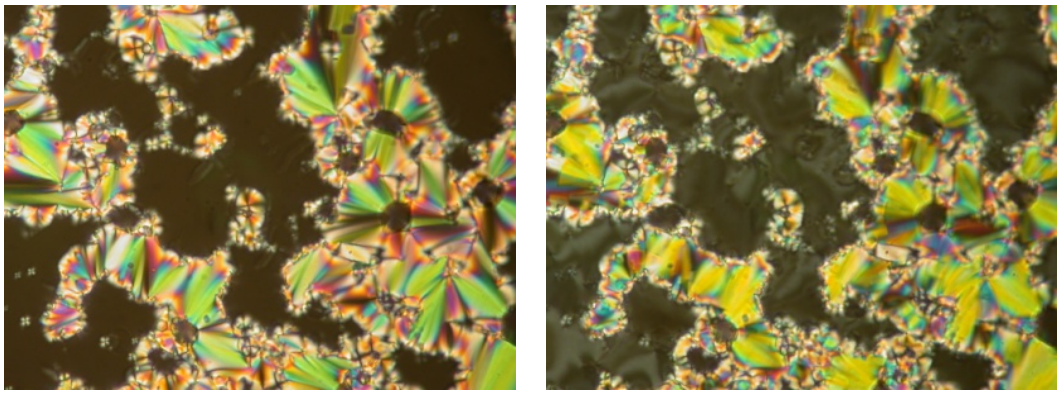

Figure A3-4: Textures of compound **1.13d** observed by polarized microscopy on cooling: in the SmA phase at 86^{o}C (left) and in the SmC phase at 81^{o}C (right). (500X Magnification)

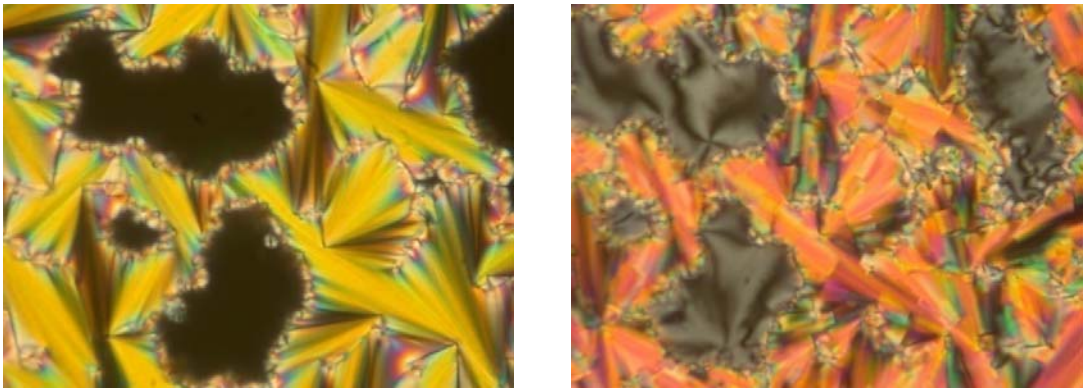

Figure A3-5: Textures of compound **1.13e** observed by polarized microscopy on cooling: in the SmA phase at 90^{o}C (left) and in the SmC phase at 86^{o}C (right). (500X Magnification)

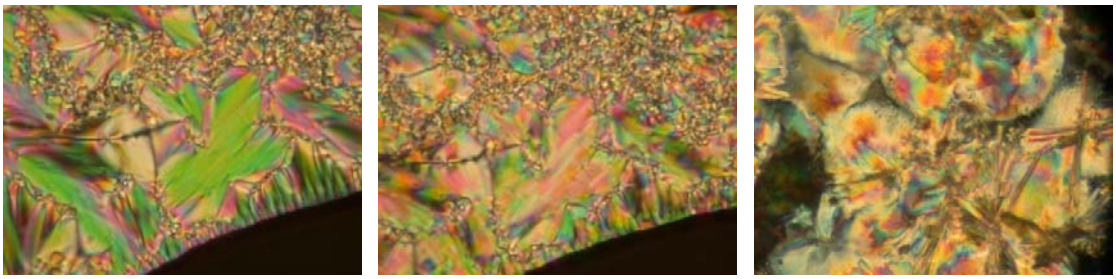

Figure A3-6: Textures of compound 1.14a observed by polarized microscopy on cooling: in the SmA phase at 60^{o}C (left), in the SmC phase at 57^{o}C (middle) and in the SmX at 20^{o}C (right). (500X Magnification)

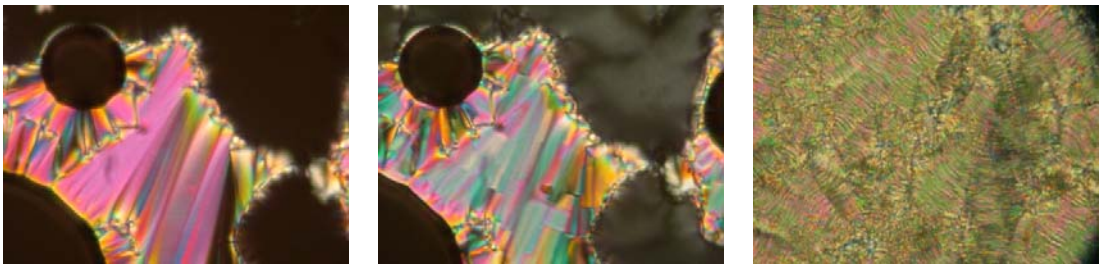

Figure A3-7: Textures of compound **1.14b** observed by polarized microscopy on cooling: in the SmA phase at 73^{o}C (left), in the SmC phase at 69^{o}C (middle) and in the SmX phase at -15^{o}C (right). (500X Magnification)

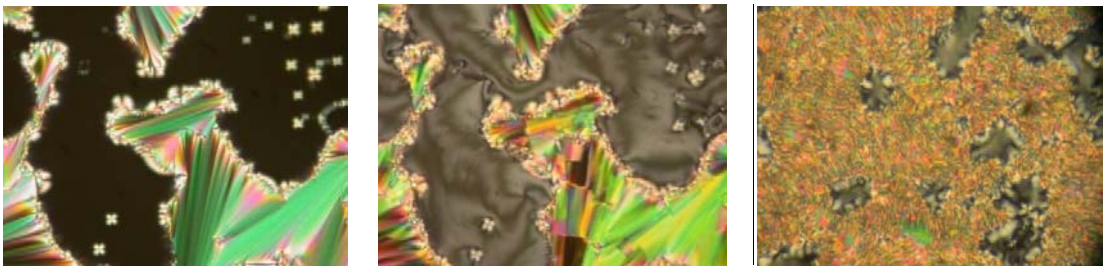

Figure A3-8: Textures of compound **1.14c** observed by polarized microscopy on cooling: in the SmA phase at 77^{o}C (left), in the SmC phase at 73^{o}C (middle) and in the SmX phase at 0^{o}C (right). (500X Magnification)

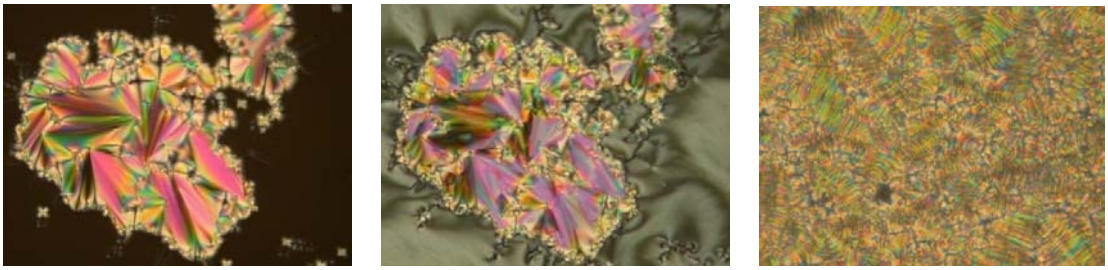

Figure A3-9: Textures of compound **1.14d** observed by polarized microscopy on cooling: in the SmA phase at 72^{o}C (left), in the SmC phase at 68^{o}C (middle) and in the SmX phase at -10^{o}C (right). (500X Magnification)

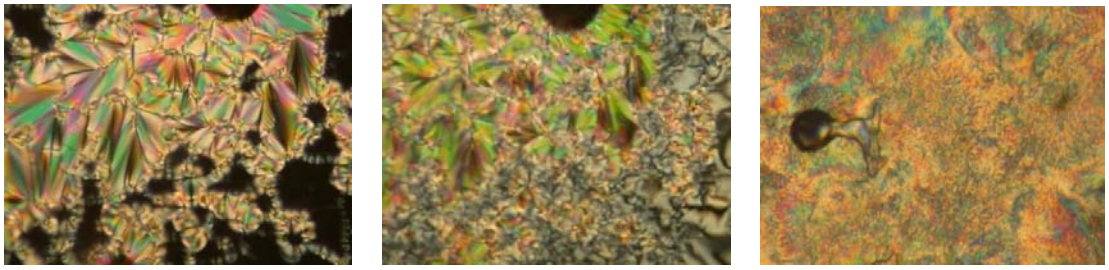

Figure A3-10: Textures of compound **1.14e** observed by polarized microscopy on cooling: in the SmA phase at 80^{o}C (left), in the SmC phase at 76^{o}C (middle) and in the SmX phase at 20^{o}C (right). (500X Magnification)

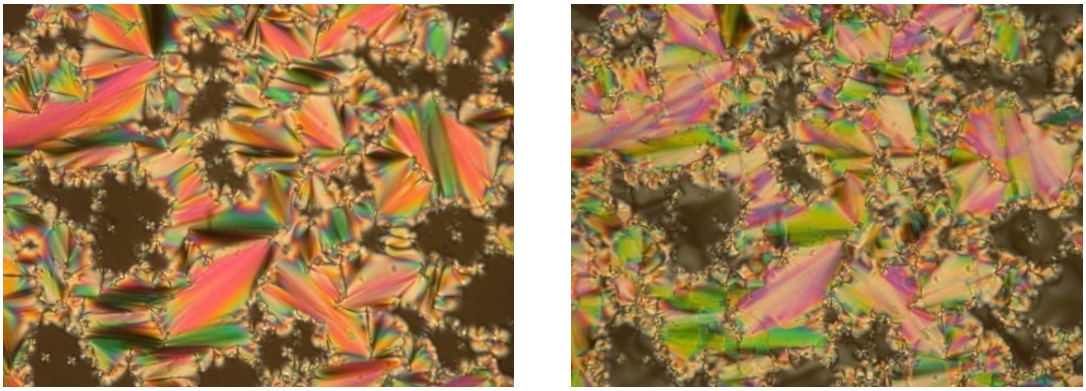

Figure A3-11: Textures of compound **1.15** observed by polarized microscopy on cooling: in the SmA phase at 106^{o}C (left) and in the SmC phase at 102^{o}C (right). (500X Magnification)

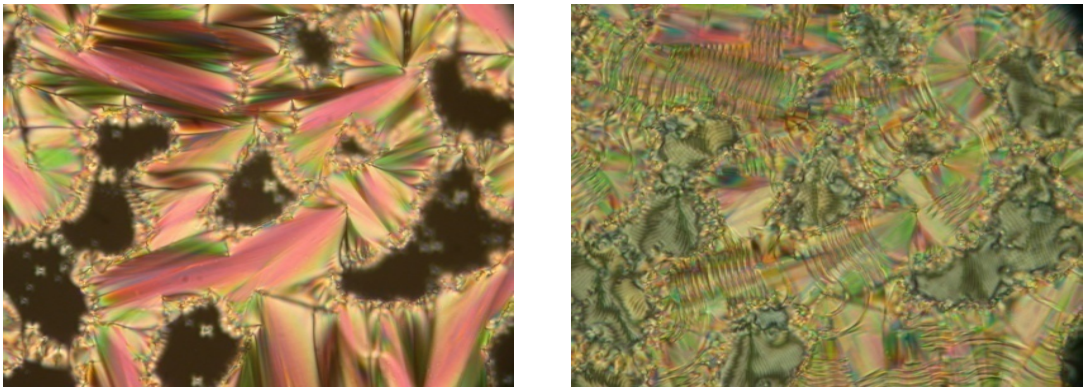

Figure A3-12: Textures of compound **1.16** observed by polarized microscopy on cooling: in the SmA phase at 94^{o}C (left) and in the SmC phase at 91^{o}C (right). (500X Magnification)